

Analysis of Parasitic Losses in Heavy Duty Diesel Engines

by

Christopher Joseph James

B.S. Mechanical Engineering
Northeastern University, 2010

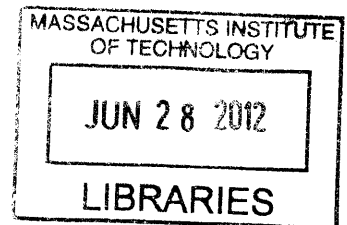
SUBMITTED TO THE DEPARTMENT OF MECHANICAL ENGINEERING IN PARTIAL
FULFILLMENT OF THE REQUIREMENTS FOR THE DEGREE OF

MASTER OF SCIENCE IN MECHANICAL ENGINEERING
AT THE
MASSACHUSETTS INSTITUTE OF TECHNOLOGY

JUNE 2012

© 2012 Massachusetts Institute of Technology
All Rights Reserved

ARCHIVES



Signature of Author.....
Department of Mechanical Engineering
May 25, 2012

Certified by.....
Victor W. Wong
Principal Research Scientist and Lecturer in Mechanical Engineering
Thesis Supervisor

Accepted by.....
David E. Hardt
Chairman, Department Committee on Graduate Students

(This page was intentionally left blank)

Analysis of Parasitic Losses in Heavy Duty Diesel Engines

by

Christopher Joseph James

Submitted to the Department of Mechanical Engineering
on May 25, 2012 in Partial Fulfillment of the
Requirements for the Degree of Master of Science in
Mechanical Engineering

Abstract

Fuel economy of large, on-road diesel engines has become even more critical in recent years for engine manufactures, vehicle OEMs, and truck operators, in view of pending CO₂ emission regulations. Demands for increased fuel economy are coupled with corresponding improvements in engine performance, durability, and emissions. This project centers on resolving the adverse effects on engine wear, durability, emissions, and oil consumption that often accompany traditional low-friction concepts. A detailed analysis of the sources of friction within a heavy-duty diesel engine was undertaken and empirical data on engine friction and component wear was collected from industry as well as from studies in literature.

The use of thermal barrier coatings (TBC) was investigated as a novel approach to strategically increase cylinder liner temperatures in order to reduce power cylinder friction. By coating selected parts of the liner where piston speeds are high, local liner temperature is raised and local lubricant viscosity decreased in that region. In the mid-stroke, the piston is in the hydrodynamic lubrication regime, and high surface speeds generate the majority of the power cylinder work losses which can be reduced through reduced lubricant viscosity. By coating the liner in selected regions only, top dead center temperatures are mostly unaffected thereby minimizing any increase in cylinder liner wear. This approach is expected to maximize friction reduction while minimizing risk to other engine components or increasing component wear rates.

A simulation was developed to model the primary physical processes that occur in a complete four stroke engine cycle. Calculations included work done by the piston, mass flow rates through the intake and exhaust valves, heat release during combustion, and heat transfer rates. The results demonstrate the potential to decrease power cylinder between 15% and 30% depending on coating thickness and application zone. This corresponds to approximately a 0.5% to 1% improvement in vehicle fuel economy. Additional fuel economy benefits from the TBC are expected from increased exhaust gas enthalpy and reduced liner heat rejection. This strategic thermal management approach within the engine has very high potential to increase engine efficiency while maintaining the performance and durability demanded in the HD engine market.

Thesis Supervisor: Victor W. Wong

Title: Principal Research Scientist and Lecturer in Mechanical Engineering

(This page was intentionally left blank)

Acknowledgements

My time at MIT has been a memorable, challenging, and extremely rewarding experience. Central to my success here at MIT has been the influence of a number of people, to whom I've tremendously grateful. I would like to thank the following people for their help in the completion of this project

First I would like to acknowledge and thank my advisor, Dr. Victor Wong, for his support and guidance throughout my time here at MIT. His vast experience in engine design and modeling exposed me to an exciting field of research and knowledge. The analytical skills gained through my research will prove invaluable in any profession.

This project would not have been possible without the support of my project sponsor, Detroit Diesel/Daimler Trucks North America. I would like to thank Kevin Sisken, Dave Maietta, and Dennis Krawczak for their support throughout the project and their expertise in engine component design.

I would like to thank the students of the Sloan Automotive Laboratory for providing an engaging, and often times entertaining work environment. I would like to thank Yin-Chun Wang for providing interesting conversation and a necessary distraction from research. Thomas Martins and Troy Niekamp for their friendship and office comradery. Justin Ketterer for the hours spent on various homework assignments and study sessions. Dr. Alex Sappok and Dr. Carl Justin Kamp for their guidance throughout my time here at MIT. Finally no acknowledgment of the Sloan Lab would be complete without thanking Janet Maslow for her tireless efforts to keep the lab running smoothly.

I would like to extend my sincerest thanks to my family and friends for their support. I am especially grateful to my parents for their unwavering support, guidance, and encouragement in my personal, academic, and professional endeavors. Most importantly, I am thankful for the love and support of my fiancée, Emily, whose daily encouragement and understanding has made my time here at MIT much more enjoyable.

(This page was intentionally left blank)

Table of Contents

Abstract	3
Acknowledgements	5
Table of Contents	7
List of Figures	11
List of Tables	13
Nomenclature	15
1. Introduction	17
1.1 Diesel Engine Principles	18
1.1.1 Typical Application of Diesel Engines	19
1.1.2 Advantages of Diesel Engines	21
1.1.3 Disadvantages of Diesel Engines	22
1.2 Regulation of Heavy Duty On-road Diesel Engines	23
1.2.1 Emissions Regulation	23
1.2.2 Emission Control Strategies	25
1.2.3 Fuel Economy Standards	26
1.3 The Motivation to Reduce Engine Friction	27
1.4 Sources of Friction in Diesel Engines	29
1.4.1 Overview of Major Engine Systems	30
1.4.2 Quantifying Friction Losses	32
1.4.3 Typical Friction Distribution in a HD Diesel Engine	34
1.5 Scope of Current Work	38
2 Friction Analysis	39
2.1 Lubrication Regimes in an Engine	39
2.2 Lubricant properties	41
2.2.1 Lubricant Additives	42
2.2.2 Viscosity Temperature Relationship	43
2.2.3 Viscosity and Shear Rate Relationship	44
2.3 Wear	45
3 Modeling of Friction in Heavy Duty Class 8 Diesel Engines	47

3.1	Numerical Friction Models	48
3.1.1	Crankshaft Numerical Friction Models	48
3.1.2	Power Cylinder Numerical Friction Models.....	50
3.2	Empirical Friction Models	55
3.3	Empirical Friction Models Applied to HD Diesel Engines.....	66
3.3.1	Crankshaft	66
3.3.2	Power Cylinder	67
3.3.3	Auxiliary Components	68
3.3.4	Summary	69
4	Local Oil Viscosity and Friction Reduction - Study of Cylinder Liner Thermal Barrier Coatings	71
4.1	Previous Studies of Thermal Barrier Coatings in Diesel Engines	72
4.1.1	Effects of TBC and LHR on Engine Emissions.....	74
4.1.2	Effects of TBC and LHR on Engine Performance Parameters.....	75
4.2	Thermal Barrier Coating Properties	76
4.3	Motivation for Research in Thermal Barrier Coatings for Super Truck Project.....	77
4.3.1	Power Cylinder Lubrication.....	77
4.4	Modeling Approach and Details	81
4.4.1	Overview of Model	81
4.4.2	Modifications to Model.....	86
4.5	Results and Discussion.....	89
4.5.1	Study of Thermal Barrier Coating Thickness and Application Zone on Cylinder Liner Temperature	89
4.5.2	Comparison of Natural Convection Combined Thermal Barrier Coatings on Selected Parts of the Cylinder Liner.....	94
4.5.3	Study of Thermal Barrier Coating Thickness and Application Zone on Lubricant Kinematic Viscosity	97
4.5.4	Friction Reduction Potential of TBC	102
4.5.5	Study of Thermal Barrier Coating Thickness and Application Zone on Coolant Heat Rejection and Exhaust Gas Enthalpy	110
4.5.6	Study of Thermal Barrier Coating Thickness and Application Zone on Engine Thermal Efficiency	115

4.6	Summary of Thermal Barrier Coating Study	117
5	Conclusions	119
5.1	Continuing Work.....	121
	Works Cited	123
	Appendix A.....	131

(This page was intentionally left blank)

List of Figures

Figure 1.1 Sulzer RT96-C Diesel Engine [5].....	19
Figure 1.2 Reduction of PM and NOx Emissions Over Time [13]	25
Figure 1.3 Weekly U.S. No 2 Diesel Retail Prices 1995-2012 [19].....	28
Figure 1.4 United States Petroleum Consumption in the Transportation Sector [7]	29
Figure 1.5 Distribution of Total Energy in a Fired Engine [20]	34
Figure 1.6 Distribution of Total Mechanical Losses of a Diesel Engine [20]	35
Figure 1.7 Typical Distribution of Power Loss in the Power Cylinder [20].....	36
Figure 1.8 Typical Distribution of Piston Ring Friction [20]	36
Figure 1.9 Flowchart of Friction Contributions by Component Group.....	37
Figure 2.1 Regimes of Lubrication Shown on the Scale of Surface Asperities [23]	39
Figure 2.2 Stribeck Curve	40
Figure 2.3 Estimated Additive use for 2006 by additive type, North America	42
Figure 2.4 Cross Equation Lubricant Viscosity Shear Rate Dependence.....	45
Figure 3.1 Lubricant Pressure Distribution in a Dynamically Loaded Journal Bearing.....	50
Figure 3.2 Stribeck Curve for Power Cylinder Components	51
Figure 3.3 Forces and Moments Acting on the Piston [36]	52
Figure 3.4 Model Layout for Each Piston Ring.....	54
Figure 3.5 Crankshaft Friction Model and Experimental Results	66
Figure 3.6 Crankshaft FMEP Analysis for SAE Oil Grades	67
Figure 3.7 Power Cylinder FMEP Analysis for SAE Oil Grades.....	68
Figure 3.8 Oil Pump FMEP	69
Figure 3.9 Total Engine FMEP as a Function of Engine Speed	69
Figure 4.1 Dry and Wet Cylinder Liner Comparison [52].....	71
Figure 4.2 Thermal conductivity of 8% YSZ at Various Measuring Temperatures [59]	76
Figure 4.3 Instantaneous Piston Velocity as a Function of Crank Angle	78
Figure 4.4 Cylinder Liner Wall Temperature Distribution.....	79
Figure 4.5 Kinematic Viscosity of Lubricant on Cylinder Liner versus Ideal Case.....	80
Figure 4.6 Geometry of Power Cylinder Without and With TBC.....	82
Figure 4.7 Thermal Resistance Circuit	85
Figure 4.8 Diagram of Cylinder Liner Segments in Model	87
Figure 4.9 Heat Transfer Element of Cylinder Liner.....	88
Figure 4.10 Conventionally Cooled Cylinder Liner and Liner with TBC on Mid-Stroke	90
Figure 4.11 Liner Wall Temperature Woschni Correlation vs Model.....	91
Figure 4.12 Liner Temperature Profile with TBC on Entire Liner.....	92
Figure 4.13 Liner Temperature with TBC on Piston Mid-stroke (Segments 4,5,6)	93
Figure 4.14 Liner Temperature with TBC on Segments 4 through 10	94
Figure 4.15 Natural Convection Applied to Various Liner Segments.....	95
Figure 4.16 Cylinder Liner Temperature Profile with Natural Convection on Bottom 30% of Liner and TBC on Mid-stroke.....	96

Figure 4.17 Cylinder Liner Temperature Profile with Natural Convection on Bottom 20% of Liner and TBC on Mid-stroke.....	96
Figure 4.18 Local Viscosity of 15W-40 with TBC on Entire Liner	97
Figure 4.19 Local Viscosity of 15W-40 with TBC on Liner Segments 4,5,6	98
Figure 4.20 Local Viscosity of 15W-40 with TBC on Liner Segments 4 through 10.....	98
Figure 4.21 Lubricant Viscosity with Natural Convection Applied to Liner Segments	99
Figure 4.22 Lubricant Viscosity with Natural Convection Applied to Segments 9-10 and TBC from 4-8	100
Figure 4.23 Lubricant Viscosity with Natural Convection Applied to Segments 8-10 and TBC from 4-7	100
Figure 4.24 Power Cylinder Lubricant Viscosity over Engine Cycle for Different TBC and Natural Convection Applications.....	101
Figure 4.25 Instantaneous Power Cylinder Friction Over Complete Engine Cycle	102
Figure 4.26 Cylinder Liner Segment Crank Angle Duration and Average Velocity.....	103
Figure 4.27 Average Friction Force for Each Liner Segment	103
Figure 4.28 Average Friction Work Losses for Each Liner Segment.....	104
Figure 4.29 Average Friction Power Losses for Each Liner Segment	104
Figure 4.30 Hydrodynamic and Boundary Friction Forces in the Ring Pack [42]	105
Figure 4.31 Hydrodynamic and Boundary Friction FMEP for Varying Mean Lubricant Viscosities [42]	106
Figure 4.32 Decrease in Liner Segment Friction Force for TBC Applications	107
Figure 4.33 Decrease in Liner Segment Friction Power Losses for TBC Applications	108
Figure 4.34 Reduction in Engine Friction for Various TBC Application Zones.....	109
Figure 4.35 Coating Thickness and Type versus Exhaust Enthalpy.....	111
Figure 4.36 Liner Heat Rejection for Different TBC Thickness and Application Zone	112
Figure 4.37 Liner Heat Rejection for Different TBC Thickness and Application Zone	113
Figure 4.38 Cylinder Gas Temperature versus Crank Angle.....	114
Figure 4.39 Cylinder Liner Full Cycle Heat Transfer by Liner Segment	114
Figure 4.40 Thermal Efficiency as a Function of TBC Thickness	115
Figure 4.41 Thermal Efficiency for TBC on the Cylinder Liner	116

List of Tables

Table 1.1 Federal Heavy Duty Diesel Engine Emission Regulations [12].....	24
Table 1.2 EPA and NHTSA Proposed Model Year 2017 Combination Trailer Standards	27
Table 4.1 Model Input Parameters for Engine Geometry, Timing, Fuel and Air Input	89
Table 4.2 TBC Parameters and Additional Model Inputs.....	90
Table 4.3 Hydrodynamic Friction Weighting Factors	106
Table A.0.1 Lubricant Properties and Constants Used in Vogel and Cross Equations Various	131

(This page was intentionally left blank)

Nomenclature

BDC - Bottom Dead Center

BMEP – Brake Mean Effective Pressure

BSFC – Brake Specific Fuel Consumption

CI - Compression Ignition

CI - Compression Ignition

CO - Carbon Monoxide

CO₂- Carbon Dioxide

DPF - Diesel Particulate Filter

EGR – exhaust gas recirculation

EHD - Elastohydrodynamic

EPA - United States Environmental Protection Agency

FMEP – Friction Mean Effective Pressure

GHG – Greenhouse Gas

GWP – Global Warming Potential

HC - Hydrocarbons

HD - Heavy Duty

ICE - Internal Combustion Engine

IMEP – Indicated Mean Effective Pressure

IPCC - Intergovernmental Panel on Climate Change

ISFC - Indicated Specific Fuel Consumption

LHR - Low Heat Rejection

NHTSA – National Highway Traffic Safety Administration

NMHC - Non-Methane Hydrocarbons

NO_x - Nitrous Oxide

OEM – Original Equipment Manufacturer

OCR - Oil Control Ring

PM - Particulate Matter

PM – Particulate Matter

RPM - Revolutions Per Minute

SCR - Selective Catalytic Reduction

SI – Spark-Ignition

TBC – Thermal Barrier Coating

TDC - Top Dead Center

VI – Viscosity Index

VI – Viscosity Modifier

1. Introduction

Fuel economy in large, on-road diesel engines has become even more critical in recent years for engine manufactures, vehicle OEMs, and for truck operators. Demands for increased fuel economy are coupled with increased demands in engine performance and durability by consumers. Additionally, more stringent emissions standards for particulate matter (PM), nitrogen oxides (NO_x), and non-methane hydrocarbon emissions (NMHC) have added significant equipment to the vehicle and a corresponding engine efficiency penalty.

Vehicle fuel economy improvements are realized through a multitude of approaches, from engine downsizing, improved vehicle aerodynamics, electrification, waste heat recovery, and increased efficiency from existing vehicle systems. Fuel economy improvements in the engine can be realized through mechanical design, advanced control systems, material improvements, and friction reduction. Reductions in engine friction increase the brake mean effective pressure (bmepp) of the engine and reduce the brake specific fuel consumption (BSFC). Engine friction reduction is accomplished through three primary methods: mechanical design of engine components, material surface texture and coatings, and improvements in engine lubrication performance.

The mechanical design of engine components dictates the friction surfaces in an engine; in addition to the loading, surface speeds, and lubrication each engine component receives. Design engineers have been improving mechanical designs since the first engines were developed. Changes in the mechanical design of a production engine can be very challenging for a variety of reasons including tooling, service, certification, and concern on overall system integrity. While these barriers can be overcome, the cost and time to implement these changes may outweigh the benefit.

Material surface texture and low friction coatings have led to improved performance, durability and lower friction in internal combustion engines. Recent studies have used various cylinder liner crosshatch patterns and angles in addition to micro texturing of the cylinder liner to mitigate wear effects associated with lower viscosity lubricants [1]. Coatings and textures can be easily applied to components but must be able to withstand the conditions within the engine throughout

the lifecycle of the engine. For class 8 trucks the B50 life, or the point at which half the engines produced are still running and half require rebuild, is typically 1 million miles. These extremely long life cycles make coating longevity of primary importance.

Engine lubricant provides critical protection and lubrication of engine components. Lubricant properties and additives therefore have a vital role in engine performance and durability along with the longevity of vehicle emission systems. Improvements in the engine lubrication system to optimize mechanical conditions such as temperature, load, and shear rate as well as advanced lubricant formulations can reduce engine frictional losses and improve performance.

Investigations into lubricant base stock, friction modifiers, anti-wear additives, high-temperature high-shear (HTHS) properties, and viscosity modifiers (VM), to optimize the friction characteristics of engine oil under various loading conditions can make notable improvements on vehicle and fleet fuel economy [2].

1.1 Diesel Engine Principles

Since the invention of the diesel engine by Rudolph Diesel in 1893 it has been utilized all over the world for power generation, locomotion, shipping, construction equipment, trucks, and automobiles. The diesel engine is an internal combustion engine that uses the heat of compression to ignite fuel that is injected into the combustion chamber, leading to heat release and expansion against a piston which results in work output. Diesel engines typically have compression ratios between 12:1 and 24:1, with peak cylinder pressures and temperatures of 4-5 MPa and 800-1000 K [3]. In comparison to spark-ignition (SI) engines, diesel engines have a higher thermal efficiency due to greater compression ratios, and also benefit from the lack of a complicated ignition system that requires maintenance. Their high efficiency and high torque output have made the diesel engine an indispensable tool in a wide spectrum of industries and uses.

Diesel engines are used for a variety of reasons, principally thermal efficiency, durability, fuel safety, and application power requirements. Diesel engines have higher thermal efficiencies compared to spark-ignition engines which allow them to burn less fuel while maintaining the same work output. Diesel engines are made from stronger materials due to higher in cylinder

pressures and therefore have high durability and reliability which is critical for marine, railroad, and transportation applications. Fuel safety is critical for applications such as marine vessels, military vehicles, school busses, and firefighting equipment. Diesel fuel is less volatile than gasoline and will not explode or release flammable vapors in open air making it more desirable in these safety critical applications. Finally, diesel engines are most useful for high power applications. Spark-ignition engines are rarely used in displacements over 10 liters or power requirements over 300 kW, whereas diesel engines come in displacements from less than a liter to more than 25,000 liters and power ratings from a few kW to over 80 MW.

1.1.1 Typical Application of Diesel Engines

Diesel engines are used in a variety of applications. They are used extensively in marine applications, 96% of the engine output of all civilian ships above 100 gross metric tons is produced with diesel engines [4]. These engines have service lives of 30 years or more and are available in power ratings that exceed 80 MW for large ships [5]. Figure 1.1 shows a picture of the Wartsila RTA96C, a 14 cylinder low speed diesel engine which generates 80 MW at 127 revolutions per minute (RPM) and weighs 2,300 metric tons. More than 90% of global trade is transported by ships. Domestic and international waterborne commerce shipped more than 7.8 billion tons of goods globally in 2009 and 2.2 billion tons into and out of the United States alone [6] [7].

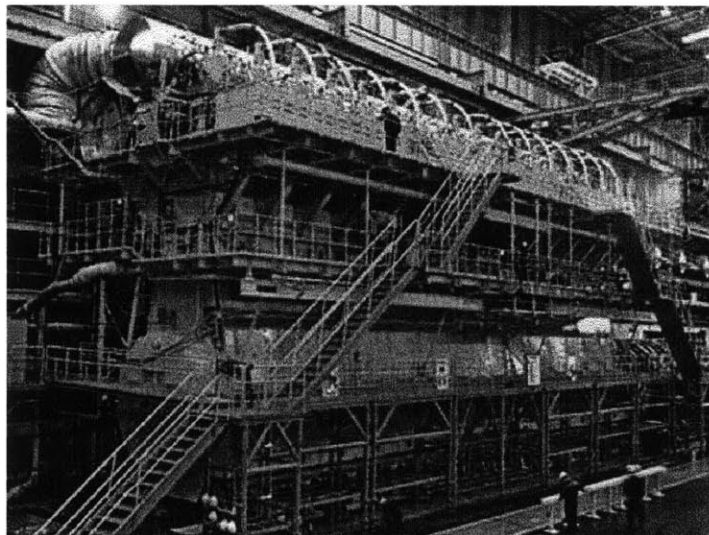


Figure 1.1 Sulzer RT96-C Diesel Engine [5]

Diesel engines are also utilized in rail transportation where electrification of rail lines is not feasible or too expensive. In these systems a large diesel engine powers a generator that provides power to electric motors which power the locomotive. These diesel locomotives transported 1.67 billion tons of freight in the United States in 2009, an average distance of 919 miles (1534.73 billion ton-miles) [7]. Class I railroad companies, defined as have operating revenues over \$401.4 million in 2008 dollars, have locomotive fleets that are approximately 95% diesel-powered [8].

Large truck transportation and a significant number of automobiles worldwide use diesel engines for their high efficiency and durability. Over 99% of all class 8 heavy duty trucks in the United States are diesel powered [8]. Heavy duty trucks moved commodities over 1342.1 billion ton-miles in 2007 [7]. In the light duty market in the United States diesels compose only 2.68% of the market but in European markets diesels have approximately 50% market share [7] [4]. This large disparity in light duty market penetration is due to substantially lower taxes on diesel fuel in European countries.

Besides the transportation of people and goods, diesel engines are used in a wide variety of other applications. Diesel engines are used in agriculture to power large tractors, vehicles, and irrigation pumps. Large construction equipment, including trucks, excavators, trenchers, rollers, asphalt pavers, bore/drill rigs, earth moving equipment, generators, and air compressors are largely powered by diesel engines. Mining is another industry that depends heavily on diesel engines. Underground they are used for their near-zero carbon monoxide emissions, making the environment safe for workers. Above ground they power nearly all the heavy equipment, including massive dump trucks and power shovels with engines in excess of 2500 horsepower [9].

Diesel engines are also used extensively by the military because of safety and for fuel standardization to simplify wartime logistics. Needless to say, diesel engines are what allow the efficient movement and production of goods in our economy and have a great influence on our lives.

1.1.2 Advantages of Diesel Engines

Diesel engines have a variety of advantages over their spark-ignition counterparts. One critical advantage is the higher thermal efficiency afforded by the higher compression ratios, which range between 12:1 and 24:1 for diesel engines compared with 8:1 to 12:1 for gasoline spark-ignition engines. The higher compression ratios of diesel engines provide for thermal efficiencies of up to 45% compared to around 30% for gasoline counterparts [3].

Besides high compression ratios, there are several other advantages of diesel engines over SI engines. Diesel engines inject the amount of fuel required for the current load and have no throttle plate or other restriction to airflow, in comparison to gasoline engines which throttle airflow to control a set air-fuel mixture. The throttling of an SI engine increases pumping losses, the energy lost as air is moved through the engine. The injection of fuel directly into the combustion chamber allows diesel engines to run a lean air-fuel ratio while modern SI engines must run at stoichiometric ratios due to emission system requirements. Lean fuel operation creates minimal carbon monoxide (CO) emissions, which allowed diesel engines use in early submarines and underground mining equipment without danger of CO poisoning. Lean operation also increases fuel economy under partial load conditions, which is a substantial portion of a typical drive cycle. The direct injection of fuel also makes diesel engines ideal for super charging and turbocharging, unlike SI engines that reach a knock limit due to the premixed mixture of air and fuel that enters the cylinder prior to compression.

Due to higher compression ratios diesel engines are made from stronger components that have increased durability and longevity. Increased lifecycles make them ideal for heavy duty transportation, industrial, and construction equipment. The lack of an electrical ignition system found on SI engines eliminates a source of failure and also makes diesel engines more suitable for damp environments.

The properties of diesel fuel itself have several advantages over gasoline. First, it is distilled directly from petroleum and therefore requires less refinement before use. Diesel fuel also has a higher energy density than gasoline per unit volume, one gallon of diesel fuel has approximately 15% more energy than a gallon of gasoline. Diesel fuel is considered safer than gasoline due to

its lower vapor pressure it will not explode or release flammable vapor in open air, making it safer in enclosed applications such as marine vessels or in mining equipment.

1.1.3 Disadvantages of Diesel Engines

Despite the numerous advantages of diesel engines, they do have several disadvantages when compared to SI gasoline engines. A gasoline engine has a better power-to-weight ratio than a comparable diesel engine. This is because gasoline engines have lower compression ratios and therefore lower peak cylinder pressures, which allows for the use of lighter weight materials in engine design. High power-to-weight ratios is important for performance vehicles and light weight vehicles such as motorcycles. The heavier construction combined with a more demanding fuel delivery system makes a diesel engine more expensive than their gasoline counterparts.

The compression ignition (CI) of fuel in a diesel engine tends to make them noisier and have greater vibration than SI engines. The high compression ratios in a CI engine lead to long piston strokes which constrains diesel engines to running within a narrower power band than a similar displacement gasoline engine. This requires more gears in the transmission to move a vehicle along.

Diesel engines produce particulate matter (PM) and nitrous oxide (NO_x) emissions that now require expensive aftertreatment systems and additional maintenance. PM is cited as a significant human health risk while NO_x leads to smog formation and is a greenhouse gas (GHG). A diesel particulate filter (DPF) is used to remove soot particles from the exhaust. The DPF requires periodic cleaning and/or replacement over the life of the engine and significantly increases exhaust system backpressure which has a corresponding efficiency penalty. In addition, extra fuel is needed to increase exhaust temperatures during periodic regenerations required to burn off accumulated soot in the filter. Selective catalytic reduction (SCR) is used to reduce NO_x, with the aid of a catalyst, into diatomic nitrogen, water, and carbon dioxide by dosing the exhaust stream with a diesel exhaust fluid (DEF). The SCR system requires the use of DEF at a rate of 2-4% of total fuel consumption. Currently, a gallon of DEF costs approximately the same as a gallon of diesel which adds a significant operating expense over the life of the engine. These

additional systems, maintenance, and the cost of DEF add significantly to the initial cost of the vehicle and lifetime costs of operation.

One final disadvantage of diesel engines is their difficulty to start in cold weather. This is because diesel engines rely on the heat of compression to ignite the fuel and low cylinder block temperatures can absorb much of this heat, preventing ignition. Small electric heaters called glowplugs are used in the compression chamber to prevent this, along with electric resistive heaters in the engine block. Also, diesel fuel can wax or gel in cold weather clogging fuel filters and starving the engine of fuel. Modern design and special winter mixes of diesel fuel have minimized these issues in today's diesel engines.

1.2 Regulation of Heavy Duty On-road Diesel Engines

1.2.1 Emissions Regulation

Major pollutants from diesel engines are particulate matter, hydrocarbons (HC) and nitrogen oxides. The major source of particulate matter emissions is in the nature of the fuel delivery of a diesel engine. Injecting the fuel into the combustion chamber leads to rich zones in the air-fuel mixture which generates soot (PM) after the mixture is ignited. NO_x formation is caused by high temperatures in the combustion chamber. The technical challenge in diesel engine emission reduction is that there is a tradeoff between reducing PM and NO_x emissions. PM is formed primarily from unburned fuel and higher in-cylinder temperatures can vaporize the fuel more readily and limit PM emissions. However, NO_x emissions are directly related to high cylinder temperatures and the availability of oxygen. Consequently, decreasing PM increases NO_x formation and vice versa.

Particulate matter is regulated by the EPA with a specific focus on PM smaller than 10 micrometers which are so small they can become deeply imbedded in the human respiratory system, even into the bloodstream, and cause serious health issues. Studies have linked particulate pollution to decreased lung function, irregular heartbeat, chronic bronchitis, nonfatal heart attacks, premature death in people with heart or lung disease, aggravated asthma, coughing, and difficulty breathing. Children and the elderly are the most susceptible to the negative effects

from PM pollution. Very fine PM (2.5 micrometers or less) is the major cause of haze in parts of the United States. Particles that travel by wind can settle in waterways turning them acidic, damaging crops, forests, and disrupting soil nutrient balance. [10]

Nitrous oxides are highly reactive gasses which contribute to the formation of ground level ozone and PM pollution. For this reason NO_x has 289 times more global warming potential (GWP) than carbon dioxide according to the Intergovernmental Panel on Climate Change (IPCC). NO_x has also been known to cause respiratory problems in humans [11].

The U.S. EPA has regulated diesel engine emissions since 1974, and has implemented a 96% reduction in NO_x and a 90% reduction in PM over 1994 levels. Table 1.1 shows the regulated levels of hydrocarbon, PM, NO_x, and CO from 1974 to present day in grams of pollutant per brake horsepower per hour of engine operation.

Table 1.1 Federal Heavy Duty Diesel Engine Emission Regulations [12]

Federal Heavy-Duty Highway Compression-Ignition Engines - Exhaust Emission Standards						
Year	HC (g/bhp-hr)	NMHC (g/bhp-hr)	NMHC + Nox (g/bhp-hr)	Nox (g/bhp-hr)	PM (g/bhp-hr)	CO (g/bhp-hr)
1974-78	-	-	16	-	-	40
1979-84	1.5	-	10	-	-	25
1985-87	1.3	-	-	10.7	-	15.5
1988-89	1.3	-	-	10.7	0.60	15.5
1990	1.3	-	-	6.0	0.60	15.5
1991-93	1.3	-	-	5.0	0.25	15.5
1994-97	1.3	-	-	5.0	0.10	15.5
1998-2003	1.3	-	-	4.0	0.10	15.5
2004-2006	-	-	2.4 (or 2.5 with a limit of 0.5 on NMHC)	-	0.10	15.5
2007+	-	0.14	-	0.2	0.01	15.5

Note: 2007 NMHC and Nox standards phased in between 2007 and 2010

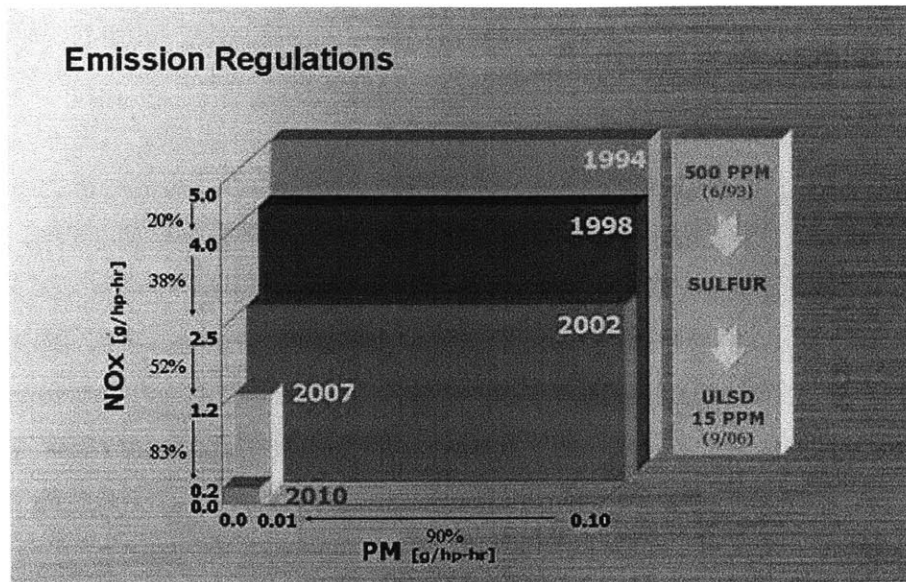


Figure 1.2 Reduction of PM and NO_x Emissions Over Time [13]

1.2.2 Emission Control Strategies

Figure 1.2 graphically displays the changes in the permitted levels of particulate and NO_x emissions from diesel engines. To meet these emissions performance requirements a variety of emission control strategies have been used. Electronic engine control, retarded injection timing, exhaust gas recirculation (EGR), reduced sulfur level in fuel, reduced oil consumption, charge air cooling, higher boost pressures, and now DPFs and SCR.

Electronic controls of the engine allow optimized fuel injection timing, duration, multiple injections, and engine management to minimize emissions and fuel consumption. Retarded injection timing is a strategy implemented to combat NO_x emissions by reducing peak combustion temperature as more of the combustion occurs during the expansion stroke in the engine. Exhaust gas recirculation was implemented to meet 2002 NO_x emissions standards, in which a portion of the exhaust gas is redirected back into the cylinder. The exhaust gas is inert in the combustion process and therefore lowers peak combustion temperatures and increases ignition delay. However EGR reduces engine power levels and increases lubricant degradation rates along with wear in the engine. One additional criteria pollutant, sulfur dioxide, is associated

with diesel exhaust and has been combated at the oil refinery by reducing sulfur levels in fuel from 500 ppm to 15 ppm in 2006.

The EPA's 2007 emission regulation on heavy duty diesel engines was targeted to particulate matter emissions. This regulation required the addition of diesel particulate filters (DPF) to be installed in the exhaust system of on-road diesel engines. These filters prevent the soot and ash particles that make up the PM emissions from entering the atmosphere. However, DPFs require regeneration cycles, which raise the temperature of the exhaust gasses enough to burn off the accumulated soot in the filter. As the vehicle is driven, incombustible particles or ash, primarily from engine lubricant additives accumulate and eventually clog the filter. The accumulation of ash requires the DPF to be maintained over their lifetime, increasing vehicle downtime and operating expense. The addition of DPFs in the exhaust stream creates backpressure which leads to a decrease in engine efficiency and fuel economy, the fuel economy penalty is on the order of 2-5% [14].

The 2007 regulations for NO_x from Table 1.1 were phased in for the 2010 model year. To meet the regulations the vast majority of manufacturers turned to selective catalytic reduction. SCR units inject a gaseous reductant, urea (DEF) in this case, into the exhaust stream and through a catalyst. The NO_x and urea is then reduced through a series of chemical reactions to diatomic nitrogen, water, and carbon dioxide. The introduction of SCR units has allowed reduced levels of EGR in diesel engines. High EGR rates were implemented along with retarded ignition timing to meet emissions regulations in pre-2010 engines, which has a corresponding fuel economy penalty due to less efficient engine operation. Therefore, the introduction of SCR has come with a corresponding engine efficiency improvement and fuel economy benefit of 3-5% in typical applications. It should be noted however that the use of DEF, which costs nearly the same per gallon as diesel fuel, is used at the rate of 2-5% of fuel consumption negating any operating cost benefit for trucking companies [13].

1.2.3 Fuel Economy Standards

The EPA and the Department of Transportation's National Highway Traffic Safety Administration (NHTSA) recently proposed fuel economy regulations for medium and heavy

duty trucks in 2011. These regulations are the first of their kind and are aggressive in their targets. Regulations are to be phased in with increased stringency each model year from 2014 to 2018. By 2017 the proposed regulation will be technology forcing, requiring advanced drivetrains and/or waste heat recovery technology. As proposed, these standards would achieve from seven to 20 percent reduction in emissions and fuel consumption over 2010 baselines.

Table 1.2 shows the proposed carbon emission and fuel consumption standards [15].

Table 1.2 EPA and NHTSA Proposed Model Year 2017 Combination Trailer Standards

Proposed MY 2017 Combination Tractor Standards						
	EPA Emissions Standards			NHTSA Fuel Consumption Standards		
	(g CO₂/ton-mile)			(gallons/1,000 ton-mile)		
	Low Roof	Mid Roof	High Roof	Low Roof	Mid Roof	High Roof
Day Cab Class 7	103	103	116	10.1	10.1	11.4
Day Cab Class 8	78	78	86	7.7	7.7	8.5
Sleeper Cab Class 8	64	69	71	6.3	6.8	7

1.3 The Motivation to Reduce Engine Friction

Mechanical friction in a diesel engine is defined as the energy lost from two surfaces moving relative to each other and the movement of lubrication fluids in the engine. It is responsible for 10-15% of the engines indicated mean effective pressure (IMEP) – a measure which is the engine’s power normalized to engine displacement. This amounts to approximately 1 million barrels of oil/day lost to friction in the transportation sector in the United States alone [16].

There are many benefits to reducing engine friction. A reduction in engine friction directly increases the engine’s brake thermal efficiency (BTE) and delivers more mechanical energy to the vehicle. Improvements in BTE reduce engine fuel consumption, reducing levels of criteria pollutants such as PM, NO_x, HC, and also greenhouse gas emissions of CO₂, CO, and methane, which has a significant environmental benefit.

There are also significant economic benefits to reducing engine friction in large trucks. The trucking industry is extremely competitive and operates on very slim profit margins, with an

average operating ratio of 97% - that is for every dollar in revenue there is 97 cents associated in operating costs. This includes fuel, repair and maintenance, insurance, tires, permits, tolls, driver's wages, and benefits [17]. Trucking companies that operate fleets spend up to 30% of their operating expenses on fuel [18]. With the steadily increasing price of diesel fuel as shown in Figure 1.3, even small improvements in fuel economy result in significant savings for heavy duty trucks that operate an average of 44,581 miles per year [7]. Over the lifetime of the vehicle this can result in thousands of gallons of fuel saved, a corresponding reduction in GHG emissions, and can save large trucking companies thousands of dollars in fuel expenses every year.



Figure 1.3 Weekly U.S. No 2 Diesel Retail Prices 1995-2012 [19]

Looking at the United States vehicle mix, heavy-duty (HD) trucks represent approximately 4% of the overall vehicle fleet. While they represent only a small fraction of all vehicles they are responsible for 21.4% of all transportation fuel consumption in 2009 as shown in Figure 1.4 [7]. Friction reduction technologies implemented into the heavy duty market can have a significant effect on total fuel consumption. High turnover rates in the HD fleet, due to high annual utilization and miles, ensure that technologies which improve emission and fuel consumption characteristics are quickly implemented into the majority of the fleet.

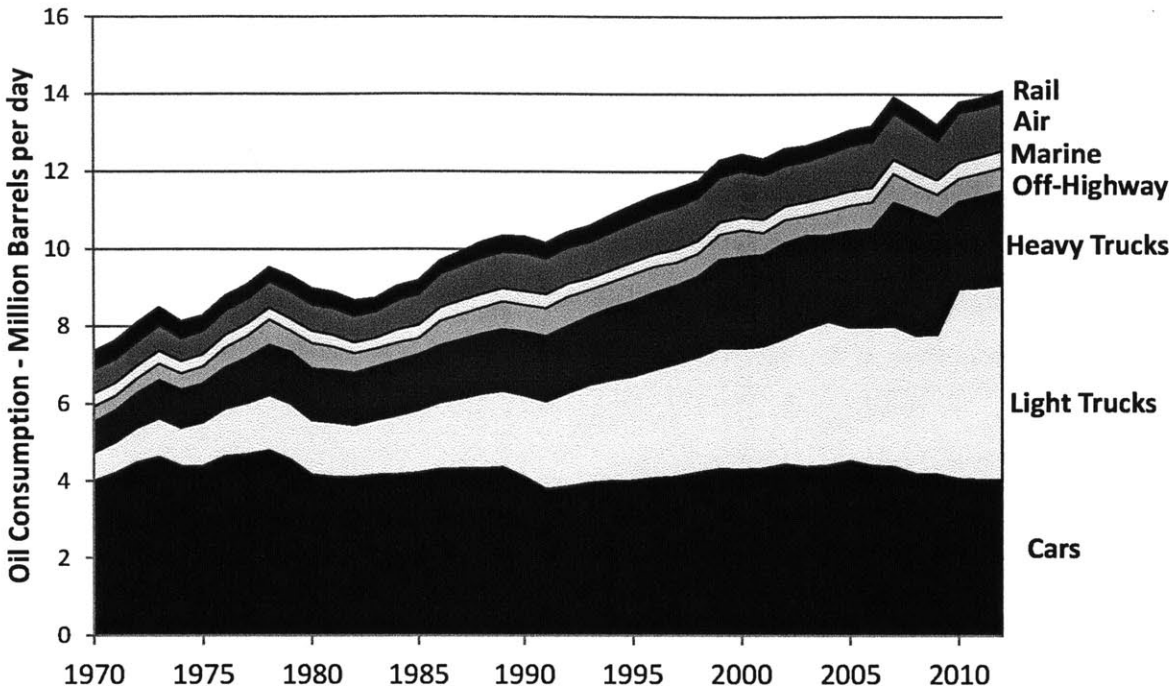


Figure 1.4 United States Petroleum Consumption in the Transportation Sector [7]

1.4 Sources of Friction in Diesel Engines

The energy lost to friction in an internal combustion engine is the difference between the indicated work done by the expansion of combustion gasses in the cylinder and the net or brake power extracted from the engine. Normalizing these results to the engine displacement and rotational speed we can calculate the friction mean effective pressure (*f_{mep}*) shown in equation (1.1):

$$f_{mep} = imep - bmep \quad (1.1)$$

Friction forces inside internal combustion engines arise from the hydrodynamic stresses in lubrication films and metal-to-metal contact. In addition to reducing engine efficiency and power output, friction generates wear in an engine which leads to reduced engine reliability and eventually component failure. In a heavy duty class 8 diesel engine friction losses come from a wide variety of sources including mechanical friction, pumping work, and auxiliary system losses.

Mechanical friction is the friction between internal parts in the engine block. Interactions between the crankshaft, connecting rods, piston, rings, cylinder liner, camshaft, geartrain, and valvetrain generate friction and waste heat which is removed by the engine lubricant and cooling system. The pumping work is the energy lost from moving air into and out of the engine during the intake and exhaust strokes. Auxiliary loads are those placed on the engine from equipment such as the oil pump, water pump, air compressor, vehicle fan, fuel pumps, and alternator. The focus in the current study is mechanical friction and auxiliary loads.

1.4.1 Overview of Major Engine Systems

A modern internal combustion engine is composed of thousands of individual components. When studying the friction performance of an entire engine it becomes necessary to group components together based on function and lubrication regime. These basic component groups are the crankshaft assembly, the power cylinder, the valvetrain, and auxiliary systems.

Crankshaft Group

The crankshaft is the component of the engine responsible for translating the reciprocating motion of the pistons into rotary motion to be delivered to the vehicle wheels. The crankshaft of a heavy-duty diesel engine is forged and has precision machined bearing surfaces. It is also carefully balanced to minimize engine vibration and excess wear. The crankshaft is supported by journal bearings at each end and between each connecting rod and piston assembly. Lubrication is delivered directly into the main bearings by the oil pump to support the large dynamic loads imposed upon it by the motion of the pistons. The crankshaft also has oil seals on each end of the assembly to prevent oil from leaving the engine block.

Power Cylinder

The power cylinder assembly is composed of the cylinder liner, piston, piston rings, connecting rod, and bearings. The piston moves up and down the cylinder liner generating the intake, compression, expansion, and exhaust strokes. The connecting rod is attached to the piston pin and the crankshaft on journal bearings allowing it to transfer the forces from the piston to the crankshaft. The ring pack is typically composed of three rings held in grooves in the piston. They

serve the primary purpose of sealing between the piston and the cylinder liner to prevent the escape or “blow by” of combustion gasses past the piston which would reduce engine power and efficiency. The piston rings also control oil transport up the cylinder liner to minimize oil consumption, in addition to helping to remove heat from the piston into the cylinder liner.

Valvetrain

The valvetrain component group includes the cylinder head, intake and exhaust valves, and the actuation mechanism which controls the movement and timing of the valves. For a typical heavy-duty diesel engine this component group would include the camshafts, intake and exhaust poppet valves, rocker arms, valve springs, and cam followers. The camshaft is a rotating component that actuates the valves through the use of a cam, one for each valve it controls. The profile of the cam and orientation dictates the valve opening crank angle, closing crank angle, duration and valve lift. It is precisely connected to the engine crankshaft to control the engines operation. The camshaft is supported by lubricated journal bearings.

In HD diesel engines the camshafts and other equipment are connected to the crankshaft through gears in lieu of a chain or belt as seen in smaller internal combustion (IC) engines. This component group is commonly referred to as the geartrain. In friction studies the geartrain is generally considered part of the valvetrain, because a large component of the geartrain is the cam gears.

Auxiliary systems

Class 8 trucks have much greater auxiliary system demands than a typical light duty vehicle. The water pump is responsible for the circulation of coolant throughout the engine block and a variety of other coolers including EGR, fuel, oil, air compressor, and the DEF tank to the radiator for removal of waste heat. The cooling system must remove approximately 30% of the chemical energy input into the engine, which requires high water pump flow rates and large radiators which contribute significantly to overall mechanical losses. The oil pump is another critical engine component that provides lubrication to all moving components in the engine block. Pumping the large volume of lubricant at high pressure through small orifices and jets accounts for a significant fraction of overall engine losses.

Additional auxiliary losses come from the air compressor, used to power air brake and suspension systems used in these large vehicles. The alternator, AC compressor, power steering pump, mechanical fuel pumps, and vehicle cooling fan can also be considered auxiliary losses on the engine. Generally however, engine designers only consider the systems necessary for engine operation, namely the oil and water pumps for a diesel engine.

1.4.2 Quantifying Friction Losses

Quantifying overall friction losses in an engine is a fairly simple measurement that can be performed on a dynamometer. It can be measured through fmep using Equation (1.1) which requires brake power output of the engine and cylinder pressure instrumentation. In this method the imep must be calculated from the cylinder pressure data and integrated using Equation (1.2), where P is the cylinder pressure, V_d is the engine displacement, V is the cylinder volume. This is integrated over one engine cycle to determine the imep. The bmep is calculated with Equation (1.3), where W_b is the brake power, N is the engine speed in RPM, V_d is the engine displacement, and 2 is the number of revolutions per cycle.

$$imep = \int_0^{720} \left(\frac{P}{2V_d} \right) dV \quad (1.2)$$

$$bmep = \left(\frac{2\dot{W}_b}{V_d N} \right) \quad (1.3)$$

It is also possible to use brake specific fuel consumption to measure changes in friction if component redesign or lubricant effects are studied. However small changes in friction are difficult to quantify without a well-controlled experimental set up and extensive statistical analysis.

Quantifying losses associated with each component or component group is much more difficult for several reasons. First the power dissipated by friction is much less than the power output of the engine, and requires accurate instrumentation and a calibrated test cell. Second is determining how much of overall friction can be contributed to individual components. Researchers have developed several ways to measure specific component contributions. Motoring friction teardown tests, firing and motoring tests, direct measurement through floating

liner engines, and component instrumentation have been used experimentally. Modeling and simulation have also proven to be a valuable resource in engine friction studies.

The easiest method to measure component friction is a motoring teardown test. In this experiment the engine is driven with a motoring dynamometer and the torque required to maintain a given speed is recorded. Components from the engine are then removed in sequence to determine the change in motoring torque which can then be converted into a fmep measurement. There are several disadvantages to this method: the engine does not experience the high cylinder pressures and temperatures from combustion, in addition, as components are removed the loading (and hence friction) is reduced which can result in misleading results. Researchers and engineers have tried to overcome these shortcomings several ways, first being a pressurized motoring test where pressurized air is used to simulate the high cylinder pressures the engine experiences during combustion. Another drawback to a motored test is that components are not up to operating temperatures, increased lubricant viscosity and reduced clearances at lower motoring temperatures lead to higher friction measurements than those in a firing engine. Researchers have tried firing an engine and then motoring to ensure all internal components and fluids are up to operating temperature.

Direct measurement of friction in the power cylinder is of particular interest due to the high contribution to overall friction. Floating bore engines elastically mount the cylinder liner and use strain gauges to directly measure the friction forces the piston and ring pack exert on the cylinder liner during operation. Other techniques have been developed that include using strain gauges on connecting rods and direct measurement on the flywheel of the engine.

Simulation and modeling has proven a valuable tool in quantifying component contributions to overall engine friction. The range of modeling includes detailed analysis of one or two components. For example, the top ring in the piston ring pack to system wide models that use basic engine parameters to predict fmep.

1.4.3 Typical Friction Distribution in a HD Diesel Engine

The distribution of total energy in a firing engine is shown in Figure 1.5. Frictional contributions from individual engine components have been studied extensively in industry and in research. Tribology theories in conjunction with specialized laboratory test rigs, motored and fired engine tests have given us a clear picture of the distribution of mechanical friction losses for a typical diesel engine, as shown below.

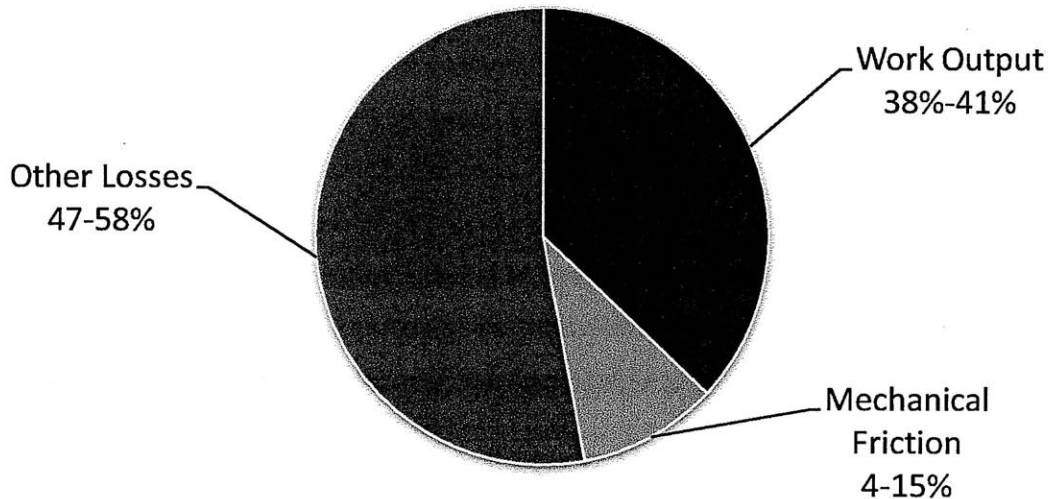


Figure 1.5 Distribution of Total Energy in a Fired Engine [20]

As mentioned in Section 1.4.1, studies of the mechanical friction breakdown typically separate engine components into the following major subgroups the power cylinder, the crankshaft group, auxiliary components, and the valvetrain. Figure 1.6 shows an approximate distribution of the mechanical losses by component group in a typical diesel engine.

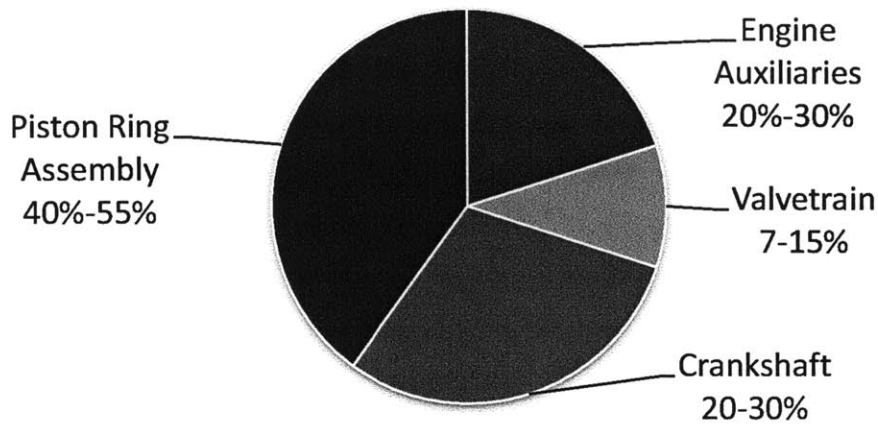


Figure 1.6 Distribution of Total Mechanical Losses of a Diesel Engine [20]

The majority of the mechanical friction is attributed to the power cylinder assembly, which is responsible for between 40-55% of the total friction in a fired engine. This large contribution has made the power cylinder a primary focus in research and modeling efforts to better understand the tribological interfaces and physical phenomenon that occur.

Reported component friction contributions in the power cylinder assembly vary greatly. Figure 1.8 details the breakdown on friction in the power cylinder assembly between the piston (25-47%), piston rings (28-45%), and the connecting rods (18-33%). The ring pack friction breakdown is shown in Figure 1.8. The largest contribution to ring pack friction is the oil control ring (OCR) which contributes 50-75% of the total ring pack friction or between 5.6% and 18.6% of total engine mechanical friction. Previous studies and research has focused on optimizing the OCR profile and tension to balance friction performance with engine oil consumption [21] [22]. The wide range of reported component friction contributions, especially in the power cylinder, highlights the need for individual analysis of each engine design and operating conditions to optimize the friction performance of the engine.

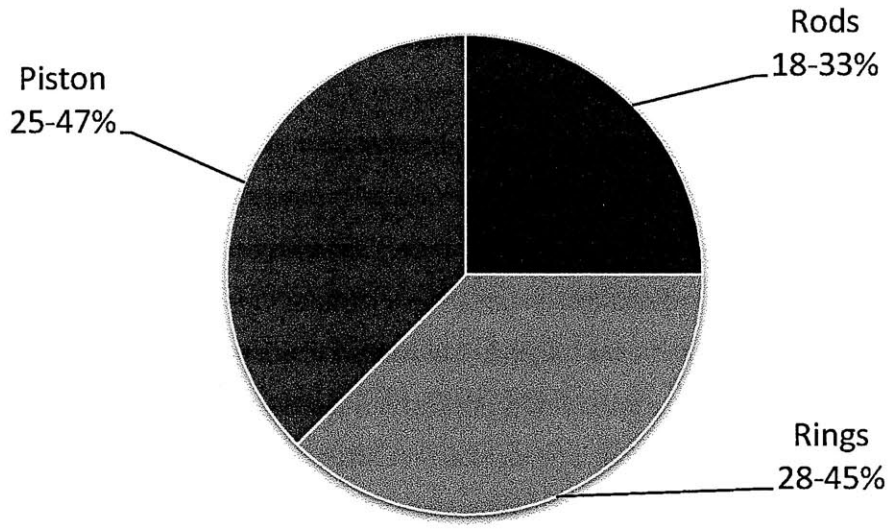


Figure 1.7 Typical Distribution of Power Loss in the Power Cylinder [20]

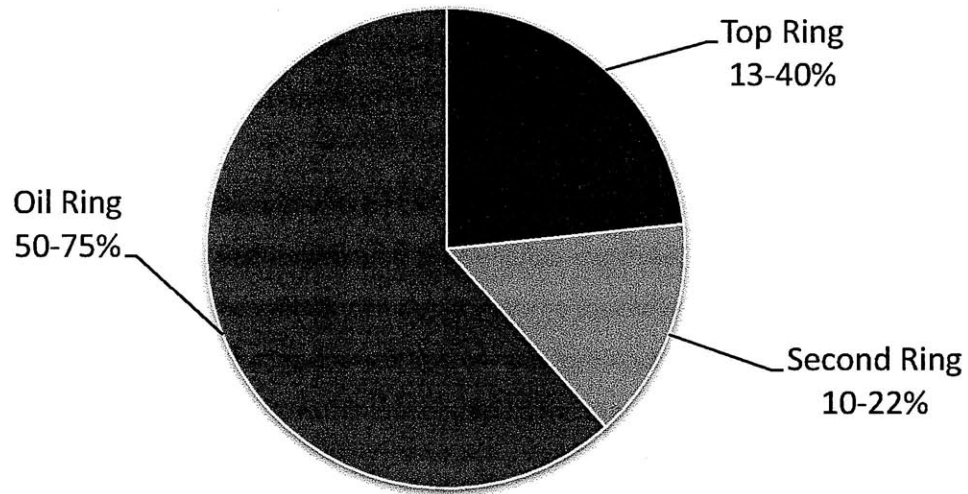


Figure 1.8 Typical Distribution of Piston Ring Friction [20]

The crankshaft group of a diesel engine is responsible for 20-30% of the total friction. The primary source of losses is the main bearings that support the crankshaft. The other sources of friction in this component group are the main oil seals.

Auxiliary component frictional losses account for 20-30% of engine mechanical friction. Heavy-duty diesel engines have significantly higher auxiliary losses than smaller SI engines due to greater vehicle demands in HD trucks. Additions of DPFs and SCR to the engine emissions system have placed increased thermal demands on engine cooling systems. Increased vehicle electronics and engine management systems have increased electrical loads. While not typically considered in engine friction tests, radiator fan loads have a dramatic effect on HD vehicle fuel efficiency.

This aggregate survey can be summarized schematically as shown in Figure 1.9.

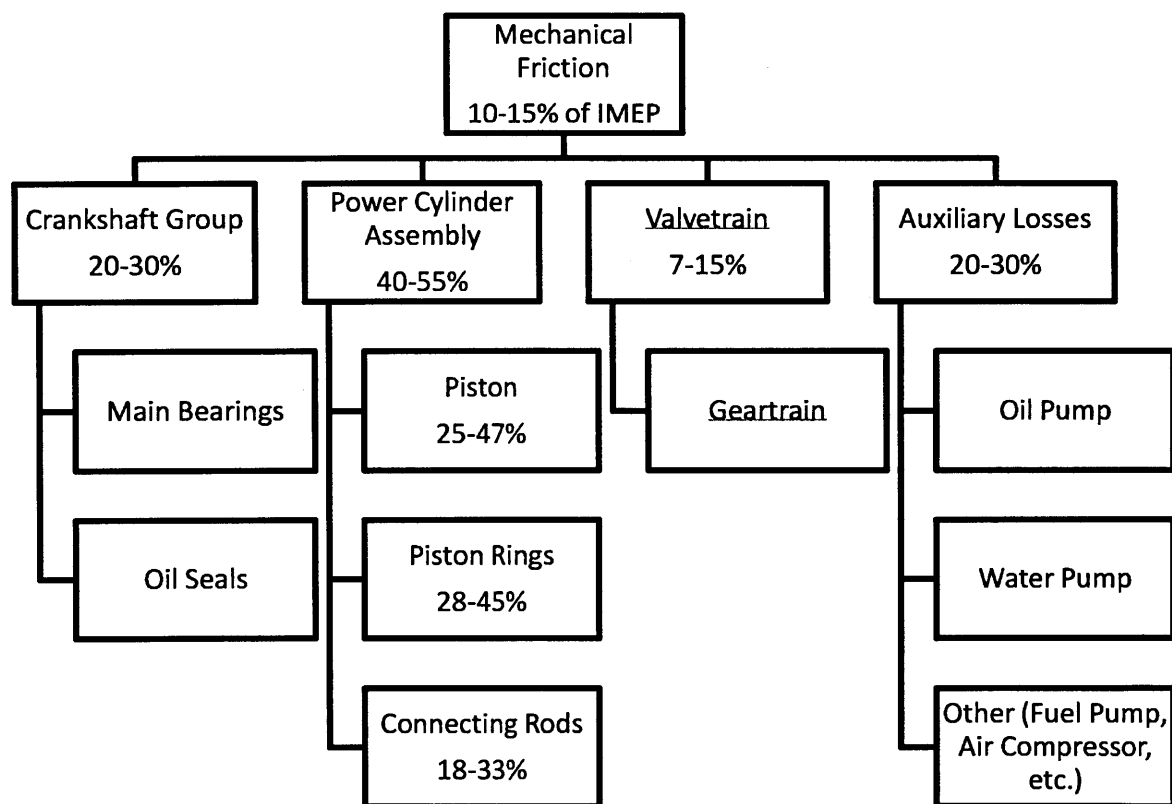


Figure 1.9 Flowchart of Friction Contributions by Component Group

The final component group is the valvetrain which is responsible for 7-15% of the total friction in the engine. The lower operating speeds found in HD diesel engines greatly reduce the mechanical friction in the valvetrain when compared to SI counterparts.

1.5 Scope of Current Work

The purpose of this work was to analyze frictional losses within a representative class 8 truck diesel engine in support of the DOE Super Truck Program. The DOE program has a goal of improving overall class 8 truck freight efficiency (measured in ton-miles per gallon) by 50%. Daimler Trucks North America enlisted MIT to demonstrate low engine friction technologies on a representative class 8 tractor truck diesel engine. The project involves an ambitious goal of a 40% reduction in the mechanical losses of the engine. The improvement targeted in this project centers on resolving the adverse effects on engine wear, durability, emissions, and oil consumption that often accompany traditional low-friction concepts such as reducing oil viscosity or contact stresses. Principal areas under investigation in this project are low-friction lubricants and additives, advanced material selection and surface modification, component mechanical design, and engine lubrication system design.

In order to accomplish the goal of the sub-program, a detailed analysis of the sources of friction within a heavy-duty diesel engine was undertaken. Empirical data on engine friction and component wear was collected from industry and from similar studies in the literature. An extensive review of analytic friction models in literature was assembled and evaluated. Potential gains from changes in lubricant viscosity were analyzed.

Additionally, this work includes analysis performed on the use of thermal barrier coatings (TBC) and their use to strategically increase cylinder liner temperatures in order to reduce power cylinder friction. By coating selected parts of the liner the local temperature is raised and lubricant viscosity decreased in that region. By coating the liner in selected regions only, top dead center temperatures are mostly unaffected thereby minimizing any increase in cylinder liner wear. Additional fuel economy benefits from the TBC were investigated from increased exhaust gas enthalpy and reduced liner heat rejection. This approach is expected to maximize friction reduction while minimizing risk to other engine components or increasing component wear rates.

2 Friction Analysis

2.1 Lubrication Regimes in an Engine

Motor oil is pumped through an engine to provide the necessary lubrication to critical components such as journal bearings, the valvetrain, and the cylinder liner. To investigate the friction losses within an engine the three modes of lubrication must be understood, namely hydrodynamic, boundary, and mixed.

The lubrication regime is determined by the thickness of the fluid film separating the two surfaces in contact. In hydrodynamic lubrication the two surfaces are supported and separated from each other by the lubricant film. There is no direct contact between the two surfaces in motion. In boundary lubrication there is constant contact between the high surface points or asperities despite the presence of a lubrication film. Mixed lubrication is the transition between hydrodynamic and boundary lubrication where the surfaces are supported both by asperity contact and by the lubricant film. The three regimes are shown graphically in Figure 2.1 on the scale of the surface asperities.

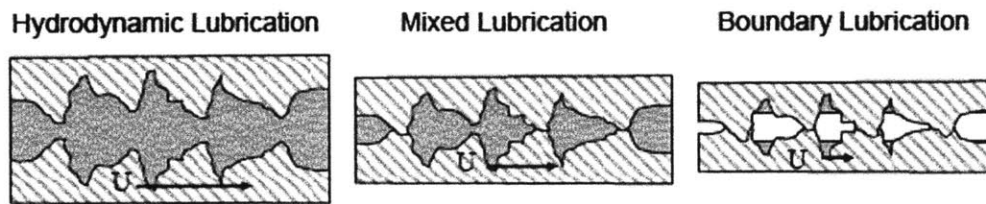


Figure 2.1 Regimes of Lubrication Shown on the Scale of Surface Asperities [23]

The relationship and transition between the three lubrication regimes can be shown graphically through a Stribeck curve, shown in Figure 2.2. The Stribeck curve plots the coefficient of friction between the sliding surfaces as a function of lubricant viscosity, surface speed, and load, and is known as the duty parameter. Looking at Figure 2.2 we can see that a low duty parameter which can be a combination of low lubricant viscosity and/or low surface speeds in conjunction with high load produces boundary lubrication with a high friction coefficient. Increasing surface speed and viscosity or reducing the load, a lubricant film begins to form and the interface is experiencing mixed lubrication, and in this regime a minimum friction coefficient is achieved. By further increasing speed and viscosity, or reducing load, the interface is fully supported by a

lubricant film and is in hydrodynamic lubrication. Friction is generally low but as the duty parameter increases the friction increases due to fluid drag in the lubricant film.

It is worth noting that the point of minimum friction lies within the mixed lubrication regime. Here is the ideal tradeoff between hydrodynamic lubrication and asperity contact. This however will produce greater wear than full hydrodynamic lubrication and must be carefully considered for each engine component.

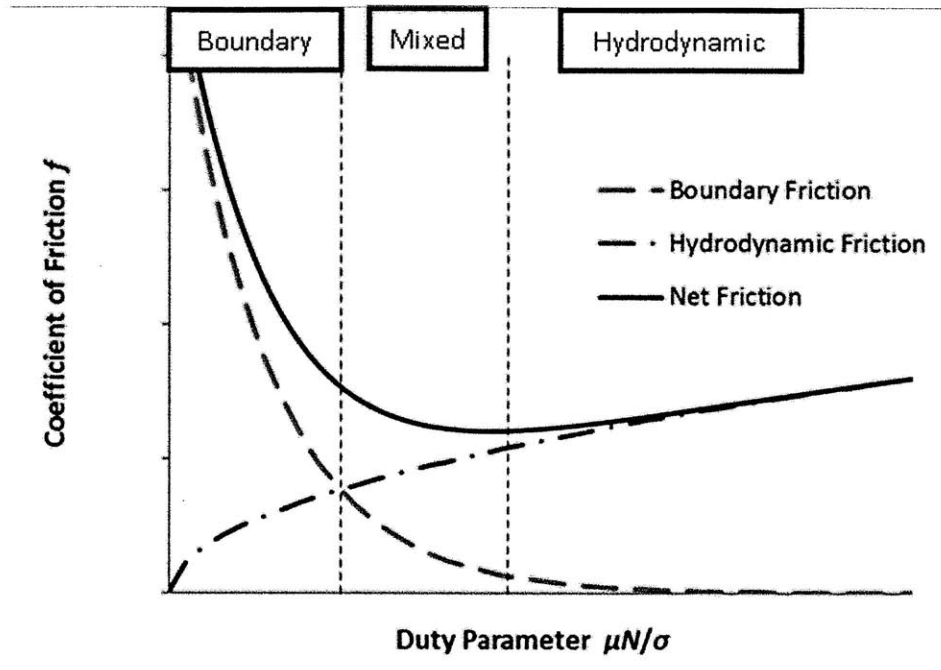


Figure 2.2 Stribeck Curve

Within an engine, components are subject to all three lubrication regimes throughout normal operation. In general engine journal bearings operate within the hydrodynamic lubrication regime as their loads are supported by maintaining a fluid film between surfaces. Journal bearings may operate under the mixed regime under extreme conditions, heavy loading, or initial engine start up. This would include the main bearings of the crankshaft, big end connecting rod bearings, the piston pin, and camshaft bearings. The engine valvetrain primarily operates in the boundary and mixed lubrication regime although some components such as valve guides operate in the hydrodynamic regime.

The piston rings and liner span the spectrum of lubrication, encountering locations or periods of boundary, mixed and hydrodynamic lubrication due to the reciprocating nature of piston motion. The piston skirt undergoes mixed and hydrodynamic lubrication. This relationship becomes very important in the power cylinder assembly where boundary or mixed lubrication at the top dead center (TDC) and bottom dead center (BDC) regions (low surface speeds) leads to wear and eventual failure of the liner and rings. However the majority of power cylinder work losses come from the high surface speeds and hydrodynamic motion in the piston mid-stroke.

2.2 Lubricant properties

A class 8 tractor trailer diesel engine requires approximately 45-55 liters of lubricant for normal engine function. Characteristics and properties of the lubricant used in are vitally important to engine function, emissions performance, reliability, and longevity. In an internal combustion engine the lubricant performs several functions listed below:

1. Lubrication – By maintaining a fluid film between moving parts the lubricant reduces metal-to-metal contact (friction). This reduces the force necessary to sustain the motion while reducing wear and premature failure of engine parts.
2. Cooling – Engine oil is used to cool critical engine components such as the piston during operation. It provides cooling to components that would not be accessible by the coolant circulated through the block and heads. It removes heat from these parts and into the cooling system through the external oil cooler.
3. Corrosion Protection – The lubricant film on the internal surfaces of the engine prevents the formation of oxidation and corrosion. Special additives in the lubricant form films on components to act as anti-wear coatings and for additional corrosion protection.
4. Suspension and Removal – Engine oils contain special detergents and dispersants which keep harmful combustion products, contaminants, and wear particles in suspension. Sources of contamination include particles entering the engine through the intake air, from metallic particles that result from surface wear during operation, and combustion by-products such as carbon. Detergents and dispersants prevent the contamination particles from being deposited on metal surfaces in the engine which can lead to wear. Contaminants are then removed by filtration or periodic replacement of the lubricant.

2.2.1 Lubricant Additives

Engine lubricants perform in a harsh environment that is subject to contamination from combustion, the open environment, and is highly corrosive. Specialized additives are used to optimize the lubricant to function in this environment. A common diesel engine lubricant will be composed of 75-83% organic base oil, 5-8% viscosity modifier, and 12-18% inorganic additive package [24]. The specialized additive package contains compounds with specific functions, namely detergents and dispersants, oxidation inhibitors, rust and corrosion inhibitors, friction modifiers, anti-wear agents, foam inhibitors, viscosity modifiers, pour point depressants, in addition to anti-seize and anti-scuffing additives. The estimated additive use in all lubricants is shown below in Figure 2.3.

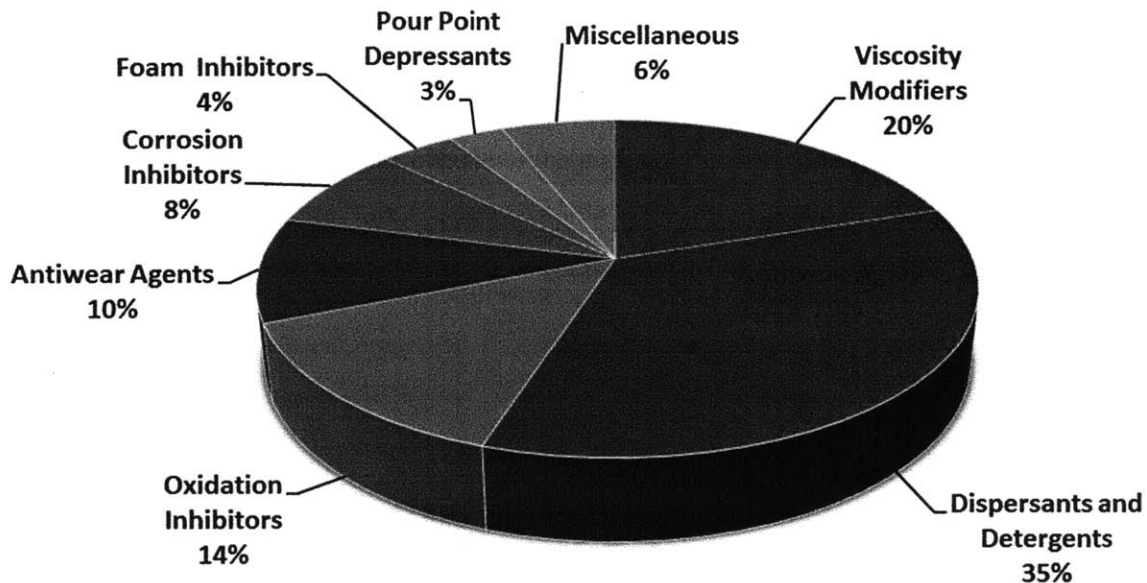


Figure 2.3 Estimated Additive use for 2006 by additive type, North America

- Detergents neutralize acids that are natural by-products of combustion and lubricant oxidation to minimize deposition on engine parts. They also serve to keep those acidic compounds suspended in the lubricant.
- Dispersants additives are used in the oil to keep detrimental compounds and particles in suspension to prevent deposit onto engine components and allow removal through the oil filter or replacement of the lubricant.

- Oxidation inhibitors are included in lubricants to limit oxidation of the lubricant.
- Rust and corrosion inhibitors form protective films or barriers on metal surfaces which prevent reaction with water, acids, and oxygen.
- Friction modifiers also form films on surfaces in the engine but with the purpose of creating a low friction surface. These additives reduce wear at low temperatures and improve fuel efficiency.
- Anti-wear, anti-seize, and anti-scuffing additives form durable films on metal surfaces which can withstand high contact pressures, temperatures, and loads.
- Foam inhibitors reduce the surface tension in foam bubbles that form from agitation and aeration of the engine oil as it is transported through the engine. Foam is detrimental because it can reduce lubricant pumping efficiency and heat transfer properties.
- Viscosity modifiers alter the lubricant temperature dependence curve; generally they work to maintain lubricant viscosity at high temperatures to ensure engine protection.
- Pour point depressants prevent separation of the oil at low temperatures.

2.2.2 Viscosity Temperature Relationship

An important characteristic of an engine lubricant is the viscosity temperature dependence. They are related through an inverse relationship i.e. as temperature increases viscosity decreases. It is advantageous to use lubricants with more stable viscosity profiles over the range of operating temperatures. The most common measurement of the viscosity temperature relationship is the viscosity index (VI). VI is an arbitrary scale from 0 to 100 based on the kinematic viscosity of the test lubricant at 40°C and 100°C with respect to two reference lubricants with VI of 0 and 100. A high VI number implies a low sensitivity to temperature while a low VI implies a high sensitivity to temperature. The formula for calculating the VI is shown below in Equation (2.1), where L is the 40°C viscosity of the 0 VI oil, U is the kinematic viscosity of the oil under study at 40°C and H is the 40°C viscosity of the 100 VI oil. The values of L and H are found from reference tables provided by ASTM [25].

$$VI = \frac{L - U}{L - H} \times 100 \quad (2.1)$$

Viscosity temperature dependence is important for components that are near combustion gasses in the engine. High combustion temperatures can generate high lubricant temperatures and low viscosity. Low lubricant viscosity leads to smaller film thicknesses which can cause a shift from hydrodynamic or mixed lubrication regime into boundary contract, where there is high friction and high wear. This relationship is of particular importance in the power cylinder, where high lubricant temperatures and limited lubricant supply at the top dead center (TDC) lead to boundary lubrication and high wear. In HD engine durability tests, the top ring reversal zone at TDC is often the failure point in the power cylinder assembly.

To calculate the viscosity of a given lubricant at any temperature the Vogel equation (2.2) may be used for straight weight oils. The parameters k , θ_1 , and θ_2 are constants determined for each lubricant with units of cSt for k and °C for θ_1 and θ_2 . T is the temperature of the lubricant in °C, and v is the kinematic viscosity at the desired temperature in cSt.

$$v = k \cdot \exp\left(\frac{\theta_1}{\theta_2 + T}\right) \quad (2.2)$$

2.2.3 Viscosity and Shear Rate Relationship

In nearly all class 8 diesel engines multi-weight oil is used as the lubricant. A multi-weight lubricant includes viscosity modifiers, mentioned in Section 2.2.1, to improve overall lubricant performance over the wide range of operating and ambient temperatures seen for an IC engine. This causes the oil to have non-Newtonian properties in that its viscosity is dependent on shear rate. Lubricants then display shear thinning where viscosity is reduced when subjected to high shear rates. The Cross equation shown below (2.3) is used to determine viscosity for multi-weight oils. In the equation v_0 is found from the Vogel equation, v_∞ is the high shear viscosity, γ is the lubricant shear rate, β is the critical shear rate, m , c_1 , c_2 are addition parameters specified for each lubricant.

$$v = v_0 \frac{1 + \frac{v_\infty}{v_0} \left(\frac{\gamma}{\beta}\right)^m}{1 + \left(\frac{\gamma}{\beta}\right)^m} \quad \beta = 10^{c_1 + c_2 T} \quad (2.3)$$

This relationship becomes important if the shear rates experienced by the lubricant film are close to the critical shear values. Figure 2.4 shows the Cross equation applied to generic 15W-40 engine oil, which is a common viscosity grade used in HD diesel engines, however the ratio of high to low shear was changed from 0.79 to 0.5 for illustration purposes.

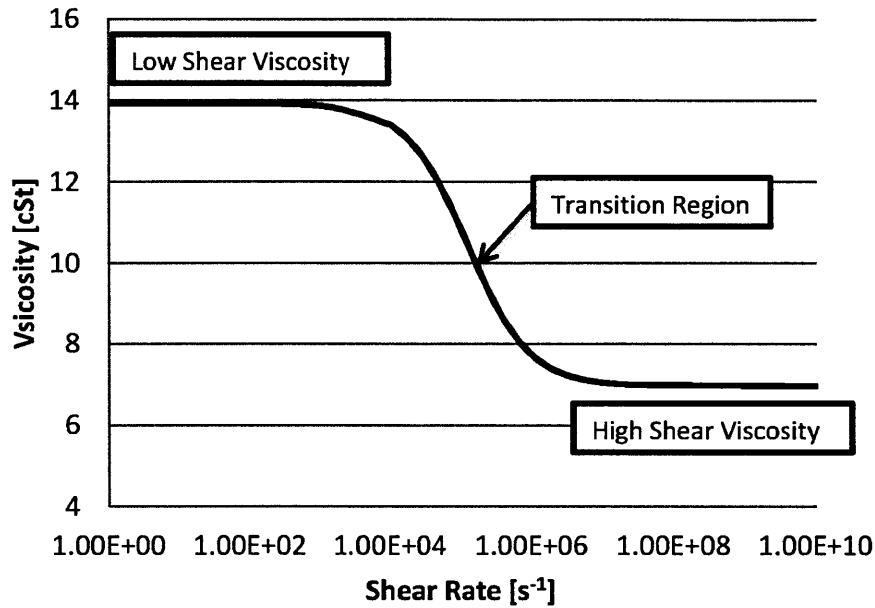


Figure 2.4 Cross Equation Lubricant Viscosity Shear Rate Dependence

2.3 Wear

Many friction reduction strategies employ reduced viscosity lubricants to lower mechanical friction in the engine to improve vehicle fuel economy. While this method can improve vehicle fuel economy it increases boundary lubrication within the engine leading to higher component wear rates. To successfully employ a reduced viscosity strategy, component wear, and the mechanisms of wear must be understood and analyzed. This is particularly true in the HD truck market, where engines are advertised for their durability and B50 lives of 1 million miles or more.

Adhesive wear is the wear that occurs when surface asperities come into contact, raising local temperatures to those that can cause the metals to weld together. This occurs when the lubricant film thickness is less than the combined depth of the surface asperities. As the asperity welds are

then broken by surface motion, the friction force increases and material is transferred from one surface to the next leaving rough edges. Reducing viscosity will reduce oil film thickness and can lead to an increase in adhesive wear, which can shorten the useful life of the engine.

Abrasive wear occurs when a harder material is in contact with a softer material; it can be between two bodies in contact or can also occur if a hard particle is trapped between the two rubbing surfaces. In diesel engines particulate matter formed during combustion in the engine can create particles large enough to impact surfaces. This can create abrasion against moving surfaces in the power cylinder, potentially increasing the wear rate. The wear associated with soot abrasive wear could be described as the polishing of the surfaces, leaving a smooth shiny surface behind. This is particularly detrimental to the power cylinder assembly where the cylinder liner has a specific roughness and hone pattern to hold lubricant on the liner surface. The use of EGR also increases soot abrasive wear because PM that would normally go to the exhaust is redirected back into the cylinder. This increases absorption into the lubricant thereby increasing wear and lubricant degradation rate.

Corrosive wear occurs in the engine due the presence of moisture or acidic compounds that result from combustion interacting with ferrous metal in the engine block. As a surface oxidizes, the motion between components removes the oxidation allowing additional oxidation to form. Large oxide particles can also cause abrasive wear as they are carried away from the surface.

3 Modeling of Friction in Heavy Duty Class 8 Diesel Engines

Engineers working on HD diesel engines must balance the demands of power, durability, emissions performance, and fuel economy. In order to make critical design decisions, it is important to understand the sources of mechanical friction within the engine. Friction is a large unknown factor in engine design and directly influences main engine performance characteristics including brake horsepower and fuel consumption. Friction from major engine components such as the piston, rings, cylinder liner, valves, camshafts, crankshafts, journal bearings, in addition to the friction from auxiliary systems such as water, fuel, and oil pumps, air compressors, etc. must be calculated and components then modified for optimum performance.

The wide varieties of parts and components in an engine have many surfaces which interact with one another and generate mechanical friction. The wide variety of operating conditions within the engine, varying in temperature, surface speed, and lubricant supply, in addition to sliding and rotating surfaces makes estimating total frictional losses difficult. Engine operating speed, load, and ambient conditions can significantly alter the conditions within the engine, further complicating the analysis.

There has been significant work both in industry and in academic research on modeling the friction losses that occur within internal combustion engines. The approaches vary from empirical models based on engine friction and laboratory tests to detailed analytical models that attempt to capture the complicated nature of the component(s) being studied. Previous research has been focused on small SI engines for the automotive and light truck market so models must be modified to the duty cycle and conditions of HD diesel engines.

An extensive literature review of existing engine friction models was evaluated. Models generally fell into one of several categories. First is empirical models based off experimental data and basic engine geometry and performance characteristics. Detailed models for the entire engine that have been developed based on simplifying assumptions and equations. Finally, detailed models of particular components or components or component groups such as big end connecting rod bearings or a model of ring pack friction. Each of these was examined and has been summarized in the following sections.

3.1 Numerical Friction Models

Detailed friction models use fundamental equations of lubrication to describe in detail the interactions between moving surfaces in an internal combustion engine. From this analysis an understanding of the critical parameters and their influence on engine friction can be quantified. This data can then be used by design engineers to improve the friction performance of newly developed engines. Detailed models have been developed for specific components, such as the piston rings, piston skirt, main and connecting rod bearings, camshaft, etc. and also for component groups such as the crankshaft, power cylinder, and valvetrain. These models can require significant computational resources and may be difficult to integrate with existing modeling software used to simulate thermodynamic conditions, engine controls, and other dynamic processes within the engine.

3.1.1 Crankshaft Numerical Friction Models

Friction is present in the journal bearings and oil seals of the crankshaft group. The journal bearing friction is dependent primarily on the dynamic motion of the engine, the mass, acceleration, loading and inertia of the rotating and reciprocating components of the engine. This loading changes dramatically in magnitude and direction throughout the engine cycle. The friction in the main bearings is mostly hydrodynamic and the lubricant is supplied to the bearing under pressure from the oil pump.

Loading on the journal bearings must be determined from the cylinder pressure and corresponding force applied to the piston, the inertia force present from the reciprocal motion of the piston assembly, in addition to the trust force from the piston skirt and liner interface. This allows direct calculation of the forces present in the connecting rod bearing. To calculate the resultant force in the crankshaft and main bearings requires simplifying assumptions because the crankshaft is a statically indeterminate structure. Generally it is assumed that the crankshaft is sufficiently rigid that reaction forces are only present on the two bearings situated between the connecting rod.

A variety of approaches have been developed to determine the friction losses in a dynamically loaded journal bearing. There are commercially available models using finite element methods and complex models for detailed bearing design. The majority of numerical friction models

surveyed used the Reynolds equation, shown below, to model the distribution of oil pressure in the bearing. In this equation h is the oil film thickness, P is the lubricant pressure, μ is lubricant viscosity, and U is the surface speed.

$$\frac{\partial}{\partial x} \left(h^3 \frac{\partial P}{\partial x} \right) + \frac{\partial}{\partial z} \left(h^3 \frac{\partial P}{\partial z} \right) = 6\mu U \frac{\partial h}{\partial x} \quad (3.1)$$

The Reynolds equation can be expressed as shown below in Equation (3.2) in polar coordinates for an isothermal dynamically loaded journal bearing as proposed by Booker [26] [27] [28] [29] [30].

$$\frac{\partial}{\partial \theta} \left[(1 + \varepsilon \cos \theta)^3 \frac{\partial P}{\partial \theta} \right] + R^2 \frac{\partial}{\partial z} \left[(1 + \varepsilon \cos \theta)^3 \frac{\partial P}{\partial z} \right] = 12\mu \left(\frac{R}{C} \right)^2 [\dot{\varepsilon} \cos \theta + \varepsilon(\dot{\phi} - \bar{\omega}) \sin \theta] \quad (3.2)$$

Where P is the fluid pressure, R is the bearing radius, ε is the journal eccentricity ratio (the ratio of distance between the center of journal from the center of bearing to radial clearance), ω is the rotational speed, ϕ is the attitude angle, and μ is the viscosity of the lubricant. Generally, engine journal bearings are narrow bearings with L/D ratios less than 0.5. Therefore the short bearing approximation developed by Ocvirk is used, where pressure, P_o , can be expressed as [31]:

$$P_o = -6\mu \left(\frac{L}{C} \right)^2 \left(\frac{1}{4} - \bar{z}^2 \right) \left(\frac{\dot{\varepsilon} \cos \theta + \varepsilon(\dot{\phi} - \bar{\omega}) \sin \theta}{H^3} \right) \quad (3.3)$$

Where H is the nondimensional film thickness, $1 + \varepsilon \cos \theta$, z is the nondimensional axial coordinate, and L is the length of the bearing. Use of the mobility method as developed by Booker allows the calculation of the minimum oil film thickness, location, and the location of the journal center in the bearing. In addition analytical methods of solution have been proposed by Hirani et al. [32] while graphical solutions have been obtains by Raimondi and Boyd [33]. Figure 3.1 shows a schematic of a journal bearing and resulting pressure distribution in the lubricant.

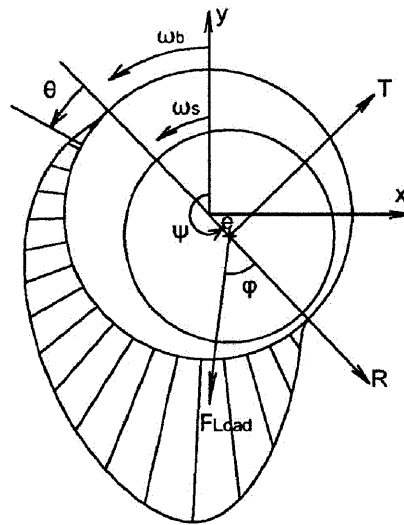


Figure 3.1 Lubricant Pressure Distribution in a Dynamically Loaded Journal Bearing

After the pressure distribution is calculated the equations of motion for the journal movement within the bearing can be calculated. From this the power losses over the engine cycle can be determined by integration as shown by Livanos [28]. This analysis is also used for other journal bearings in the engine, namely the connecting rod bearing, piston pin, and camshaft bearings [34].

3.1.2 Power Cylinder Numerical Friction Models

Power cylinder friction is the largest contribution to overall engine fmep and has been the focus of a wide array of research programs. One challenge to modeling the power cylinder is that the various components, the ring pack, the piston skirt, the connecting rod bearings, and the wrist pin all operate over a wide range of lubrication regimes over the spectrum of engine operation. Generally the connecting rod bearing and wrist pin operate in the hydrodynamic regime, but under high loading can be in mixed lubrication. The piston skirt operates in the mixed and the hydrodynamic lubrication regimes, and the friction contribution is heavily dependent on piston secondary motion and surface finishes. Finally the ring pack operates across the entire lubrication spectrum, from boundary to hydrodynamic. This changes over the engine cycle as the piston moves up and down the liner, but also as loading and engine speeds vary. Additionally, different models are required for each ring, as the top ring, second ring, and oil control ring are

each subjected to different forces and lubricant supply. The spectrum of operation for the power cylinder components is shown graphically in Figure 3.2.

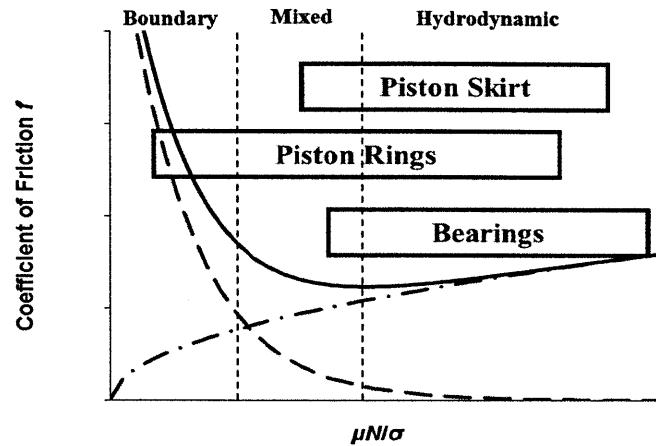


Figure 3.2 Stribeck Curve for Power Cylinder Components

Numerical models of the power cylinder have been created here at MIT and by numerous other researchers throughout the world. A review of the governing equations for each component in the power cylinder, the ring pack, the piston skirt, and the bearings follows below.

Piston Skirt Modeling

The piston skirt is generally modeled assuming hydrodynamic lubrication. Piston secondary motion is very important to the lubricant film properties around the piston skirt. In addition, the piston skirt and cylinder liner have normal asperities in addition to machining grooves or waviness which have a significant effect on oil film thickness and friction.

Piston secondary motion has a significant impact on the lubrication regime and friction losses associated with the piston skirt. Equations of piston primary motion, that is motion along the cylinder liner, are defined based on the crankshaft rotational speed and crank angle. The equations of secondary motion for the piston are developed considering the interaction of the piston with cylinder liner, the piston rings, wrist-pin, connecting rod, cylinder pressure, and inertia. Figure 3.3 shows these forces and moments schematically. They are solved about the wrist pin of the piston to develop a set of governing differential equations [35].

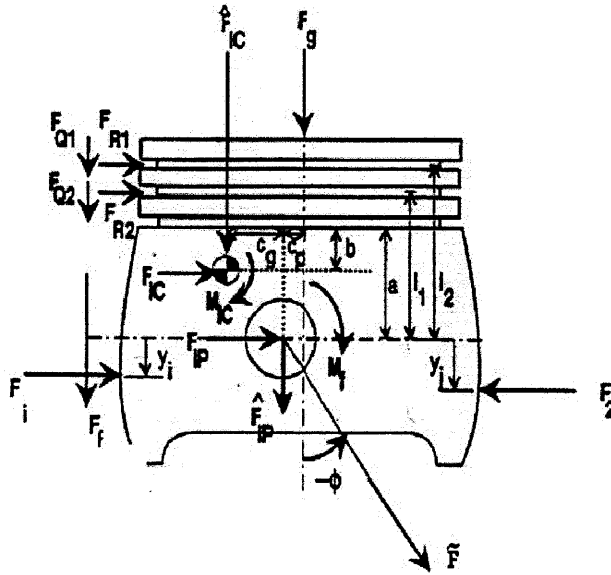


Figure 3.3 Forces and Moments Acting on the Piston [36]

Patir and Cheng developed a system of friction factors to account for the surface roughness and variation [37]. The modified unsteady Reynolds equation included constants which evaluate the piston surface stochastically to simulate the surface roughness present on the piston skirt surface and cylinder liner. Shown in Equation (3.4), Φ_x and Φ_y are pressure flow factors that adjust the oil film pressure based on the surface characteristics and Φ_s and Ω are shear flow factors that modify the shear stress in the oil film.

$$\frac{\partial}{\partial x} \left(\Phi_x h^3 \frac{\partial P_h}{\partial x} \right) + \frac{\partial}{\partial y} \left(\Phi_y h^3 \frac{\partial P_h}{\partial y} \right) = -6\mu U \left(\frac{\partial h}{\partial y} + \Omega \frac{\partial \Phi_s}{\partial y} \right) + 12\mu \frac{\partial h}{\partial t} \quad (3.4)$$

Wong et al. developed a detailed piston skirt lubrication model using the above formulation. This model includes predictions for partially-flooded skirts in mixed lubrication and in hydrodynamic lubrication. Piston skirt geometry, including waviness, roughness, and axial surface profile is included. In addition piston skirt compliance and thermal deformation was also included. These are important factors to consider as the deformation of the piston skirt under load is on the same order as the thickness of the lubrication film [35].

Equation (3.4) is used to determine the pressure distribution given a distribution of the clearance between the piston skirt and liner as function of space and time, $h(x,y,t)$. It is solved iteratively using a finite difference method. Boundary conditions are imposed to specify the pressure for

fully-flooded and partially flooded piston skirts. The model calculates the friction work losses, and the contributions of boundary and hydrodynamic friction to total piston skirt friction [35]. This model was updated by Moughon and Wong to include the effects of variable lubricant viscosity along the cylinder liner. These changes were used to perform a parametric study on the influence of piston skirt design parameters on piston skirt friction [36] [38] [39].

Ring Pack Modeling

The piston ring has been extensively studied and optimized as it generally accounts for 20-30% of overall mechanical friction in the engine. A typical ring pack is composed of three piston rings, the first the compression ring which is the primary seal against the combustion gasses and pressure. The second is the scraper ring whose function is to scrape oil down the liner and also to provide some sealing from combustion gasses. The final ring is the oil control ring (OCR) whose purpose is to distribute the lubricant evenly onto the liner to provide adequate oil supply to the entire liner surface. Each ring experiences different tribological conditions due to their position and function. The compression ring experiences boundary lubrication due to limited oil supply and exposure to high combustion temperatures. The second and oil control rings experience boundary, mixed, and hydrodynamic lubrication throughout the engine cycle.

One ring-pack model that has been used extensively in the automotive industry was developed at MIT by Tian, Wong, and Heywood [40]. The model is used to predict oil film thickness, friction, and oil transport in the piston ring and liner system. The model accounts for all lubrication regimes, shear thinning of multigrade viscosity oils, unsteady ring wetting conditions. Like the piston skirt model it uses the average flow model developed by Patir and Cheng in addition to Greenwood and Tripp's asperity contact model [37] [41]. A diagram of the ring pack and liner interface is shown in Figure 3.4.

The piston ring pack is modeled using the Reynolds equation with the average flow factors as shown below in Equation (3.5). U is the sliding velocity, h is the local fluid film thickness, μ is the lubricant viscosity, R_q is the combined RMS roughness of the liner and ring surface, and Φ_p , Φ_g and Φ_s are flow factors that adjust the oil film pressure based on the surface characteristics.

$$\frac{\partial}{\partial x} \left(\Phi_p \frac{h^3}{\mu} \frac{\partial P}{\partial x} \right) = 6U \frac{\partial}{\partial x} (h\Phi_g + R_q\Phi_s) + 12 \frac{\partial h}{\partial t} \quad (3.5)$$

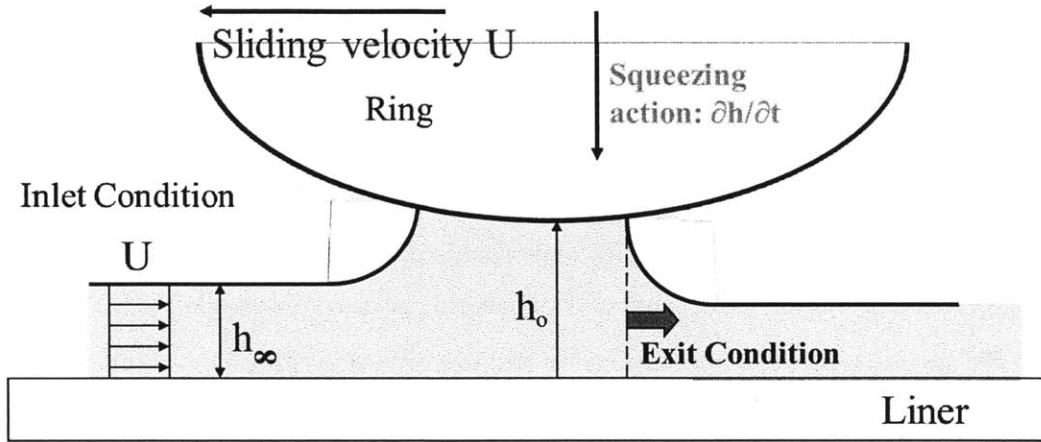


Figure 3.4 Model Layout for Each Piston Ring

The oil flow rate per unit width of the cross flow section can then be written as shown below in Equation (3.6).

$$q_x = -\Phi_p \frac{h^3}{12\mu} \frac{dP}{dx} + \frac{U}{2} (h\Phi_g + R_q\Phi_s) \quad (3.6)$$

Boundary conditions are required to solve the above equations. Oil inlet and exit conditions can vary from fully flooded to starved. The model tracks oil transport and updates the oil film thickness for each part of the cylinder liner throughout the engine cycle.

Calculation of the friction force involves the simultaneous solution of the forces imposed on the rings, mass and momentum conservation for the lubricant, and the appropriate contact model for the lubrication regime. This is difficult because each of the factors are interrelated. Both hydrodynamic and boundary lubrication are dependent on film thickness [42]. The friction force is calculated for the boundary friction and hydrodynamic friction. For boundary friction the coefficient of friction, $f_{c,boundary}$ and the film pressure is represented by $P_{boundary}$. These are integrated over the running face of the piston ring to find the total force. The hydrodynamic friction is calculated with Equation (3.8).

$$F_{boundary} = \int f_{c,boundary} P_{boundary} dA \quad (3.7)$$

$$F_{hydrodynamic} = \int \left[\frac{\mu U}{h} (\Phi_{fg} + \Phi_{fs}) - \Phi_{fp} \frac{h}{2} \frac{dP}{dx} \right] dA \quad (3.8)$$

3.2 Empirical Friction Models

Empirical models use global engine variables to allow rapid calculation and estimation of frictional losses within the engine. Complexity of empirical models varies from simple two to three terms equations to describe overall engine friction to equations with multiple terms for each engine component subgroup. Several models are reviewed below.

Several researchers have proposed global equations to calculate total engine fmep based on results from experimental data. A commonly encountered model is that of Chen and Flynn, who determined the fmep depends on the maximum cylinder pressure and engine speed through the formula shown in Equation (3.9), where C_1 is a constant applied for engine accessory friction, C_2 is a factor accounting for the load on the engine, and C_3 and C_4 are used to account for variations in friction due to engine speed [43] [44].

$$fmep = C_1 + C_2 P_{max} + C_3 N + C_4 N^2 \quad (3.9)$$

Millington and Hartles based the following formulation on engine motoring tests performed on engines near operating temperature. Shown below in Equation (3.10), where R_c is the compression ratio, N is engine speed, and V_p is the mean piston speed [45].

$$fmep = 6895(R_c - 4) + 48.2N + 401V_p^2 \quad (3.10)$$

Winterbone and Tennant proposed a friction formula based on maximum cylinder pressure for a given operating condition [46]. Using cylinder pressure the equation included engine load implicitly. However this requires experimental or additional simulations to determine the maximum cylinder pressure. Their result is shown in Equation (3.11), where P_{max} is the maximum cylinder pressure [44] [44].

$$fmep = 6100 + 29.4N + 0.16P_{max} \quad (3.11)$$

Yagi et al. proposed the following formulation based on experimental friction from over 300 different engines. The following equations account for friction from the piston rings, main bearings, and connecting rod. V_s is the stroke volume, D_{cm} is a crankshaft diameter parameter

depends on the number of cylinders, main bearings, crank pins, and the diameter of the main bearings and crank pins, Z is the effective valve opening area, v is lubricant viscosity, and ϕ_1 , ϕ_2 , ϕ_3 , and ϕ_4 are constants [47] [44].

$$fmep = \frac{\sqrt{SD_{cm}}}{B} \left[\left\{ \phi_1 \left(\frac{V_s}{Z} \right)^2 + \phi_2 \right\} N^2 + (\phi_3 v + \phi_4) \right] \quad (3.12)$$

In the mid-1960s Bishop developed one of the first empirical friction models based on experimental results obtained by motoring a Cooperative Fuel Research engine [48]. Bishop considered five contributions to total engine friction, crankcase mechanical friction, piston friction, blowby losses, inlet and exhaust throttling losses, combustion chamber and valve pumping losses.

The crankcase mechanical friction was defined as shown in Equation (3.13), where N is the engine speed, G is the intake valves per cylinder, H is the intake valve head diameter, B is the engine bore, S is the engine stroke, K is the journal bearing size coefficient. The first term represents the contribution from pumps and miscellaneous, the second represents valve gear, and the final term the friction from the journal bearings [48].

$$fmep = 0.085N^{1.5} + (2100 - 0.28N) \frac{GH^{1.75}}{B^2S} + 6.9 \frac{BK}{S} N \quad (3.13)$$

The piston mechanical friction terms are shown below in Equation (3.14). The first term represents friction due to the wall tension of the piston rings where n_{pre} is the number of piston rings per cylinder. The second term accounts for viscous friction in the piston skirt and piston rings, where M is the projected area of the piston skirt divided by the bore, V_p is the mean piston speed, and P_a is atmospheric pressure. P_1 is calculated from Equation (3.15), where $imep_c$ is a corrected $imep$ term excluding heat losses, for diesel P_1 is zero. The final term represents the engine friction due to cylinder gas pressure loading on the piston rings, where R_c is the compression ratio [48] [44].

$$fmep = 370 \frac{Sn_{pr}}{B^2} + 756 \frac{M}{BS} V_p + 0.0042(P_a - P_1) \frac{S}{B^2} \left(0.088R_c + 182R_c^{1.33-0.0238V_p} \right) \quad (3.14)$$

$$P_1 = P_a - \left(\frac{imep_c}{12.8} \right) - 10135 \quad (3.15)$$

The blowby, pumping, and throttling losses are not included as the current study is focused on mechanical friction only.

In the mid-1980s Kenneth Patton, Ronald Nitschke, and Professor John Heywood of MIT created a friction model to predict the friction mean effective pressure for spark-ignition engines [49]. This model requires only basic engine configuration, geometry, and operating conditions as input parameters. The model based its predictions on fundamental scaling laws and empirical results, and predicts the fmep for the rubbing losses from the crankshaft, power cylinder, and valvetrain, pumping losses from the intake and exhaust systems, in addition to predictions of auxiliary losses. The model was correlated to friction data from several production engines.

Major component groups were identified as the crankshaft group (crankshaft main bearings and bearing oil seals), reciprocating assembly (connecting rod bearings, piston skirt and rings), valvetrain (camshafts, cam followers, and valve actuation mechanisms), and auxiliary losses from the oil pump, water pump and alternator. Key input parameters included inline or vee configuration of cylinders, bore, stroke, main and big end bearing diameter, length, quantity, and clearance, valve diameters and lift, valvetrain configuration, oil viscosity, and engine speed. These basic parameters allow the model to be quickly applied to any engine configuration to provide a reasonable estimation of total fmep and develop understanding how each parameter affects friction performance of the engine.

To relate a mechanical or rubbing friction interface fmep to the engine operating parameters required several assumptions. First was the lubrication regime in which the component group primarily operated. A duty parameter was then identified and related to operating parameters based on the Stribeck curve (Figure 2.2). When a component group operated in the hydrodynamic lubrication regime it was assumed that the friction term varied proportionally with the duty parameter. In mixed lubrication the friction coefficient was assumed to vary inversely with engine speed. When boundary lubrication was expected the friction coefficient was assumed to be constant and independent of design and operating parameters. These friction coefficients were then multiplied by a normal force and velocity to obtain friction work losses. These terms were derived from the friction interface and geometry. This result was then normalized by dividing by engine speed and displacement to obtain the friction mean effective

pressure (fmep). Finally constants were applied to each term to calibrate the results with experimental data.

For the case of the crankshaft group, hydrodynamic lubrication was assumed for the journal bearings, while the oil seals were assumed to operate in the boundary lubrication regime. Finally, a term was added to account for the pumping losses through the journal bearing and associated passages. Engine parameters used to determine crankshaft friction were main bearing diameter, D_b , length, L_b , and the number of bearings, n_c . The main bearing friction was determined from the duty parameter for a journal bearing shown in Equation (3.16) where μ is lubricant viscosity, V is the surface speed, A is the bearing area, F_n is the normal force or loading, and c is the bearing clearance.

$$f \propto \frac{\mu V A}{F_n c} \quad (3.16)$$

Friction force is calculated from the duty parameter and the normal force. Surface speed and area are converted to bearing and engine parameters, engine speed, N , times bearing diameter, D_b replace V and D_b times L_b replaces area in the equation. The power dissipated is calculated as the friction force time surface speed times the number of bearings. This is then normalized to engine displacement and a constant of 3.03×10^{-4} was calculated. This derivation is shown below in Equation (3.17).

$$\begin{aligned} F_f &= f F_n \propto \left(\frac{\mu V A}{F_n c} \right) F_n \propto \left(\frac{\mu \pi}{2c} \right) N D_b^2 L_b \\ P_f &\propto F_f V n_c \propto \left(\frac{\mu \pi}{4c} \right) N^2 D_b^3 L_b n_c \\ f_{mep} &= \frac{P_f}{N V_d} \propto C_1 \left(\frac{\mu}{c} \right) \frac{N D_b^3 L_b n_c}{B^2 S n_c} \\ C_1 \left(\frac{\mu}{c} \right) &= 3.03 \times 10^{-4} \end{aligned} \quad (3.17)$$

For the oil seals the contact pressure between the lip of the seal and the crankshaft was assumed to be constant across all engine speeds. This was considered reasonable because the spring element in the seal maintains a constant contact pressure to minimize leakage as the seal wears. The friction force, F_f , was assumed to be constant and equal to the friction coefficient time the

normal force of the seal. The power dissipated or P_f is proportional to the friction force times surface speed, where N is the engine RPM and D_b is bearing diameter. Finally this result was normalized to engine displacement where B is the bore, S is stroke, and n_c is the number of cylinders. This derivation is shown below in Equation (3.18). From experimental data the constant was determined to be 1.22×10^5 .

$$\begin{aligned}
 F_f &= fF_n = \text{constant} \\
 P_f &\propto F_f V \propto \text{constant} \times ND_B \\
 fmep &\propto \frac{P_f}{NV_d} \propto C \frac{D_B}{B^2 S n_c} \\
 C &= 1.22 \times 10^5
 \end{aligned} \tag{3.18}$$

A term to account for the viscous losses from pumping lubricant to the bearings was also included and was assumed to be proportional to the pressure drop through the bearings, ρV^2 . Equation (3.19) shows the $fmep$ term and the constant of 1.35×10^{-10} .

$$\begin{aligned}
 fmep &\propto \frac{D_B^2 N^2 n_B}{n_c} \\
 C &= 1.35 \times 10^{-10}
 \end{aligned} \tag{3.19}$$

The previous results can be combined into one term for crankshaft friction which is shown in Equation (3.20).

$$fmep_{crank} = 3.03E^{-4} \frac{ND_B^3 L_B n_B}{B^2 S n_c} + 1.22E^5 \frac{D_B}{B^2 S n_c} + 1.35E^{-10} \frac{D_B^2 N^2 n_B}{n_c} \tag{3.20}$$

For the power cylinder a mixed lubrication model was adopted as both hydrodynamic and boundary lubrication is present in the power cylinder. As previously mentioned the majority of the work losses for the piston and rings occur in the piston mid-stroke where velocity is highest. Boundary lubrication is present, especially at TDC and BDC of the stroke, and is greatest at low engine speeds. Therefore, for the piston and ring pack hydrodynamic lubrication was assumed to dominate total friction at high engine speeds while a boundary lubrication component has increasing importance at lower speeds. The piston was assumed to operate in the hydrodynamic regime while the piston rings were modeled under mixed lubrication.

The friction coefficient for the piston skirt was based off a duty parameter that includes the length of the piston skirt, L_s . In this case they assumed the piston skirt length was proportional to the bore of the engine and the velocity could be defined using the mean piston speed, S_p . The derivation of this term is shown in Equation (3.21)

$$\begin{aligned}
 F_f &= fF_n \propto \left(\frac{\mu VL_s}{F_n} \right) F_n \propto VL_s \propto S_p B \\
 P_f &\propto F_f V \propto S_p^2 B \\
 fmep &= \frac{P_f}{NV_d} \propto \frac{S_p^2 B}{B^2 SN} = \frac{S_p}{B} \\
 C &= 2.94 \times 10^2
 \end{aligned} \tag{3.21}$$

The piston ring terms includes terms with and without gas pressure loading. Friction was determined from empirical data and was scaled using a term $1+1000/N$ as shown in Equation (3.22) to decrease the friction coefficient as engine speed increases. The velocity used in this case was also the mean piston speed.

$$\begin{aligned}
 F_f &= fF_n \propto \left(1 + \frac{1000}{N} \right) \times \text{constant} \\
 P_f &\propto F_f V \propto \left(1 + \frac{1000}{N} \right) S_p \\
 fmep &= \frac{P_f}{NV_d} \propto \left(1 + \frac{1000}{N} \right) \frac{S_p}{NB^2 S} = \left(1 + \frac{1000}{N} \right) \frac{1}{B^2} \\
 C &= 4.06 \times 10^4
 \end{aligned} \tag{3.22}$$

The term that includes gas pressure loading was based on an expression developed by Bishop from firing friction experimental data [48]. Terms included are the intake pressure P_i , atmospheric pressure P_a , and the compression ratio of the engine. The expression is shown below, where K is a constant equal to 2.38×10^2 .

$$fmep = 6.89 \frac{P_i}{P_a} [0.088r_c + 0.182r_c^{(1.33-KS_p)}] \tag{3.23}$$

The connecting rod bearing was assumed to be hydrodynamic and had an identical formulation to the crankshaft bearing friction above in Equation (3.17), with the appropriate terms input for the connecting rod bearing geometry.

$$fmep \propto \frac{ND_B^3 L_B n_B}{B^2 S n_c} \quad (3.24)$$

The summation of these expressions is shown below:

$$fmep_{PC} = 3.03E^{-4} \frac{ND_B^3 L_B n_B}{B^2 S n_c} + 4.06E^4 \left(1 + \frac{1000}{N}\right) \frac{1}{B^2} + 6.89 \frac{P_i}{P_a} [0.088r_c + 0.182r_c^{(1.33-KSP)}] \quad (3.25)$$

For the valvetrain friction contribution several valvetrain configurations were considered, single overhead camshaft, dual overhead camshaft, and a cam in block overhead valve configuration. The same journal bearing friction term from the crankshaft and connecting rod bearing was used for the camshaft with a modified constant of 2.44×10^2 and a constant value added to account for the oil seals. In addition camshaft dimensions were considered constant for the SI engines under consideration. Two terms were developed for cam and cam follower interface based on flat and roller follower configurations. A mixed lubrication regime was assumed for the flat follower with high boundary contact at low engine speeds and decreasing friction as engine speed increased. The normal force in this assembly was based off the mass and acceleration of the valvetrain components. It was determined that valve area was an effective measure for the valvetrain mass, and was assumed proportional to the engine bore. The same $1+1000/N$ term was used to decrease boundary friction at high engine speeds. The flat follower friction term is shown in Equation (3.26)

$$fmep \propto \frac{P_f}{NV_d} \propto \left(1 + \frac{1000}{N}\right) \frac{B^2 N n_v}{B^2 S n_c N} = \left(1 + \frac{1000}{N}\right) \frac{n_v}{S n_c} \quad (3.26)$$

Roller cam follower friction was assumed to be proportional to the duty parameter of the roller, which varies linearly with engine speed. The resulting $fmep$ term is shown below in Equation (3.27).

$$fmep \propto \frac{P_f}{NV_d} \propto \frac{N^2 B^2 n_v}{B^2 S n_c N} \propto \frac{N n_v}{S n_c} \quad (3.27)$$

The final term in the valvetrain friction was an oscillating friction term which included a hydrodynamic component and a boundary lubrication component similar to the power cylinder assembly. The hydrodynamic term was based on the results of Cameron as is shown below, where L_v is the maximum valve lift [50].

$$f_{mep} \propto \frac{P_f}{NV_d} \propto \frac{(L_v N)^{1.5} B n_v}{B^2 S n_c N} \propto \frac{L_v^{1.5} N^{0.5} n_v}{B S n_c} \quad (3.28)$$

Because oscillating components have surface speeds that vary from zero to a maximum value there is boundary lubrication which contributes to the overall component friction. The same $1+1000/N$ term was used to scale the boundary friction contribution with engine speed.

$$f_{mep} \propto \frac{P_f}{NV_d} \propto \left(1 + \frac{1000}{N}\right) \frac{B^2 L_v N n_v}{B^2 S n_c N} = \left(1 + \frac{1000}{N}\right) \frac{L_v n_v}{S n_c} \quad (3.29)$$

The constants for each term were determined separately for each valvetrain configuration and can be located in the reference paper [49]. This model also included empirical correlations for auxiliary losses based on engine speed, these have been omitted as they do not apply to the current study. Pumping loss estimation has also been omitted from this review as the current study is focused on mechanical friction.

This model was then updated by Sandoval and Heywood in 2003 to reflect improvements in engine design and to also include lubricant viscosity as a parameter under study [51]. This modification allowed the analysis of lower friction lubricants and cold engine friction. Hydrodynamic friction terms included viscosity scaling of the form shown below in Equation (3.30).

$$\mu_{scaling} = \sqrt{\frac{v(T)}{v_o(T_o)}} \quad (3.30)$$

The updated model included changes to constants and adding variables in each of the three original component groups, the crankshaft, the power cylinder, and the valvetrain. For the crankshaft group the viscosity scaling from Equation (3.30) was included with no other changes. The power cylinder was modified to reflect the improvements in the ring liner interface. Viscosity scaling was applied to the hydrodynamic terms for the piston skirt and connecting rod friction. For the piston ring friction terms several modifications were made. The speed scaling that was originally $1+1000/N$ was reduced to $1+500/N$ due to lower boundary friction contact in modern engine designs. In addition two additional parameters, piston ring tension and surface roughness were added. In the gas pressure loading ring expression, viscosity scaling was added to the first term, piston ring tension and surface roughness added to the second and the constant

K was doubled to 2.8×10^{-2} . In the valvetrain component expression, viscosity scaling was added to the camshaft bearing and oscillating hydrodynamic friction terms.

Taraza, Henein, and Bryzik developed a simplified friction model for multi-cylinder diesel engines based on the tribological interfaces within the engine [34]. The piston ring, piston skirt, bearings, valvetrain and engine auxiliaries were considered separately. This model used basic engine parameters and fuel input to determine cylinder pressure, engine speed, and torque output. These outputs were then used to model the dynamics of the engine to determine resultant forces and conditions within the engine. The friction was calculated from these forces to determine total engine fmep.

The piston skirt was assumed to always operate in the hydrodynamic regime. The friction force was calculated based on the duty parameter of the interface shown in Equation (3.31). In this equation S is the duty parameter, μ_{oil} is lubricant viscosity, V_p is mean piston speed, F_N is normal force, and L_s is the length of the piston skirt.

$$S = \frac{\mu_{oil}|V_p|}{F_N/L_s} \quad (3.31)$$

In this simplified model the piston skirt is assumed to always operate in the hydrodynamic regime. Since friction force is expected to vary with the square root of the duty parameter the piston skirt friction coefficient was assumed to take the form of Equation (3.32), where C_s is a constant. This friction force was correlated to experimental data and has the final form seen in Equation (3.33) below.

$$f = C_s \sqrt{\frac{\mu_{oil}|V_p|}{F_N/L_s}} \quad (3.32)$$

$$F_S \cong 2.5 \sqrt{\mu_{oil}|V_p|L_s F_N} \quad (3.33)$$

The piston rings the duty parameter as shown above in Equation (3.32). For hydrodynamic lubrication the piston ring friction coefficient is expected to vary with the square root of the duty parameter. To model this relationship a logarithmic function was used, where C and m are constants based on the ring profile curvature, ranging from 1.9 to 2.25, and from 0.425 to 0.525, respectively, and S is the duty parameter.

$$f = C \times S^m \quad (3.34)$$

In mixed lubrication the friction coefficient was assumed to vary linearly with the duty parameter. The friction coefficient was calculated using Equation (3.35), where f_0 is the dry rubbing coefficient between the two metals in contact, S_{cr} is the duty parameter where lubrication moves from mixed to hydrodynamic

$$f = f_0 \left(1 - \frac{S}{S_{cr}}\right) + f_{cr} \left(\frac{S}{S_{cr}}\right) \quad (3.35)$$

To calculate the friction force a different normal force was considered for the first ring, second ring, and OCR. Input parameters were the ring tension, T_1 , T_2 , T_3 , the cylinder pressure p_{cyl} , B is the cylinder bore, and geometry factors a , b , and h were determined from the specific ring size and geometry which be found in the reference [34].

$$\text{First Ring} \quad F_N = 2T_1 + \pi B h p_{cyl} \quad L = 0.25a \quad (3.36)$$

$$\text{Second Ring} \quad F_N = 2T_2 \quad L = 0.75a_1 \text{ (upstroke)} \quad L = a_2 \text{ (downstroke)} \quad (3.37)$$

$$\text{Oil Control Ring} \quad F_N = 2T_3 \quad L = 2b \quad (3.38)$$

The crankshaft losses were modeled using Booker's mobility method [26] the result is shown below in Equation (3.39). The first two terms account for the shearing force in the oil film and the pressure component due to the journal's eccentricity. These correspond to the short bearing approximation by Ocvik for a constantly loaded bearing. The third term considers the resistance against the motion of the journal inside the bearing [34]. The bearing parameters and loading are calculated using the cylinder pressure to find the resultant loading force and friction force.

$$F_c \cong \frac{2\pi\mu_{oil}R^2\omega L}{c\sqrt{1-\varepsilon^2}} + \frac{eW}{2R} \sin\phi + \frac{VW}{R\omega} \cos\gamma \quad (3.39)$$

The valve train friction is heavily influenced by the kinematics and dynamics of the system. In addition, elasticity of mating components is an important consideration for a detailed model. Taraza, Henein, and Bryzik considered the friction generated in an overhead valve engine. For the simplified model, the majority of valvetrain friction was assumed to come from the cam and tappet interface. The average friction force between the cam and tappet is assumed to be:

$$F_c = \left(F_0 + K_s \frac{L_v}{2}\right) \frac{r_1}{r_2} + m_c a_{tip} \quad (3.40)$$

Where F_0 is the preload force on the valve spring, K_s is the spring stiffness, L_v is the maximum valve lift, r_1/r_2 is the arm ratio of the rocker arm, m_c is the mass of the valvetrain, and a_{ip} is the acceleration of the tappet at the cam. The interface is assumed to be elastohydrodynamic (EHD) and an oil film parameter, λ , is calculated as shown below. H is a correlation parameter based on the geometry and sliding speed of the cam and tappet in addition to the pressure viscosity coefficient of the lubricant. R_c is the average cam radius and σ is the combined roughness of the cam and tappet surfaces.

$$\lambda = \frac{HR_c}{\sigma} \quad (3.41)$$

The friction force is then calculated as shown below in Equation (3.42) and (3.43). Values of λ greater than one assumes EHD lubrication while values less than one assume boundary friction.

$$\lambda > 1 \quad F_f = \frac{2b\mu_{oil}L}{h} \quad (3.42)$$

$$\lambda < 1 \quad F_f = 0.11F_c(1 - \lambda) \quad (3.43)$$

3.3 Empirical Friction Models Applied to HD Diesel Engines

For this project an approach similar to Patton et al. has been adopted. A simple model provides insight into the dominant lubrication regimes in various engine components. The model includes relevant lubricant properties and has been correlated to baseline data from a representative class 8 HD diesel engine currently in production.

3.3.1 Crankshaft

The empirical model of Patton et al. was used to model the friction losses in the crankshaft assembly. Equation (3.20) was used to model the friction losses in the crankshaft group. These results were compared with experimental data and were found to be in good agreement. Figure 3.5 shows the model f_{mep} prediction compared with experimental results, the values have been normalized to the experimental f_{mep} at 1000 RPMs. Friction was found to vary linearly at lower engine speeds and increase with a square root dependence at higher engine speeds as hydrodynamic drag increases. Crankshaft friction was predicted to account for approximately 20% of the total friction losses.

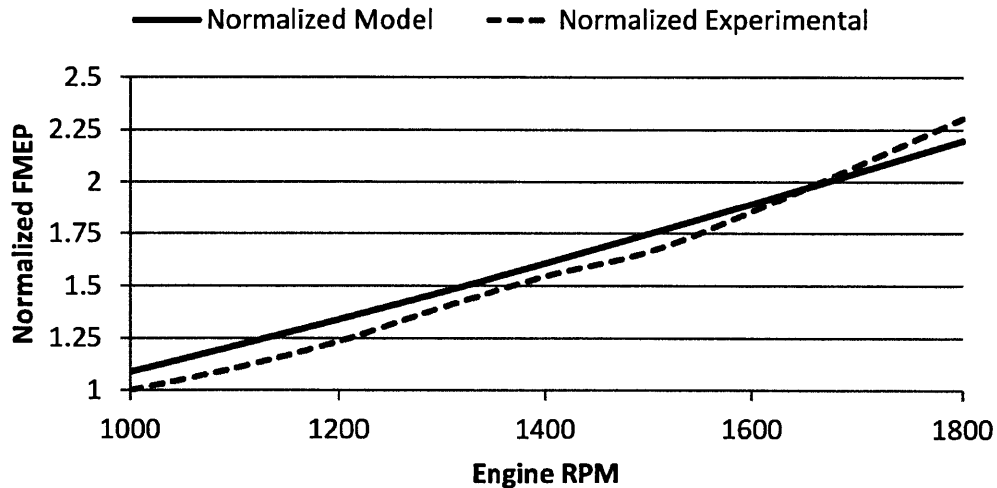


Figure 3.5 Crankshaft Friction Model and Experimental Results

The model was used to estimate the effects of viscosity changes on the crankshaft group at 100°C lubricant temperatures for 15W-40, 5W-30, and 5W-20 lubricants normalized to the 15W-40 data. Figure 3.6 shows the predicted f_{mep} values for three different oil viscosity grades. The 15W-40 oil is Mobil Delvac Elite 15W-40 fully synthetic oil with a viscosity of 15.2 cSt at

100°C and a VI of 141, this viscosity grade is a common specification for HD diesel engines. The 5W-30 oil represented is the Mobil Delvac 1 LE fully synthetic oil with a viscosity of 12.2 cSt at 100°C and a viscosity index of 161. The 5W-20 was again Mobil fully synthetic oil with a viscosity of 9 cSt at 100°C and a VI of 158. Results of this modeling analysis suggest that a fmep reduction of approximately 10% in the crankshaft assembly is possible through a lubricant viscosity reduction from 15W-40 to 5W-30.

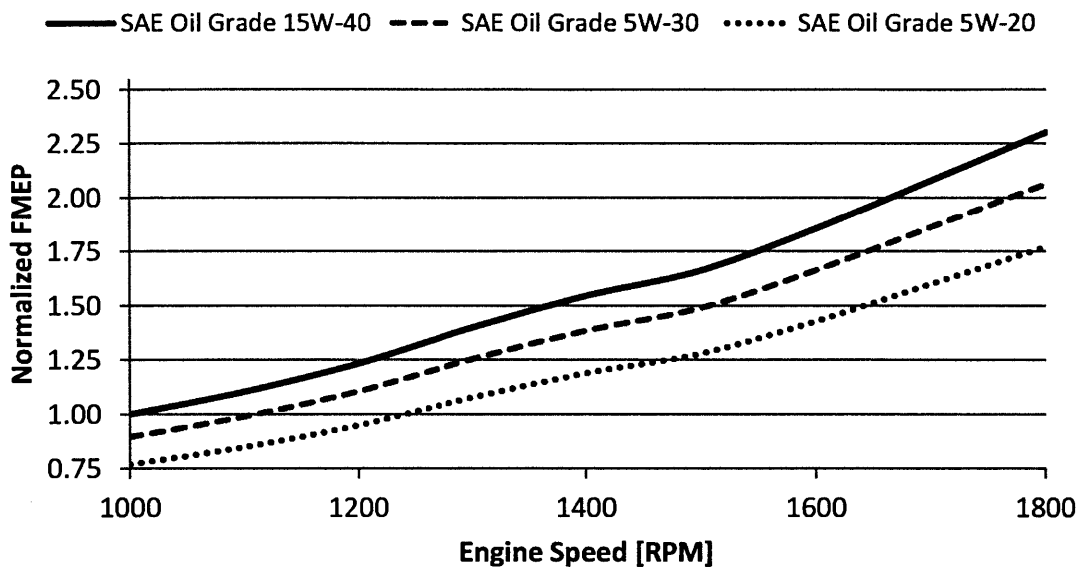


Figure 3.6 Crankshaft FMEP Analysis for SAE Oil Grades

3.3.2 Power Cylinder

The power cylinder was modeled using the piston skirt lubrication model developed by Wong et al., empirical relationships, and a piston ring pack model also developed at MIT [35]. The power cylinder assembly represents approximately 40% of total frictional losses in the engine, which falls well within the expected values from previous studies. Analysis was performed on the piston skirt and ring pack using analytical models developed at MIT. These models showed good agreement with the empirical model as well as experimental data. Figure 3.7 below shows the results for the predicted power cylinder assembly fmep for the three lubricants studied, normalized to the values at 1000 RPM. Friction reduction in the power cylinder has approximately a square root dependence on the lubricant viscosity. In this analysis a 50% reduction in lubricant viscosity predicted approximately 25% decrease in power cylinder friction.

It should be noted that a 50% reduction in lubricant viscosity would dramatically increase wear rates in the power cylinder and would not be technically feasible without aggressive wear mitigation strategies.

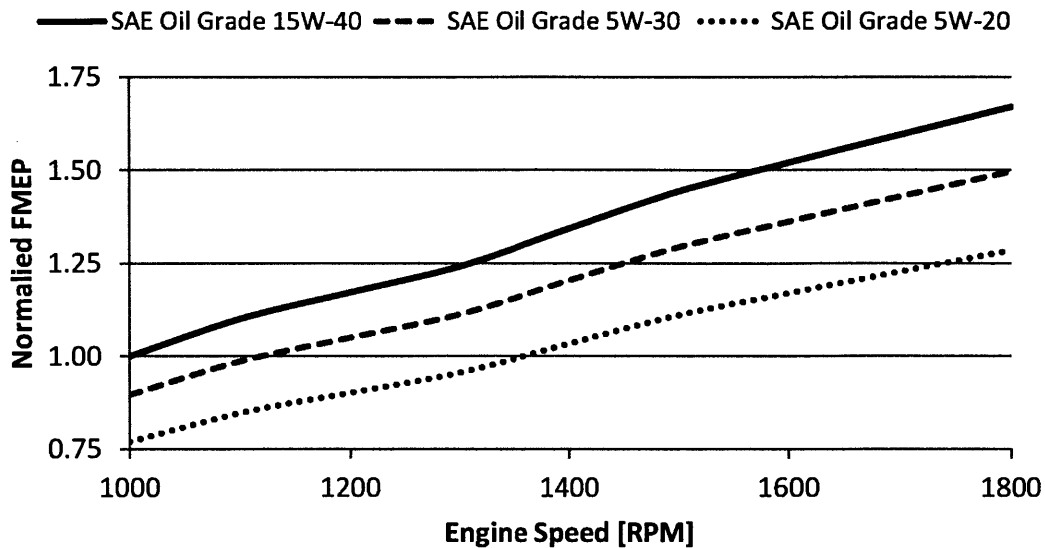


Figure 3.7 Power Cylinder FMEP Analysis for SAE Oil Grades

3.3.3 Auxiliary Components

In the HD diesel engines under study auxiliary loads are a significant source of parasitic losses in the engine. The majority of these losses are from the oil pump, used to circulate lubricant throughout the engine and accessories, and the water pump used to move coolant through the engine and maintain operating temperatures. Additional losses occur from the fuel pump and air compressor. In total, auxiliary components are responsible for approximately 30% of the total engine friction. Modeling of these losses was done through empirical correlation, due to the varied nature and interfaces within each auxiliary component. Shown in Figure 3.8 are experimental results of the oil pump losses normalized to the values at 1000 RPM. Unlike other internal engine components, lubricant viscosity does not have a significant effect on friction in the oil pump due to its geared design.

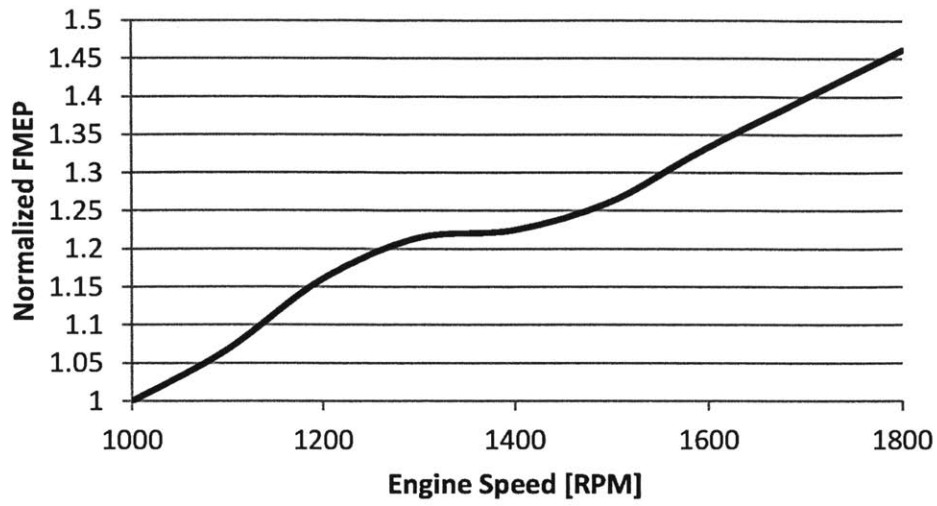


Figure 3.8 Oil Pump FMEP

3.3.4 Summary

Figure 3.9 below shows the individual component group contributions to total engine fmeep as a function of engine speed normalized to the total fmeep at 1000 RPMs.

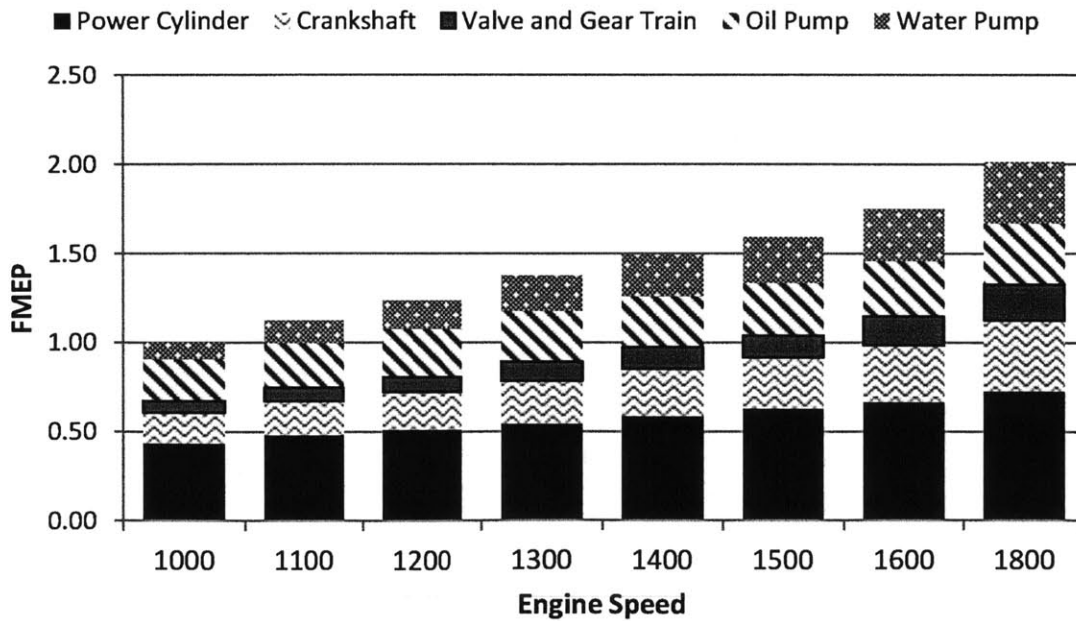


Figure 3.9 Total Engine FMEP as a Function of Engine Speed

(This page was intentionally left blank)

4 Local Oil Viscosity and Friction Reduction - Study of Cylinder Liner Thermal Barrier Coatings

In this research program, the use of TBC was investigated for a novel approach of strategically increasing cylinder liner temperatures in the piston mid-stroke to reduce local lubricant viscosity. By raising the temperature in the mid-stroke region the hydrodynamic drag between the cylinder liner and the piston skirt and ring pack is reduced, thereby lowering power cylinder frictional losses.

In this study the use of thermal barrier coatings on the cylinder liner of a heavy duty diesel engine was investigated using a computer simulation. The cylinder liner of a HD diesel engine is a separate component that is installed into the engine block using special gaskets. This configuration is called a wet liner because the outer walls of the cylinder liner come in direct contact with the engine coolant. Many light duty and automotive engines have dry liners which are sleeves supported by the cylinder block material. The difference between wet and dry liners is illustrated by Figure 4.1. The advantages of a wet liner system are that the power cylinder is in more direct contact with engine coolant and the liners can be replaced easily during an engine overhaul. Additionally the manufacturing of the cylinder liner as a separate component requires less handling and machining of the large engine block as the liners can be made separately with smaller, less expensive machine tools, with greater process control and quality.

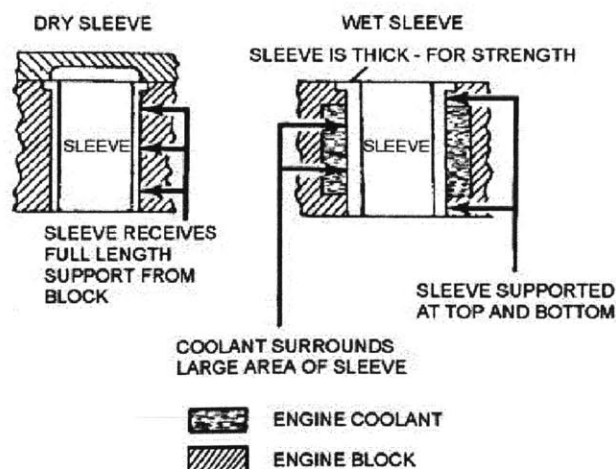


Figure 4.1 Dry and Wet Cylinder Liner Comparison [52]

Thermal barrier coatings (TBC) are advanced material systems generally applied to metallic surfaces that operate at high temperatures. The ceramic coatings insulate the base material and protect it from high heat sources. They have been extensively used in the aerospace and gas turbine industries to protect components from the extreme operating temperatures present in those devices. They have also been used in automotive applications as a way to insulate exhaust components with the goal of reducing ambient temperatures in the engine bay and decreasing catalytic converter light-off time. Additional research has been conducted to insulate internal engine components such as pistons, cylinder heads, and cylinder liners to improve thermodynamic efficiency, emissions performance, and to reduce cooling system loads.

In this research program, the use of TBC was investigated for a novel approach of strategically increasing cylinder liner temperatures in the piston mid-stroke to reduce local lubricant viscosity. By raising the temperature in the mid-stroke region the hydrodynamic drag between the cylinder liner and the piston skirt and ring pack is reduced, thereby lowering power cylinder frictional losses.

4.1 Previous Studies of Thermal Barrier Coatings in Diesel Engines

Approximately 60% of the chemical fuel energy input into a diesel engine is lost through the exhaust gasses and heat rejected to the engine coolant. This then requires additional energy input through water pumps and fans to remove the heat from the engine coolant. The concept of using thermal barrier coatings was first investigated for use in diesel engines during the 1980s.

According to second law of thermodynamics, insulating the combustion chamber of the engine increases the thermal efficiency. Efforts focused on reducing heat transfer to the engine block and coolant, allowing that energy to be partially recovered by the turbocharger in addition to reducing engine cooling loads. The use of TBC in the combustion chamber raises temperatures and can cause an increase in NO_x emission levels. Durability of the coating over the life of the engine is also a concern, as thermal cycling and the harsh combustion chamber environment can lead to failure of the coating.

Research in TBC and its application to diesel engines and more specifically low heat rejection (LHR) engines has been pursued both theoretically and experimentally. In general, theoretical

and simulation based studies find benefits from the use of TBC and varying degrees of insulation in the combustion chamber. These benefits include increased thermal efficiency, reductions in BSFC, in addition to lower PM, HC, and CO emissions with an increase in NO_x formation. Experimental investigations have had mixed results as the physical and engineering limitations of insulating the engine and running at extremely high operational temperatures are realized. Experiments on naturally aspirated engines generally report poor performance and high fuel consumption as the volumetric efficiency of the engine is degraded at high temperatures. Challenges in controlling combustion due to decreased ignition delay and optimizing engine timing at high temperatures creates additional complications. Research on turbocharged engines reports mixed results, with some researchers reporting substantial gains in engine efficiency and fuel economy while others experienced high fuel consumption. Below is a brief review of previous investigations and their results.

Simulations are often used by researchers to evaluate the potential of concepts and designs prior to investing in costly experiments and prototypes. Such simulations have been used to predict the performance of diesel engines equipped with TBC. Generally, turbocharged heavy duty diesel engines are studied. One advantage of engine simulations is that critical engine parameters such as air-to-fuel ratio and peak cylinder pressure can be easily maintained between different configurations. Some simulations include the benefits of turbocompound units and Rankine waste heat recovery systems. Results from these simulations show an improvement in the thermal efficiency of an LHR engine and improvements in specific fuel consumption from 2 to 17% depending on the degree of thermal insulation and the degree of energy recovery from the exhaust stream by turbochargers, turbocompound, and Rankine cycle systems [53].

Studies also show increases in the surface temperatures in the top ring reversal zone due to insulation. Morel et al show this region increasing from 530 K to 900 K when moving from the baseline engine to the fully insulated engine [54]. This dramatic increase in surface temperatures can cause significant issues for traditional engine lubricants which degrade above 350°C [53]. Increases in exhaust temperatures have also been recorded; K.L. Hoag et al predict exhaust temperature increases of 100°C depending on the level of in-cylinder heat rejection [55]. Increases in exhaust stream temperatures would be beneficial in today's diesel engines, as

turbochargers, turbocompound units, and waste heat recovery systems benefit from the increase in available energy. Another windfall benefit may be reduced regeneration times and/or frequency for the diesel particulate filter (DPF) systems.

Experimental studies on LHR engines using TBC have shown varying results in engine performance. Some have shown positive results: increased fuel efficiency and engine thermal efficiency. Other studies have shown mixed or even detrimental effects on insulating the combustion chamber, liner, and pistons. Studies performed by W.R. Wade et al. on an air cooled single cylinder diesel engine with an insulated cylinder head, valves, piston crown, and cylinder liner above TDC showed a 4-7% increase improvement in fuel efficiency [56]. R.H Thring, using a single cylinder diesel engine, reported fuel economy improvements of 7% for turbocharged engine and nearly 15% for a turbocharged and turbocompounded engine. The report also indicates 80% reduction in PM, 50% reduction in HC and CO emissions, but a 15% increase in NO_x emissions [57]. Other studies on LHR engines report deterioration in engine performance with insulation, generally attributed to poor combustion characteristics due to the increased in-cylinder temperatures.

4.1.1 Effects of TBC and LHR on Engine Emissions

TBC and LHR engines cause a substantial increase in the in-cylinder temperatures. This increase can dramatically alter the fuel injection, ignition delay, quenching distance, and the lean flammability limit. These key engine performance parameters then alter the emissions performance of the engine, which was optimized for uninsulated combustion chamber temperatures and current regulations.

Increased in-cylinder temperatures from TBC lead to reduced hydrocarbon, particulate matter, and carbon monoxide emissions. Unburned hydrocarbon emissions are reduced as the high temperatures decrease the quenching distance of the fuel spray from the injectors, resulting in more complete vaporization which allows oxidation reactions to proceed to completion. HC emissions could increase in the case of inefficient combustion or the increased vaporization of lubrication oil due to higher wall temperatures. CO emissions, while already low for diesel engines, are expected to decrease for similar reasons to HC emissions [53].

Particulate matter emissions are also expected to decline as the high temperatures promote greater fuel vaporization. In experimental investigations PM emissions have had mixed results. Poor combustion characteristics' have led to increased soot formation while other investigations have shown significant reductions in PM emissions [53].

Nitrous oxide emissions are highly dependent on cylinder temperatures but generally high temperatures, like those found in LHR engines, generates higher NO_x emissions. Results from experimental investigations reveal mixed results.

4.1.2 Effects of TBC and LHR on Engine Performance Parameters

TBC and LHR engines have significant effect on critical engine performance parameters including volumetric efficiency, thermal efficiency, and brake specific fuel consumption.

The volumetric efficiency is a mass ratio that compares the mass flow of air induced into the cylinder and the mass that would occupy the displaced volume at the density in the intake manifold. This ratio decreases as combustion chamber temperatures increase because the greater temperatures of the residual cylinder gasses and cylinder liner reduce the density of the intake air. Turbocharging of the engine can negate this effect.

Thermal efficiency measures the energy conversion efficiency of the engine, and has been the primary reason for the investigation into TBC use in diesel engines. Reducing the heat rejected to the engine coolant theoretically provides an increase in the thermal efficiency. This has been demonstrated by simulation studies and by some experimental researchers. Other researchers report a decrease in the thermal efficiency of the engine; this is attributed to increases in the convective heat transfer coefficient which causes greater heat flux. Also non-optimized combustion conditions in the LHR engine can cause deterioration of the thermal efficiency. Greater cylinder temperatures reduce ignition delay and therefore require modification of engine timing to perform at peak efficiency.

4.2 Thermal Barrier Coating Properties

Desirable material characteristics of a thermal barrier coating for use in a diesel engine are low thermal conductivity and specific heat to provide insulating qualities. To survive in the engine a TBC must have high flexure strength, fracture toughness, and wear resistance to withstand the loads imposed on the TBC over time; thermal shock resistance to withstand the thermal cycles from engine on-off time; and chemical inertness. Also critical is that the TBC have a coefficient of thermal expansion that is approximately the same as the metallic substrate it is to be applied on iron, steel, and aluminum.

Zirconia is a ceramic that has many of the desired qualities for use as a TBC. However it tends to change phases at higher temperatures and must be stabilized to prevent the magnitude of the phase changes. Ytria Partially Stabilized Zirconia (YSZ) has been one of the most commonly used coating for diesel engines in recent studies. YSZ has proven performance in the coating of turbine blades that operate at temperatures around 1100 °C in thickness on the order of 100 μ m. YSZ is applied to metallic surfaces such as the cylinder liner using a thin metallic bond coat and then the insulating ceramic topcoat. The most common application method is plasma spray which creates a splat structure with 10-20% volume fraction of voids and cracks [58]. Figure 4.2 shows the thermal conductivity of 8% YSZ from 100 to 1200°C, an approximate value of 1.3 W/m-K was used in this study.

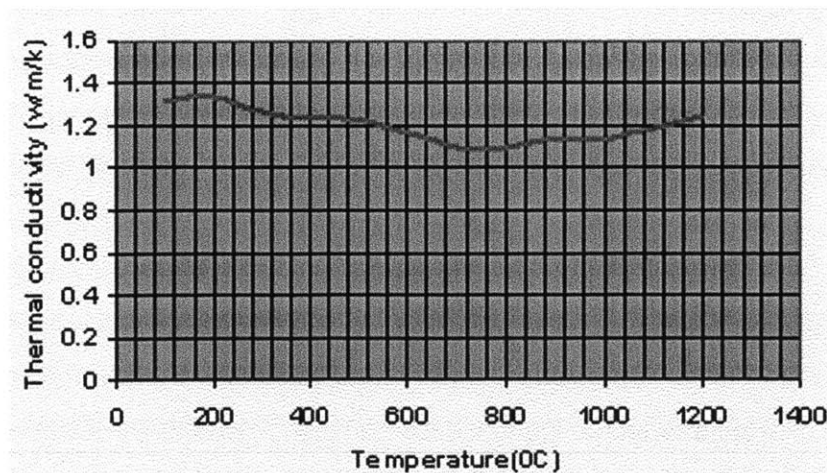


Figure 4.2 Thermal conductivity of 8% YSZ at Various Measuring Temperatures [59]

4.3 Motivation for Research in Thermal Barrier Coatings for Super Truck Project

Recently the requirement for aftertreatment of exhaust gasses for NO_x emissions through catalysts in the exhaust stream has relaxed the demands for in-cylinder NO_x reduction. This allows for increased combustion chamber temperatures and optimized engine timing.

Additionally, upcoming fuel economy regulations, which will be phased in from 2014-2018, will be technology forcing, requiring advanced vehicle technologies and drive systems. Many OEMs are investigating the use of Rankine cycle waste heat recovery in the exhaust stream. Waste heat recovered can be used to drive vehicle accessories and reduce auxiliary component demands on the engine. Preliminary investigations and tests of these systems have shown that ~5% BSFC improvement can be expected [60]. These factors allow for greater combustion chamber temperatures and increases the benefits associated with a low heat rejection engine as more energy is available in the exhaust stream for turbochargers, Rankine cycle waste heat recovery, and turbocompounding.

In this research program the use of TBC was investigated for a novel approach of strategically changing cylinder liner temperatures to improve the power cylinder frictional losses. By coating selected parts of the liner where piston speeds are high, the piston mid-stroke, local liner temperature is raised. In this region the lubrication regime of the piston and liner interface is hydrodynamic, and is the region where the majority of the power cylinder work losses occur due to the high sliding speeds. At the TDC and BDC regions the majority of power cylinder wear occurs and the lubrication regime is primarily boundary lubrication. While friction forces are high, surface speeds are very low resulting in low work losses. Increasing liner temperature in this region is undesirable because it further decreases the oil film thickness and therefore increases wear. This is especially true in the top ring reversal zone.

4.3.1 Power Cylinder Lubrication

In an internal combustion engine the power cylinder is an extremely demanding environment for lubricants. Oil films in this region must promote a air-tight seal between the piston rings and the cylinder liner to ensure that no combustion gasses “blow by”; thereby reducing engine efficiency and increasing emissions. The lubricant provides critical cooling to the power cylinder, namely

the piston, which is cooled only by the splash or spray of oil onto its surface. Lubricant migration to the combustion chamber must be minimized because excess lubricant can vaporize or burn off generating unwanted emissions and requiring constant make-up of fresh lubricant to be added to the engine. Finally, and perhaps most importantly, the lubricant provides the low friction surface that minimizes wear and allows proper engine functionality.

Speeds, forces, and temperatures all vary greatly within the power cylinder, making lubrication a greater challenge. Surface speeds dramatically fluctuate as the piston travels along its stroke from BDC to TDC. Instantaneous piston speed changes from 0 m/s at BDC to a peak speed of over 15 m/s at the mid-stroke before decreasing back to 0 m/s and reversing direction at TDC. Piston velocity and a function of crank angle can be seen in Figure 4.3.

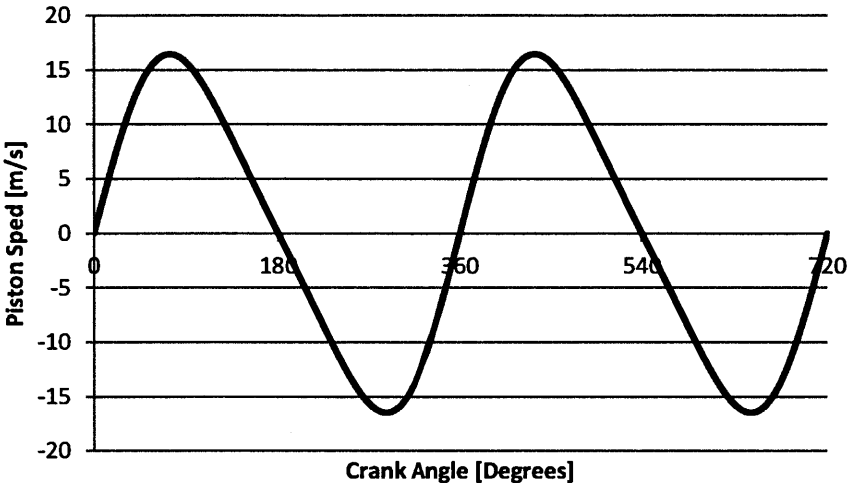


Figure 4.3 Instantaneous Piston Velocity as a Function of Crank Angle

High combustion temperatures present at the top of the cylinder liner cause a substantial temperature gradient from the TDC to the BDC of the engine. A common correlation is that proposed by Woschni, shown in Equation (4.1) where T_{TDC} and T_{BDC} are the liner temperatures at TDC and BDC, x is the position on the liner measured from TDC, and L is the cylinder liner length or piston stroke.

$$t(x) = T_{TDC} - (T_{TDC} - T_{BDC}) \sqrt{\frac{x}{L}} \tag{4.1}$$

Figure 4.4 shows a typical temperature distribution for the cylinder liner of a diesel engine. The peak liner temperature at TDC is around 170°C and decreases to approximately 100°C at BDC. This temperature distribution means that at TDC the lubricant viscosity is low and the oil film is very thin. This combination of high loading and poor lubrication leads to increased boundary contact and wear in this region. Typically wear in top ring reversal zone is the only visible wear on a modern HD diesel engine cylinder liner after durability tests or during engine overhauls.

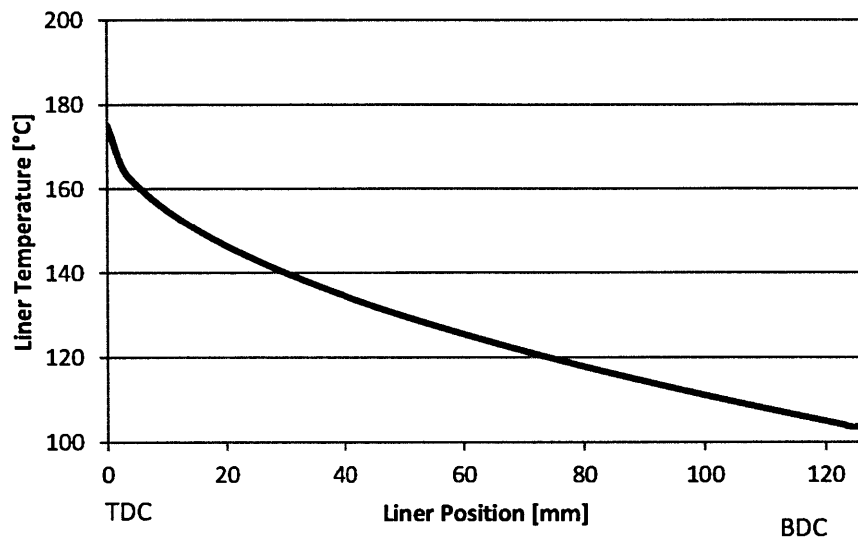


Figure 4.4 Cylinder Liner Wall Temperature Distribution

With the low surface speeds and high temperatures present at TDC region, a thick lubricant film is desirable to reduce friction, boundary contact, and wear. A thick lubricant film is also desirable at BDC where low surface speeds exist. Moving away from the TDC and BDC as piston speeds increase, the lubrication regime becomes hydrodynamic. Hydrodynamic drag and the high piston speeds at the mid-stroke lead to high work losses. This translates into a substantial amount of the power cylinder friction. Ideally, work losses would be minimized in this region by reducing hydrodynamic drag. Reductions can be accomplished by decreasing the duty parameter of the contact surfaces. Surface speed and loading forces cannot easily be changed, whereas the lubricant viscosity can be changed significantly with a simple oil change. Lowering lubricant viscosity will generate lower hydrodynamic drag in the piston mid-stroke and lower frictional losses. This strategy however, will lead to increased friction and wear and the TDC and BDC regions. Ideally the lubricant employed would have high viscosity at TDC and

BDC regions and a low viscosity in the mid-stroke. This would optimize friction performance while maintaining engine durability.

Using the Woschni correlation of cylinder liner wall temperature and the Vogel equation outlined in Section 2.2.2 (pg. 43) and shown below in Equation (4.2) the lubricant viscosity along the cylinder liner can be plotted. This result is shown in Figure 4.5 for several reference oils of various viscosity grades. Properties of the oils used can be found in Appendix A. As can be seen the actual lubricant viscosity is markedly different than the ideal viscosity curve shown. While it may not be possible to reach the ideal viscosity curve, selectively increasing the cylinder liner temperature in the mid-stroke region will decrease the lubricant viscosity, bringing the actual viscosity curve closer to the ideal case. This leads to reduced power cylinder friction without the normal drawbacks of traditional low engine friction technologies – increased wear, emissions, and reduced durability.

$$v = k \cdot \exp\left(\frac{\theta_1}{\theta_2 + T}\right) \quad (4.2)$$

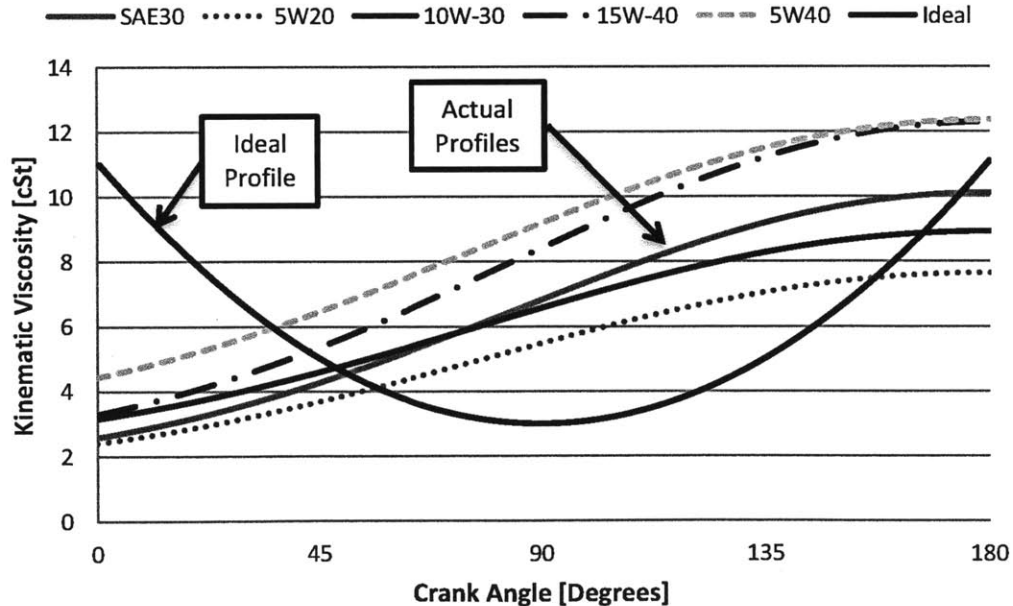


Figure 4.5 Kinematic Viscosity of Lubricant on Cylinder Liner versus Ideal Case

4.4 Modeling Approach and Details

This study involved the use and modification of a model developed by Wong et al. to illustrate the fundamental physical basis of applying thermal barrier coatings to improve the performance of IC engines [61]. A thermodynamic model is used to simulate engine performance and heat release rates within the cylinder. Additional parameters are used to model the heat transfer and wall temperatures to critical combustion chamber components, the piston, cylinder head, and the cylinder liner. The focus of this study was the application of TBC on the cylinder liner.

Parameters varied were application region on the cylinder liner, TBC thickness, and convective heat transfer coefficients from the cylinder liner to the engine coolant.

4.4.1 Overview of Model

This model is a mathematical model of the primary physical processes that occur in a complete four stroke engine cycle. Work done by the piston; mass flow rates through the intake and exhaust valves; heat release during combustion; and heat transfer rates at the piston, cylinder head, and liner surfaces are calculated. Overall engine performance characteristics, including thermal efficiency, indicated specific fuel consumption (isfc), indicated power, exhaust gas enthalpy, and turbocharger boost pressure ratio are also determined.

This model assumes simple combustion chamber geometry as shown in Figure 4.6. The model allows the application of TBC in any thickness and conductivity to any individual or combination of components. The thermodynamic model of the engine cycle consists of three parts, the intake stroke from 0-180° crank angles, the compression and expansion strokes which occur from 180-540° with the intake and exhaust valves closed, and finally the exhaust stroke from 540-720°.

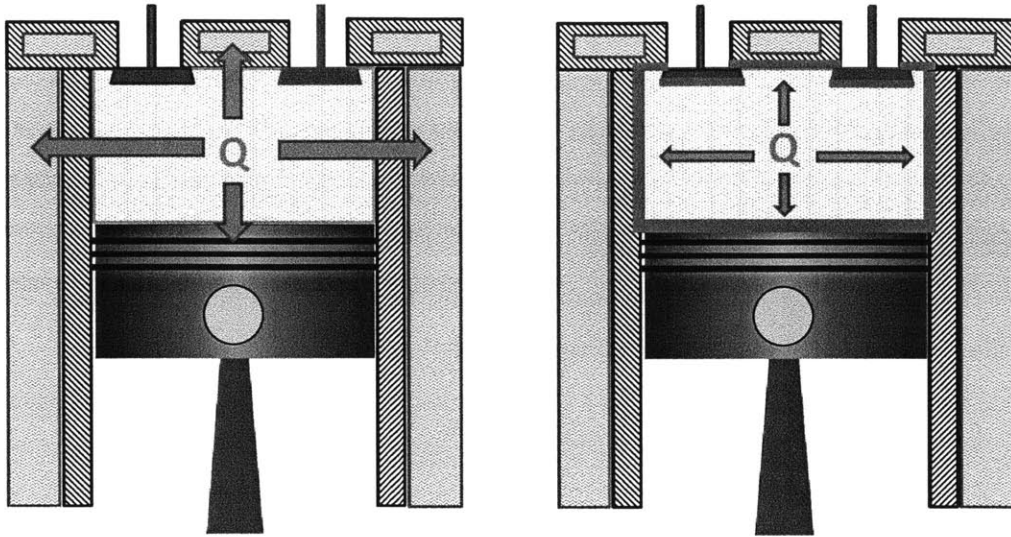


Figure 4.6 Geometry of Power Cylinder Without and With TBC

Cylinder pressure and mass contained in the combustion chamber are the primary variables in the simulation, and all other parameters are calculated from these values. Mass flow is determined by air flow through the valves during the gas exchange process. Valve area, the opening duration and timing within the engine cycle, in addition to a discharge coefficient are input variables for each unique engine configuration. The First Law of Thermodynamics determines the cylinder pressure development during the compression and expansion strokes. Key parameters that control cylinder pressure include the work done by the piston, heat release from combustion, and heat transfer rates to the piston, cylinder head, and liner.

$$\left(\frac{C_v}{R+1}\right)p \frac{dV}{d\theta} + \left(\frac{C_v}{R}\right)V \frac{dp}{d\theta} = \frac{dQ_{ch}}{d\theta} - \frac{dQ_{ht}}{d\theta} \quad (4.3)$$

Equation (4.3) is used to calculate the cylinder pressure versus time where:

- p is the cylinder pressure
- V is the cylinder volume
- θ is the crank angle
- C_v is the specific heat at constant volume
- R is the gas constant
- Q_{ch} is the chemical heat release from fuel combustion
- Q_{ht} is the heat transfer to the surroundings

Ideal gas properties are assumed during the cycle for simplicity. A Wiebe-function type equation models the cumulative heat release fraction x_b based on several input parameters. These inputs are the start of combustion θ_s , the combustion duration θ_d , the Wiebe form factor n , and the Wiebe efficiency factor, a [62].

$$x_b(\theta) = 1 - \exp \left[-a \left(\frac{\theta - \theta_s}{\theta_d} \right)^n \right] \quad (4.4)$$

Mass flow through the intake and exhaust valves is derived from one-dimensional isentropic compressible flow through a restriction. These equations are calibrated using empirical data to determine a discharge coefficient, C_D . A valve reference area A_R is used due to the complex nature of valve flow area as the cam opens and closes the valve. In this study the valve curtain area was used, shown below in Equation (4.5) where D_v is the head diameter of the valve and L_v is the valve lift [3].

$$A_R = \pi D_v L_v \quad (4.5)$$

Equation (4.6) was used to calculate valve mass flow. Important parameters are the upstream stagnation pressure, p_0 , and temperature, T_0 , and the static pressure immediately following the flow restriction, p_T . R is the gas constant and γ is the specific heat ratio, which is an input parameter in the model [3].

$$\dot{m} = \frac{C_D A_R p_0}{(RT_0)^{1/2}} \left(\frac{p_T}{p_0} \right)^{1/\gamma} \left\{ \left(\frac{2\gamma}{\gamma-1} \right) \left[1 - \left(\frac{p_T}{p_0} \right)^{\frac{\gamma-1}{\gamma}} \right] \right\}^{1/2} \quad (4.6)$$

For choked flow, Equation (4.7) is used to calculate the mass flow. For the intake valve p_0 is the intake pressure and p_T is the cylinder pressure. For the exhaust valve p_0 is the cylinder pressure and p_T is the exhaust system pressure [3].

$$\dot{m} = \frac{C_D A_R p_0}{(RT_0)^{1/2}} \gamma^{1/2} \left(\frac{2}{\gamma+1} \right)^{\frac{1+\gamma}{2(\gamma-1)}} \quad (4.7)$$

The model includes a generic turbocharger which is modeled after Equation (4.8) shown below

$$\left(\frac{P_c}{P_{atm}} \right)^{\frac{r_c-1}{r_c}} = \eta_c \eta_t \eta_m \frac{c_{p,t}}{c_{p,c}} \left(1 - \frac{P_{atm}}{P_t} \right)^{\frac{r_t-1}{r_t}} \frac{T_e}{T_{atm}} \quad (4.8)$$

Where:

- P_c, P_t, P_{atm} pressure are compressor outlet, turbine inlet, and atmospheric pressure
- T_e, T_{atm} exhaust and ambient temperature
- $c_{p,t}, c_{p,c}$ specific heat of gasses at turbine and at the compressor
- r_c, r_t specific heat ratio of gasses at compressor and at the turbine
- η_c, η_t, η_m compressor, turbine, and mechanical efficiencies of the turbocharger

These equations allow the calculation of cylinder pressure against crank angle, from this the work output can be determined for different shape and time-phasing of the combustion heat release. These outputs are then used to calculate the heat transfer to the cylinder liner, piston, and cylinder head.

For the heat transfer calculations, an initial wall temperature for each component is input into the model. The combustion gas properties are used to calculate an instantaneous convective heat transfer coefficient between the combustion gasses and the engine for each crank angle interval specified in the program. First a Reynolds number is calculated. The length scale to characterize the combustion gasses is the lower of the exposed liner height or half the cylinder bore.

Characteristic velocity is taken as the greater of the instantaneous piston speed or the average piston speed. This is shown below in Equation (4.9), where L is the length scale, V is the velocity, ρ is the density of the combustion gasses, and μ is the viscosity of the combustion gasses, based on Equation (4.10).

$$Re = \frac{LV\rho}{\mu} \quad (4.9)$$

$$\mu = 3.3 \times 10^{-4} T_{gas}^{0.7} \quad (4.10)$$

From this, a Nusselt number is calculated based on the correlation shown in Equation (4.11), where the parameter a is an input variable in the model allowing the heat transfer to be modified by the user for each phase on the engine cycle (intake, power, exhaust). An overall heat transfer coefficient is then calculated using Equation (4.12) where k is the thermal conductivity. The overall heat transfer from the combustion gasses to the piston, head, and liner walls for that time interval is calculated using Equation (4.13) where A is the wall area of the respective component. It should be noted that only the instantaneous area of the cylinder liner exposed (e.g. the area between the cylinder head and the piston) to the combustion gasses was considered in the heat transfer calculation.

$$Nu = aRe^{0.7} \quad (4.11)$$

$$h = \frac{k}{L} Nu \quad (4.12)$$

$$Q = hA(T_{gas} - T_{wall}) \quad (4.13)$$

This calculation is repeated over the engine cycle at the user specified crank angle step. The heat transfer between the combustion gasses and the piston, cylinder head, and each 10 cylinder liner segments is summed to find cycle totals.

In order to calculate the correct wall temperatures for the piston, head, and liner the total cycle convective heat transfer from the combustion gasses to the wall is compared with the conductive heat transfer through the respective engine components to the engine coolant. In the model, two solid layers were assumed between the combustion gasses and the engine coolant, one representing the base metal of the engine component and the other the thermal barrier coating.

An overall thermal resistance is calculated for the TBC/base metal/coolant based on the diagram seen in Figure 4.7. Please note this is shown for the cylinder liner where cylindrical coordinates have been used, and for the piston and cylinder head the resistances through the TBC/metal are simply L/k .

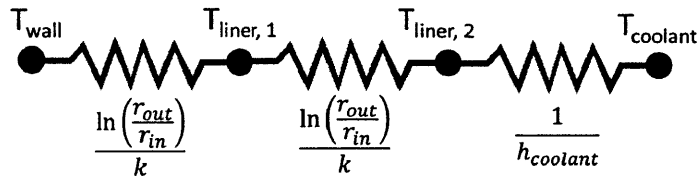


Figure 4.7 Thermal Resistance Circuit

The wall temperature, T_{wall} , is determined from the previous iteration or the initial input by the user, and the coolant temperature, $T_{coolant}$, is also specified by the user. The overall resistances are calculated using Equations (4.14) and (4.15) below, the former used for the cylinder head and piston, while the latter is use for the cylinder liner. The program was also run initially assuming that the wall and coolant interface had a negligible thermal resistance when compared to that of a TBC and therefore was not included in the calculation.

$$U_i = \frac{1}{\frac{L_1}{k_1} + \frac{L_2}{k_2} + \frac{1}{h_{coolant}}} \quad (4.14)$$

$$U_i = \frac{1}{\frac{r_1}{k_{1,i}} \ln\left(\frac{r_{2,i}}{r_{1,i}}\right) + \frac{r_1}{k_{2,i}} \ln\left(\frac{r_{3,i}}{r_{2,i}}\right) + \frac{r_1}{r_{3,i}} \frac{1}{h_{coolant}}} \quad (4.15)$$

$$T_{wall,i} = \frac{Q_i}{A_i U_i} + T_{coolant,i} \quad (4.16)$$

Finally, Equation (4.16) is used to predict the wall temperature required to match the convective heat transfer from the combustion gasses. The program then iterates until the two values of heat transfer are equal to one another. This is typically obtained in less than 30 iterations.

4.4.2 Modifications to Model

This model allows TBC coatings to be applied to all the components of the combustion chamber, including the piston, cylinder head, and cylinder liner. The cylinder liner has been discretized into 10 different segments which can have varying liner thicknesses, conductivities, TBC coating thickness, and TBC conductivity. Effects of conduction in the axial direction along the cylinder liner were included in the model to provide an accurate prediction of the axial liner temperature distribution. In addition, an external heat transfer coefficient from the cylinder liner wall to the engine coolant can be input to represent values typical of water cooled engine or an air cooled engine. This modification of the cylinder liner parameters allows the study of selective coating of the cylinder liner to maximize power cylinder efficiency while minimizing the risk to the durability, emissions performance, and power of the engine.

Previous simulations using the model were focused on engine performance parameters such as thermal efficiency and exhaust gas enthalpy. To study the cylinder liner temperature profile it was necessary to modify the model to discretize the liner into 10 separate, equally-spaced segments along its length. Figure 4.8 shows each of the segments, with segment 1 corresponding to the top 1/10th of the liner near the TDC region and segment 10 the bottom 1/10th of the liner near BDC. This allowed the heat transfer through each liner segment to be calculated in addition to the liner temperature.

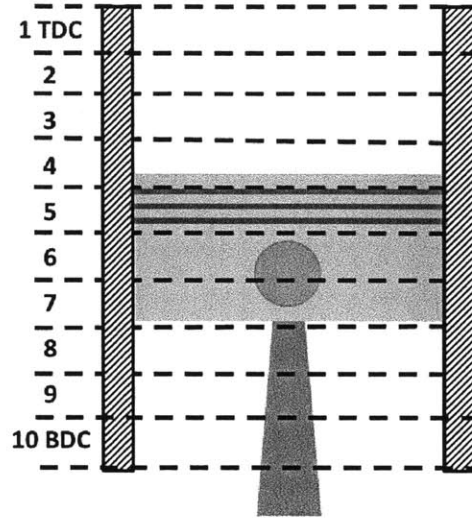


Figure 4.8 Diagram of Cylinder Liner Segments in Model

The program calculates the heat transfer from the combustion gasses to the cylinder liner wall for each crank angle. This heat flux is then used to determine the cylinder liner wall temperature using Equation (4.17) and Equation (4.18) for each liner segment over the entire engine cycle. In these equations r_1 is half the engine bore, r_2 is the radius at the interface of the TBC and base metal, r_3 is the outer radius of the cylinder liner and TBC, k_1 and k_2 correspond to the thermal conductivity of each layer (eg base metal and TBC). These factors are represented by an overall heat transfer coefficient U . This is used in Equation (4.18) to calculate the liner temperature, T_{liner} , based on the heat transfer from the combustion chamber, Q , the area of the cylinder liner, A , and the engine coolant temperature, $T_{coolant}$. The program uses an initial prediction of liner, piston, and head temperatures and is iterated until the previous and current calculated temperatures converge. The program allows for each liner segment to have different thermal conductivities, thicknesses, and different convective heat transfer coefficients.

$$U_i = \frac{1}{\frac{r_1}{k_{1,i}} \ln\left(\frac{r_{2,i}}{r_{1,i}}\right) + \frac{r_1}{k_{2,i}} \ln\left(\frac{r_{3,i}}{r_{2,i}}\right) + \frac{r_1}{r_{3,i}} \frac{1}{h_{o,i}}} \quad (4.17)$$

$$T_{liner,i} = \frac{Q_i}{A_i U_i} + T_{coolant,i} \quad (4.18)$$

Axial conduction within the cylinder liner is an important mechanism when considering the cylinder liner temperature profile. These effects were included in the model by using the

temperature history of each liner segment as the model is iterated. Simple one-dimensional conduction is assumed based on the cylinder liner's small thickness relative to its length. Figure 4.9 represents a liner segment control volume, the axial conduction in and out of the segment and the convective heat transfer from the combustion chamber gasses and the heat rejection to the engine coolant.

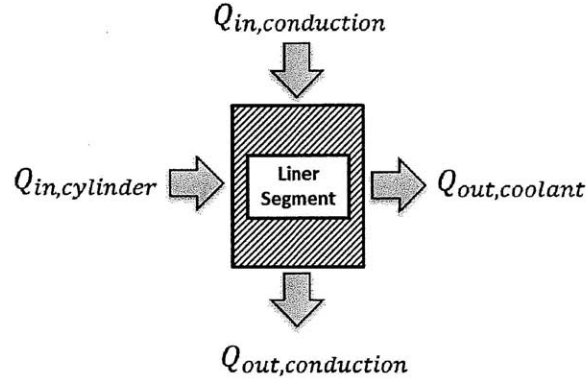


Figure 4.9 Heat Transfer Element of Cylinder Liner

Governing equations were assembled based on Figure 4.9 to derive an expression for the cylinder liner temperature with axial conduction. Equation (4.19) is an energy balance, energy in is from $Q_{in,cylinder}$ and the axial conduction from the previous segment, where k_i is the thermal conductivity, A_i is the area of the cylinder liner looking down its axis, H is the segment height, $T_{L,i-1}$ is the temperature of segment above, and $T_{L,i+1}$ is the temperature of the segment below. Energy removed from the segment is done by convection with the engine coolant and by conduction down the cylinder liner. U is the same as calculated in Equation (4.17), and A_1 is the area of the liner exposed to engine coolant. This equation is simplified and re-arranged to find an expression for the liner temperature, shown in Equation (4.20).

$$0 = Q_{in,cylinder} - UA_1(T_{L,i} - T_{coolant}) + \frac{k_i A_i}{2H}(T_{L,i-1} - T_{L,i}) - \frac{k_i A_i}{2H}(T_{L,i} - T_{L,i+1}) \quad (4.19)$$

$$T_{L,i} = \frac{Q_{in,cylinder} + UA_1 T_{coolant} + \frac{k_i A_i}{2H}(T_{L,i-1} + T_{L,i+1})}{\frac{k_i A_i}{2H} + UA_1} \quad (4.20)$$

The final modification to the existing model was to incorporate the convective heat transfer coefficient between the cylinder liner and the engine coolant. The equations above all

incorporate this coefficient. Previous studies focused on fully insulated engines, where the thermal resistance between the cylinder liner and coolant was negligible in comparison to the TBC applied to the entire cylinder liner.

4.5 Results and Discussion

Simulations were run using a generic 5.9L diesel engine whose input parameters are outlined in Table 4.1. Since heat transfer between different cylinders in a multi-cylinder engine is not expected to vary significantly this simulation is run for a single cylinder only. An engine operating point of 2500 RPM and a fueling rate of 45 kW was used for this generic simulation; which would correspond to approximately half load for an engine of this size.

Table 4.1 Model Input Parameters for Engine Geometry, Timing, Fuel and Air Input

<u>Engine Parameters</u>		<u>Timing Parameters</u>	
Bore	102 mm	Intake Valve Closing	280°
Stroke	120 mm	End of Expansion Stroke	540°
Connecting Rod Length	192 mm	Start of Combustion	335°
Compression Ratio	17.5	90% Burn Duration	30°
Intake Valve Flow Area	1408 mm ²		
Exhaust Valve Flow Area	1432 mm ²		
Intake Valve Discharge Coefficient	0.9		
Exhaust Valve Discharge Coefficient	0.9		
Compressor Efficiency of Turbo	0.8		
Turbine Efficiency of Turbo	0.8		
Mechanical Efficiency of Turbo	0.9		
Boost Pressure Ratio of Turbo	2.3		
RPM	2500 RPM		

<u>Fuel and Air Properties</u>	
Gamma Intake Air	1.35
Intake Air Temperature	300 K
Intake Air Pressure	101.3 kPa
Fueling Rate (Fuel Energy)	45 kW
Fuel Lower Heating Value	43 MJ

4.5.1 Study of Thermal Barrier Coating Thickness and Application Zone on Cylinder Liner Temperature

Simulations were run for varying TBC thickness from 0.5 to 3mm on the cylinder liner. The application zone of the TBC included the entire cylinder liner, the bottom 60% of the cylinder liner, and the piston mid-stroke only (Shown in Figure 4.10). No TBC was applied to the cylinder head or piston. Cylinder liner cooling was assumed to be provided by water at a temperature of 375 K and a heat transfer coefficient of 5000 W/m²-K, based on values provided in literature [63]. The thermal barrier coating was assumed to be PSZ with a thermal conductivity

of 1.3 W/m-K. Additional input parameters for key component materials, thermal conductivities and thicknesses are found in Table 4.2.

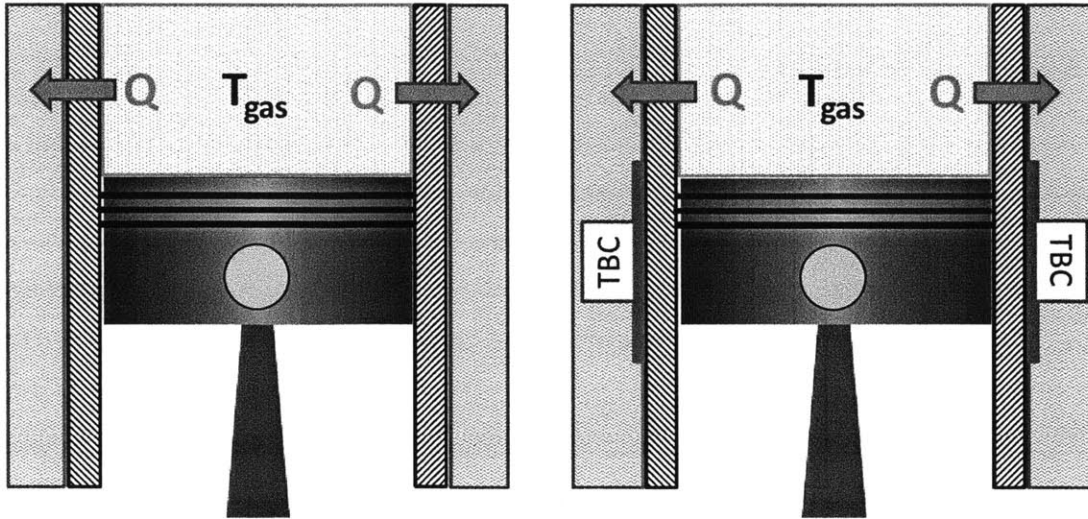


Figure 4.10 Conventionally Cooled Cylinder Liner and Liner with TBC on Mid-Stroke

Table 4.2 TBC Parameters and Additional Model Inputs

TBC Conductivity	1.3 W/m-K
Cylinder Liner Conductivity	80 W/m-K
Cylinder Head Conductivity	80 W/m-K
Piston Conductivity	80 W/m-K
Cylinder Liner Thickness	1 cm
Cylinder Head Thickness	6 cm
Piston Thickness	1.5 cm
Engine Coolant Temperature	375 K

A baseline case was run with no TBC and compared with the Woschni square root correlation of the axial cylinder liner temperature profile shown in Equation (4.1). The results are shown in Figure 4.11. The temperature profile along the liner is the cycle average calculated from the total heat transfer, it does not take into account the fluctuation in surface temperature due to cylinder gas temperature during the combustion and exhaust strokes. The correlation and the model are in good agreement on the cylinder liner temperature profile for the baseline case. This has been compared against empirical observations from engine tests and is also in good agreement.

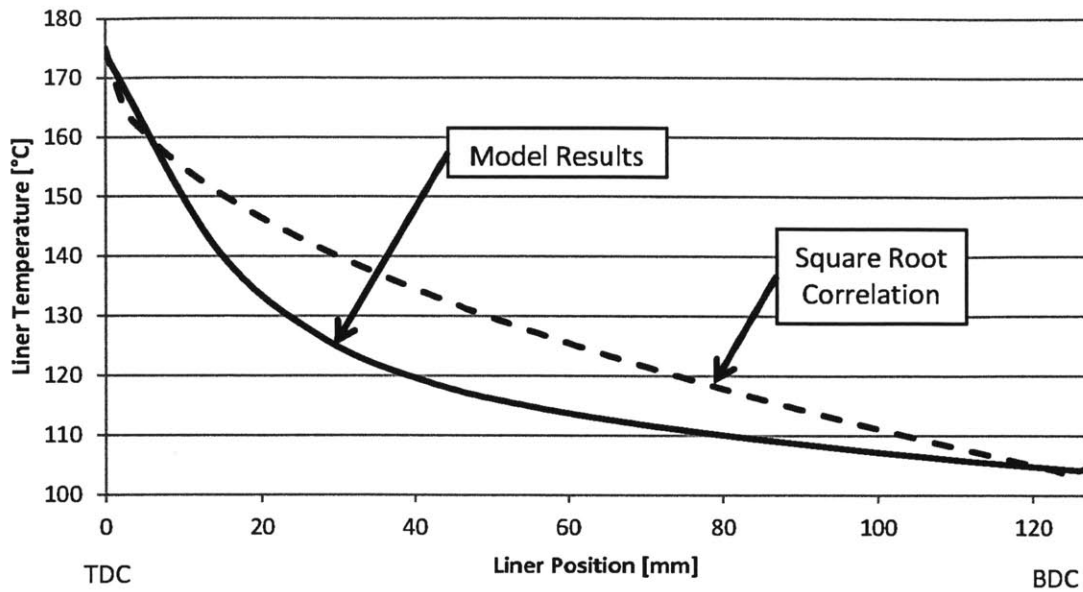


Figure 4.11 Liner Wall Temperature Woschni Correlation vs Model

With the baseline case established and a temperature distribution from TDC to BDC of approximately 175°C to 100°C, applications of TBC from 0.5 to 3 mm thick were applied to the entire cylinder liner. The results are shown in Figure 4.12. Please note that the x-axis represents each liner segment in the model with segment 1 occupying the top 1/10th of the liner length, and segment 10 corresponding to the bottom 1/10th of the liner length as shown schematically in Figure 4.8.

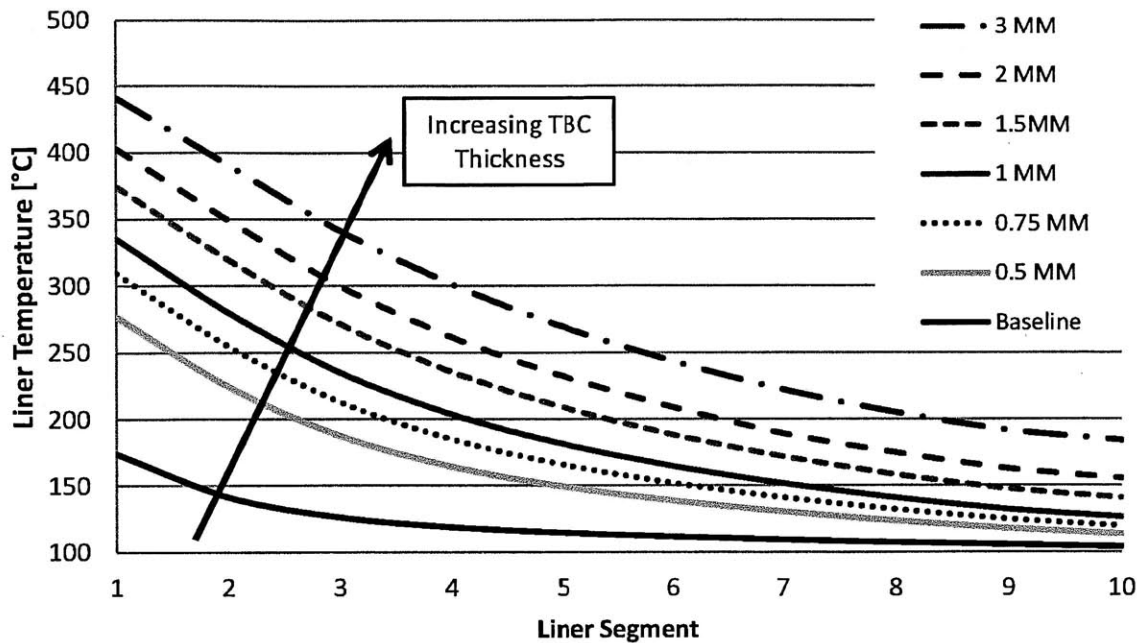


Figure 4.12 Liner Temperature Profile with TBC on Entire Liner

As expected, the cylinder liner temperature increases dramatically when the entire cylinder liner is coated. Increased coating thickness, and hence insulation value, causes a further rise in cylinder liner temperatures close to a maximum of 450°C. At these high temperatures along the liner, lubricant degradation rates would be high in addition to increased boundary friction and component wear. As mentioned previously, conventional lubricants used in HD Diesel engines will breakdown above 350°C. The TBC did increase the exhaust gas enthalpy 10.43% with the 3 mm coating in addition to a small increase in thermal efficiency, despite the piston and head remaining uncoated.

Figure 4.13 and Figure 4.14 show two different application zones of TBC. The first application involves coating just the piston mid-stroke section of the liner, which corresponds to segments 4,5,6 in the model. As can be seen in Figure 4.13, this causes the temperature in the mid-stroke region to raise approximately 35 to 60°C, depending on coating thickness. This profile is a substantial improvement over the fully coated liner as the TDC region does not experience any significant increase in temperature because of the TBC. As noted previously, increasing TDC temperature has significant effects on engine durability, a key performance metric for HD diesel engines.

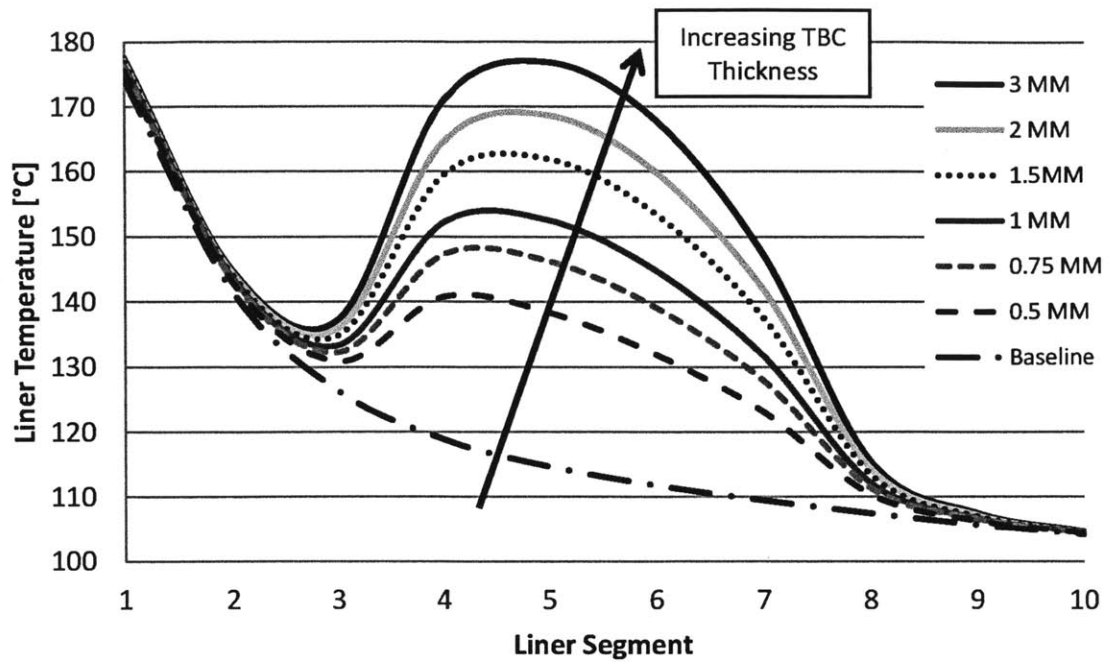


Figure 4.13 Liner Temperature with TBC on Piston Mid-stroke (Segments 4,5,6)

Figure 4.14 displays the results for a liner TBC coating that extends from the beginning of the piston mid-stroke to BDC (segments 4-10). Similar to the results above, the TDC region does not experience any significant increase in temperature. The mid-stroke increases in temperature 35 to 60°C and at BDC the temperature increases 10 to 55°C depending on thermal barrier coating thickness.

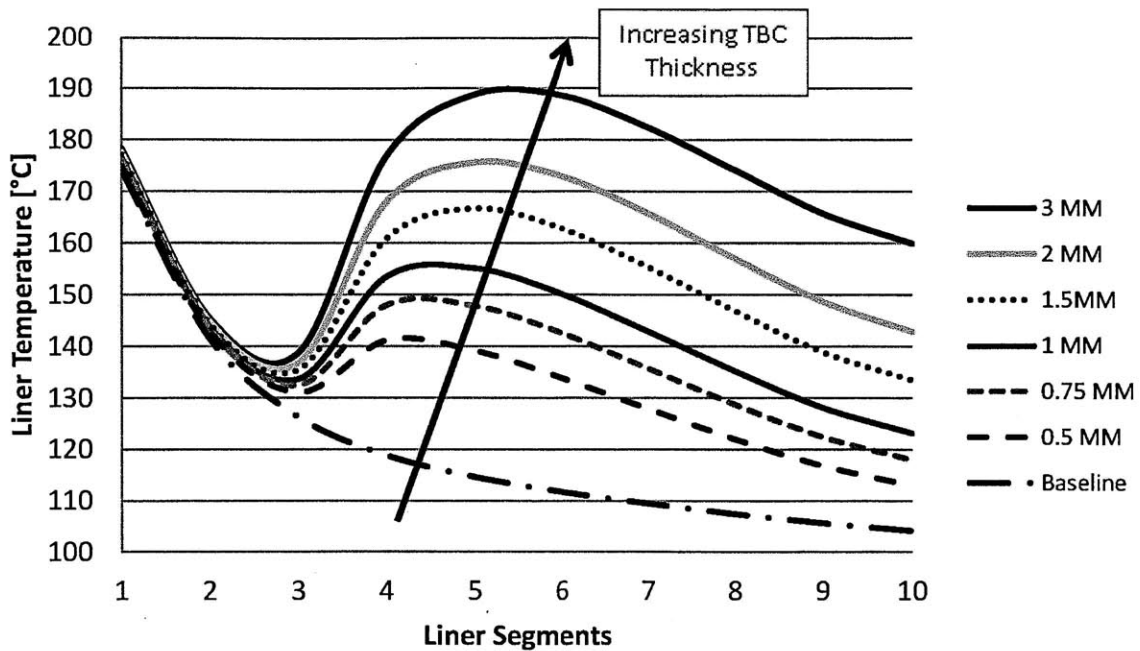


Figure 4.14 Liner Temperature with TBC on Segments 4 through 10

4.5.2 Comparison of Natural Convection Combined Thermal Barrier Coatings on Selected Parts of the Cylinder Liner

The use of wet liners in heavy duty diesel engines provides the potential of eliminating or reducing coolant flow to selective parts of the cylinder liner. Eliminating the coolant flow would place a large resistance to heat transfer between the outside liner surface and the surrounding air. Using natural convection along the liner surface would reduce the convective heat transfer coefficient by a factor of 100. This will lead to a much greater temperature rise than with the use of the thermal barrier coating.

To simulate the effects of using natural convection on the outside of the liner, a convective heat transfer coefficient was input for each cylinder liner segment. For natural convection, a coefficient of $35 \text{ W/m}^2\text{-K}$ was used based on previous literature [63]. Figure 4.15 shows the cylinder liner temperature distribution for a liner cooled by various amounts of natural convection. When natural convection is employed anywhere but the bottom 20-30% of the liner, extremely high liner temperatures are observed. For the case of segments 4-10 covered, peak liner temperature is predicted to be over $285 \text{ }^\circ\text{C}$ at the piston mid-stroke. Applying natural

convection to segments 8 through 10 and segments 9 and 10 raises temperatures to a peak of 165 and 137 °C respectively.

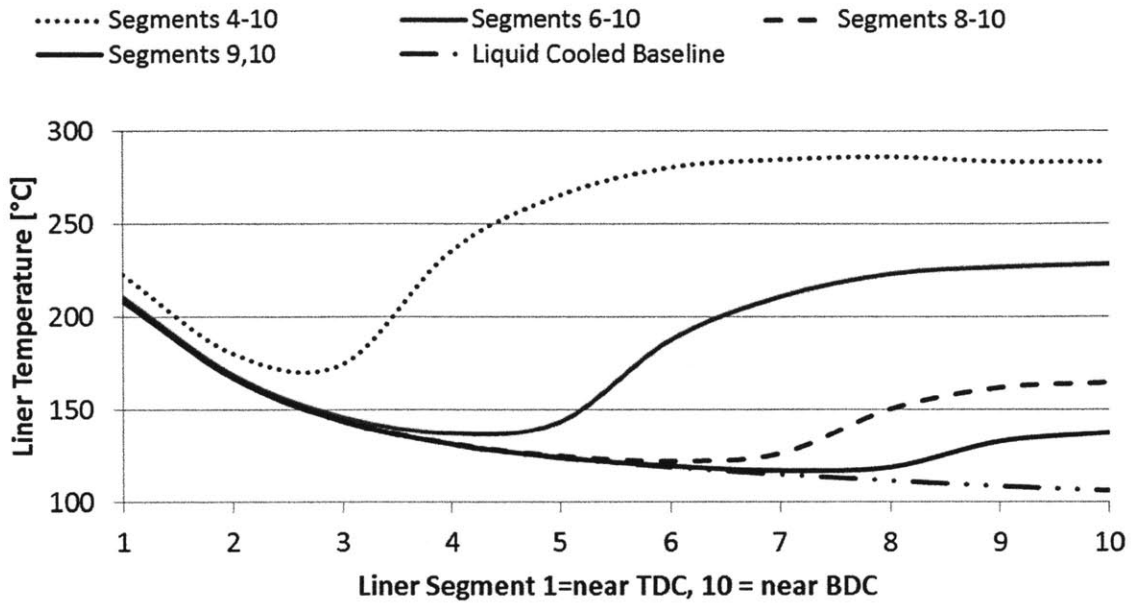


Figure 4.15 Natural Convection Applied to Various Liner Segments

The use of a combination of natural convection in the BDC region of the cylinder liner and thermal barrier coating in the piston mid-stroke was also examined. Figure 4.16 is the simulation results for a cylinder liner that has a coating on the mid-stroke region (segments 4 through 7) and natural convection applied to the BDC region (segments 8-10). This predicts a substantial rise in liner temperature for the bottom 60% of the cylinder liner when compared to the baseline case with water cooling and no thermal barrier coating. In this case the BDC liner temperature of 200°C is nearly the same as the temperature at TDC.

Raising BDC temperatures to the same level as TDC temperatures is not desirable, as higher liner temperatures and reduced lubricant viscosity will increase boundary friction in this region. To reduce BDC temperatures, the simulation was executed for a cylinder liner that was coated for the bottom 20% and had a 1 mm thick TBC applied on the middle 40% of the liner (segments 4-8). The results are shown in Figure 4.17. This application maintains the liner temperature in the bottom 60% of the liner around 165 °C.

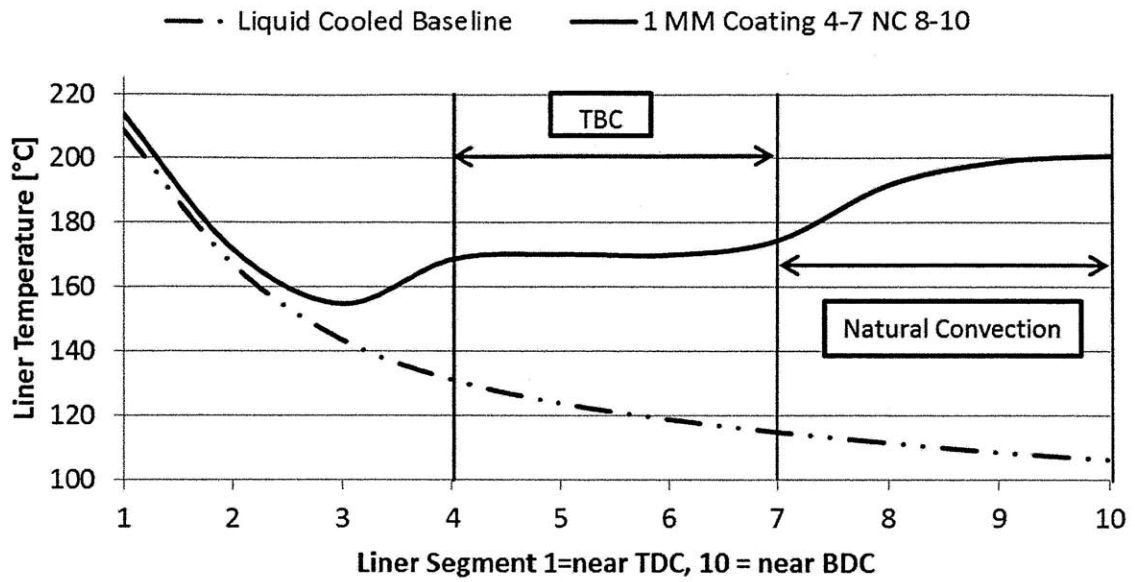


Figure 4.16 Cylinder Liner Temperature Profile with Natural Convection on Bottom 30% of Liner and TBC on Mid-stroke

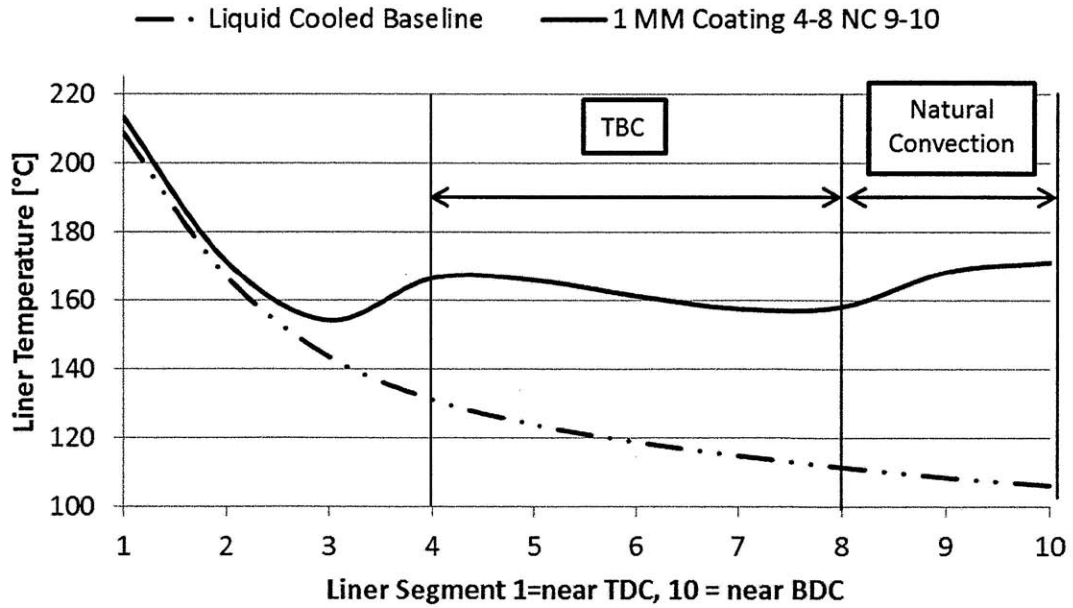


Figure 4.17 Cylinder Liner Temperature Profile with Natural Convection on Bottom 20% of Liner and TBC on Mid-stroke

4.5.3 Study of Thermal Barrier Coating Thickness and Application Zone on Lubricant Kinematic Viscosity

Lubricant viscosity is the critical parameter in improving mechanical friction losses in the power cylinder through lubricant properties. Using the cylinder liner temperature profiles generated in the previous section (Figure 4.12, Figure 4.13, and Figure 4.14), the Vogel equation was used to generate the corresponding lubricant viscosity profile. The baseline lubricant selected for this part of the study was the 15W-40 whose properties are specified in Appendix A.

Figure 4.18, Figure 4.19, and Figure 4.20 show the viscosity profiles along the cylinder liner for a fully coated liner, a liner coated in the mid-stroke, and a liner coated from mid-stroke to BDC, respectively. A fully coated liner results in extremely low lubricant viscosity, most notably at TDC where increased temperatures decrease viscosity from the baseline value of 3.33 cSt to 0.40 to 1.09 cSt depending on TBC thickness. Coating of the mid-stroke region and the coating from the mid-stroke to BDC produces actual lubricant viscosity curves much closer to the ideal curve illustrated in Figure 4.5.

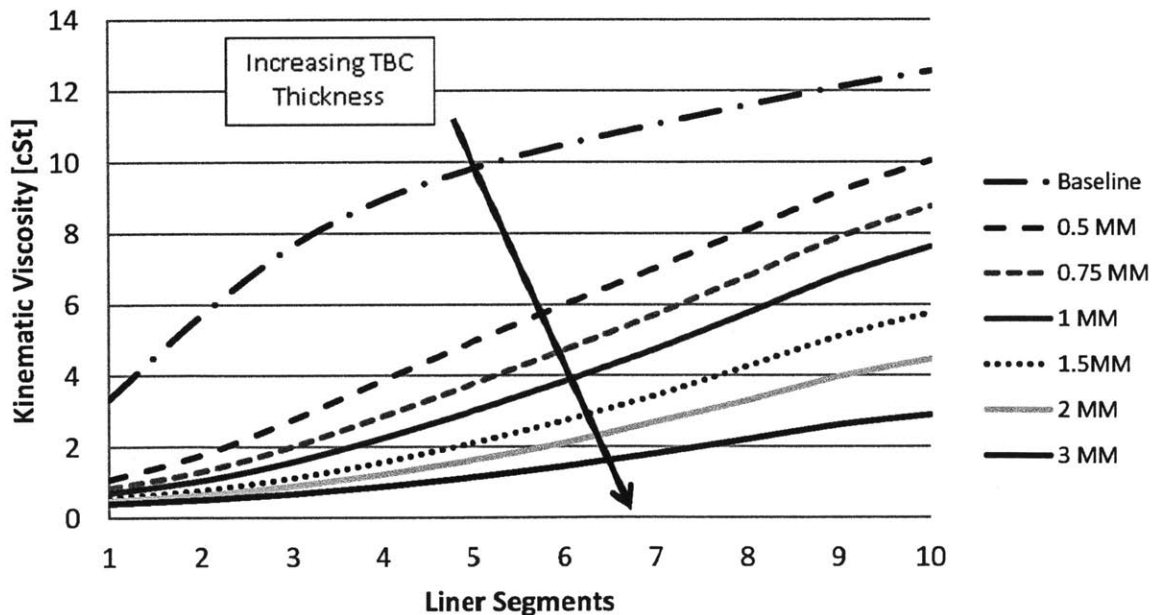


Figure 4.18 Local Viscosity of 15W-40 with TBC on Entire Liner

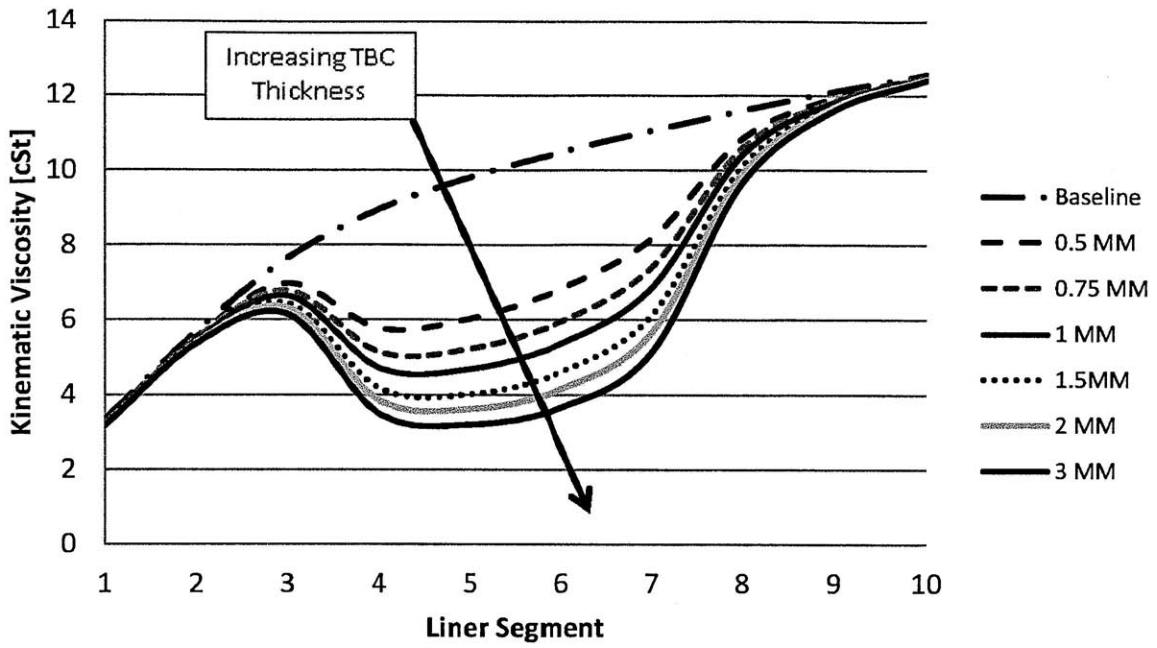


Figure 4.19 Local Viscosity of 15W-40 with TBC on Liner Segments 4,5,6

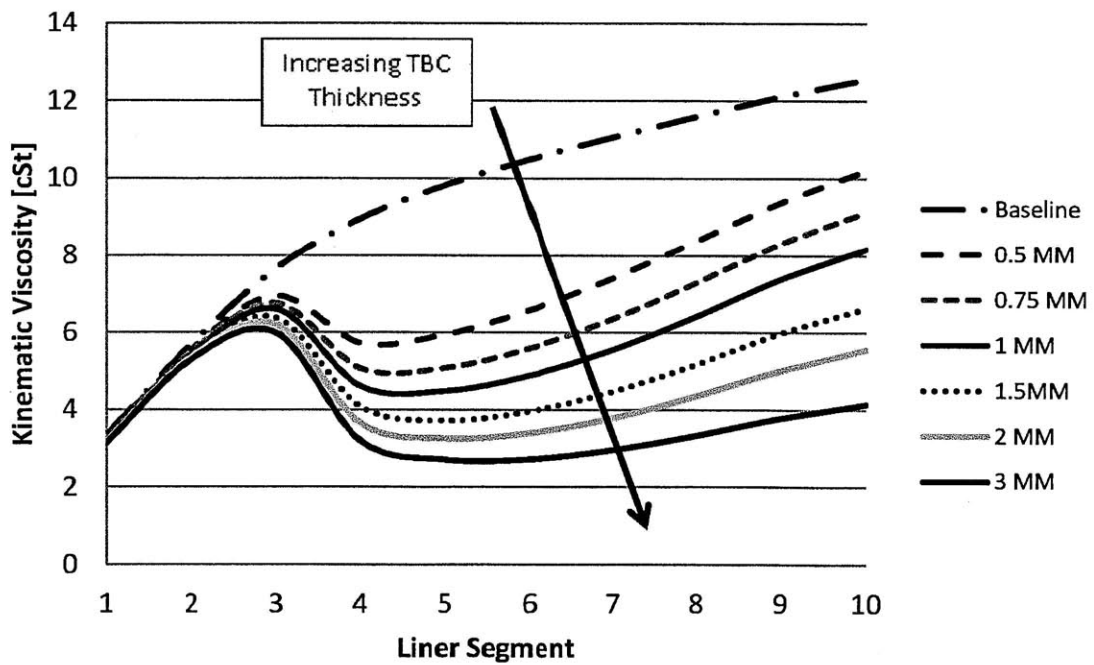


Figure 4.20 Local Viscosity of 15W-40 with TBC on Liner Segments 4 through 10

Viscosity curves were also constructed for the combined natural convection and TBC coating cases. Figure 4.21 shows the lubricant kinematic viscosity for natural convection applied to liner segments 4-10, 6-10, 8-10, and 9-10. Applying natural convection to segments 4-10 and 6-10 creates very low mid-stroke and BDC viscosities, which will lead to increased wear and boundary friction between the liner and piston. When applied to the bottom of the liner, natural convection does little to reduce mid-stroke viscosity, where the greatest friction reduction potential exists.

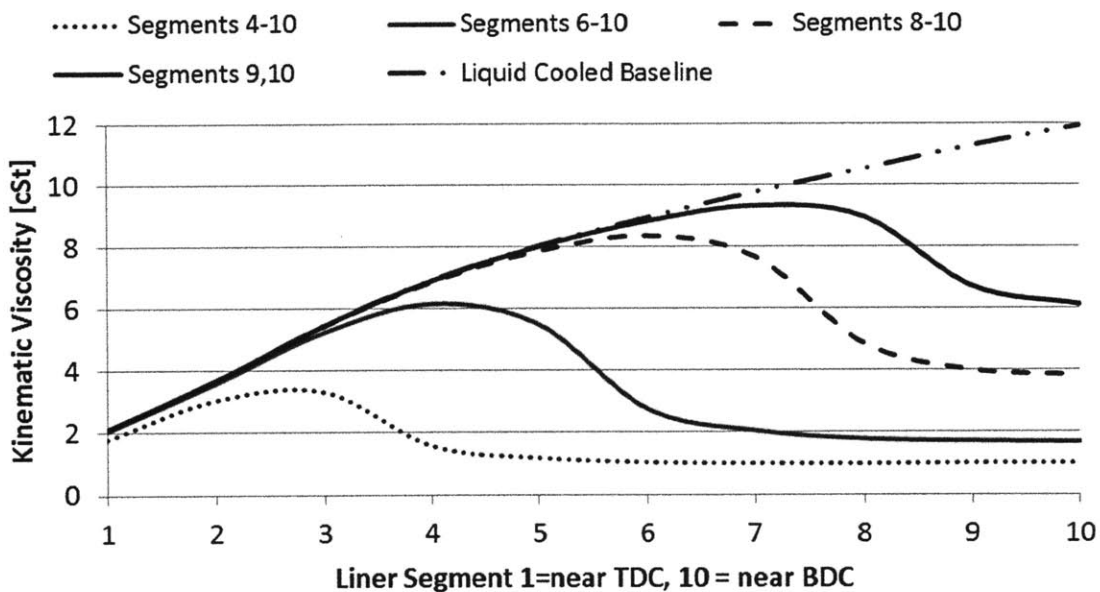


Figure 4.21 Lubricant Viscosity with Natural Convection Applied to Liner Segments

While the use of natural convection alone is not a viable method of raising mid-stroke temperatures without increased wear, there is potential for combining natural convection and a TBC. This approach will raise BDC temperatures, which raises concerns regarding boundary friction and increased wear. However, the BDC region has adequate lubricant supply, unlike TDC where the lubricant supply is very limited by design to minimize oil consumption. Therefore it is likely that increased liner temperatures at BDC will not generate high levels of liner wear and may also reduce power cylinder friction performance. Lubricant kinematic viscosity for a cylinder liner with TBC on segments 4 through 8 and natural convection on segments 9 and 10 is shown in Figure 4.22. This generates a relatively flat viscosity profile for

the lower 70% of the liner with a value of 4 cSt. Figure 4.23 shows results for segments 4 through 7 and natural convection on segments 8 through 10.

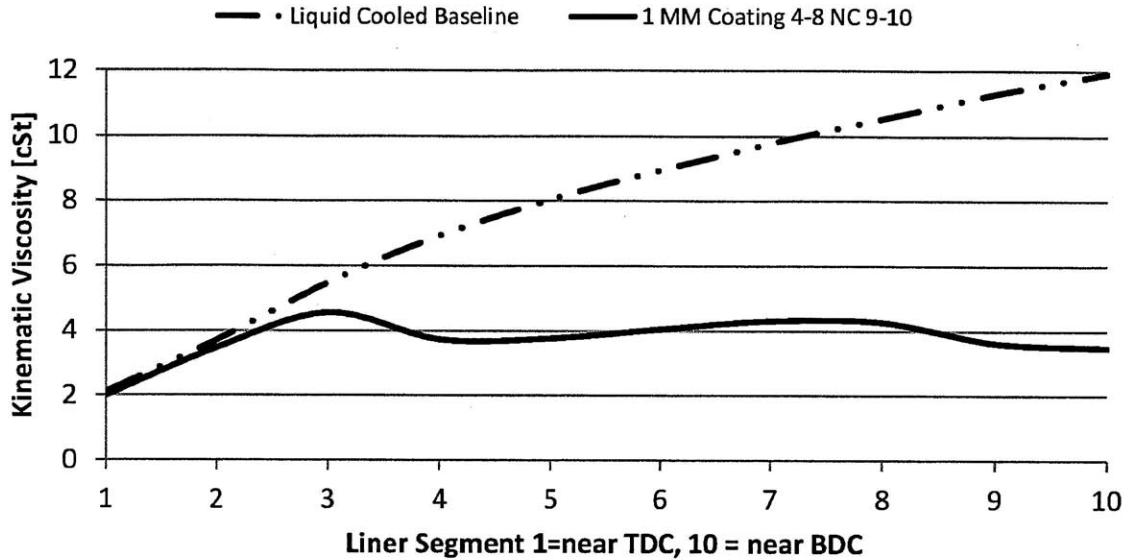


Figure 4.22 Lubricant Viscosity with Natural Convection Applied to Segments 9-10 and TBC from 4-8

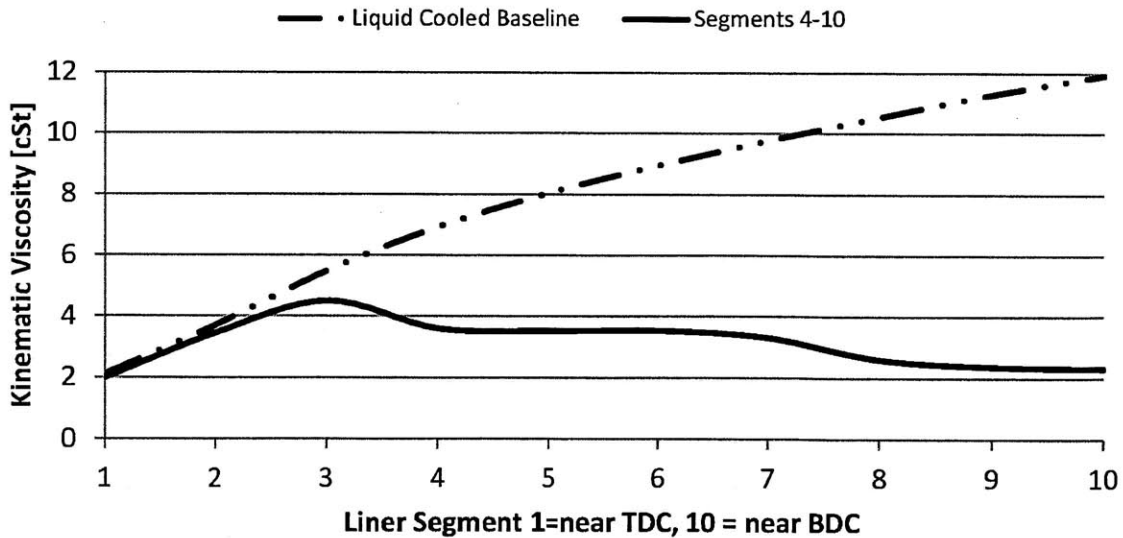


Figure 4.23 Lubricant Viscosity with Natural Convection Applied to Segments 8-10 and TBC from 4-7

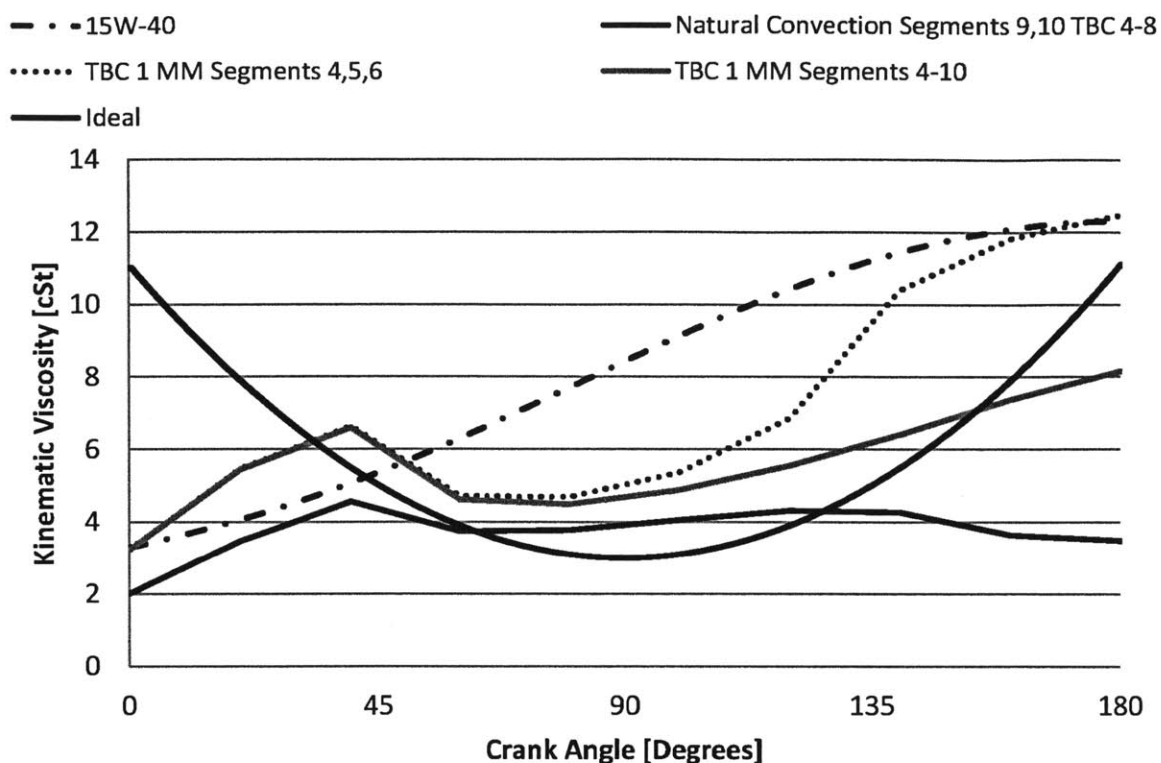


Figure 4.24 Power Cylinder Lubricant Viscosity over Engine Cycle for Different TBC and Natural Convection Applications

Figure 4.24 shows the lubricant viscosity as a function of liner position for 15W-40 oil with an uncoated and conventionally cooled liner. Also shown are viscosity profiles for a cylinder liner coated with a 1 mm TBC on the mid-stroke (segments 4, 5, 6), and the bottom 60% of the liner (segments 4-10). The same 15W-40 reference lubricant was used for the TBC and natural convection cases. These profiles reduce mid-stroke viscosity, and reduced BDC viscosity is seen when the bottom 60% of the liner is coated. Finally, a profile is shown that represents a TBC application on liner segments 4-8 and natural convection on the last 20% of the liner (segments 9-10). This case generates an essentially constant viscosity profile throughout the engine cycle, except for in the TDC region.

Referencing the baseline cases in Figure 4.24, it is clear that TBC coating and natural convection can fundamentally alter the lubricant properties in the power cylinder assembly. The friction benefit from the modified viscosity profiles is quantified in Section 4.5.4.

4.5.4 Friction Reduction Potential of TBC

The outputs from these simulations were used to predict the reduction in power cylinder friction for each TBC application. Baseline data for cylinder liner lubricant viscosity was taken from the 15W-40 lubricant used in the model simulation. Representative data of the friction forces exerted by the piston skirt and ring pack on the cylinder liner was taken from experimental results on a floating liner engine. Figure 4.25 is a graph of the instantaneous piston/ring/liner friction force over a complete engine cycle for various lubricant temperatures [64]. Representative data was used because data for the engine under study was not readily available. While the absolute value of friction force is inaccurate the friction force trend is typical of that seen in many research studies [64] [65] [66] [67] [68].

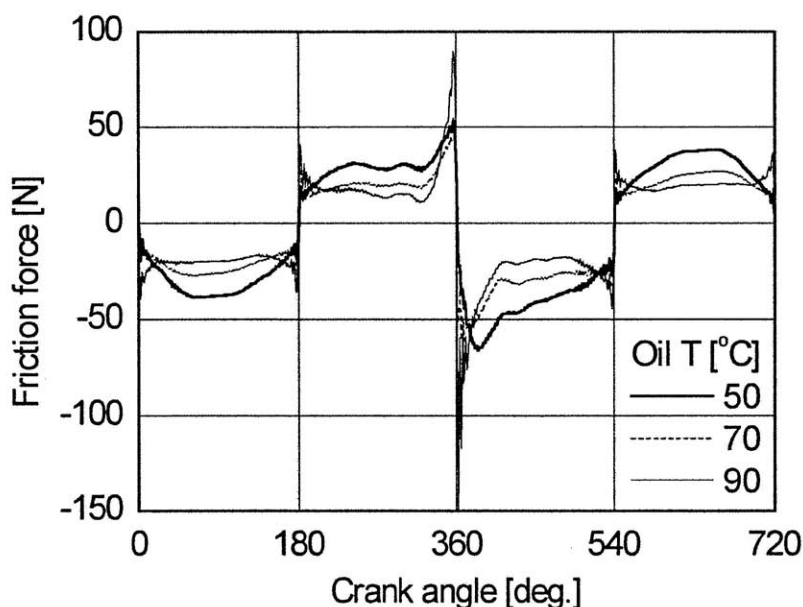


Figure 4.25 Instantaneous Power Cylinder Friction Over Complete Engine Cycle

The crank angle duration for each liner segment was calculated from Equation (4.21) below, where y is the instantaneous stroke length, l is the connecting rod length, a is the crank radius, and θ is the crank angle [62]. Due to variations in sliding speed as the piston moves up and down the liner each cylinder liner segment corresponds to a different number of crank angles. TDC and BDC have low surface speeds; therefore, it takes more crank angles to traverse these segments of the liner. At the mid-stroke, piston velocity is at a maximum and liner segments are traversed in much fewer crank angles.

$$y = l + a - [(l^2 - a^2 \sin^2 \theta)^{1/2} + a \cos \theta] \quad (4.21)$$

Figure 4.26 show the results of the above calculations. The crank angle duration for each liner segment is shown on the left and the average segment velocity is shown on the right.

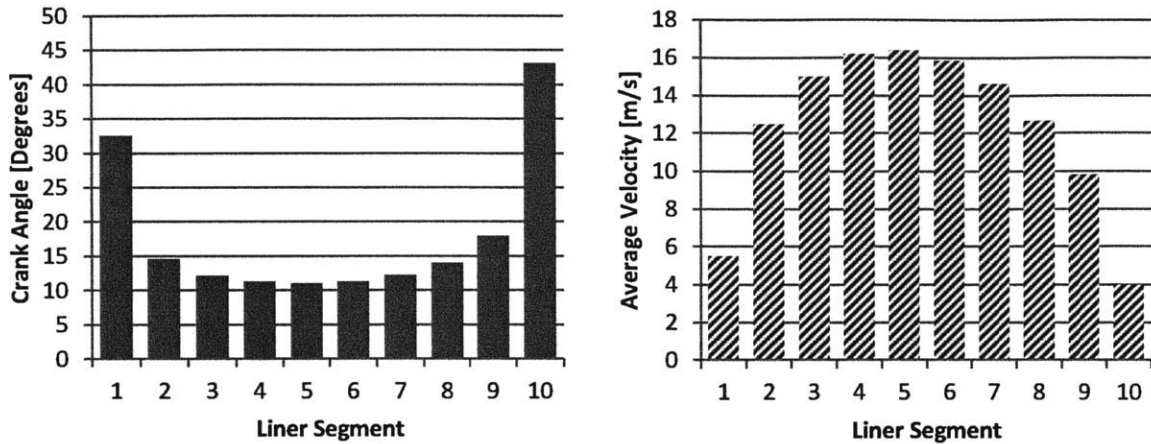


Figure 4.26 Cylinder Liner Segment Crank Angle Duration and Average Velocity

An average friction force was calculated for each cylinder liner segment over one engine cycle based on available data and is shown in Figure 4.27 [69]. High friction forces are noted at TDC and BDC regions (segments 1 and 10) because of high boundary contact between the cylinder liner and piston due to low sliding speeds. Friction forces are lower in the mid-stroke region where the lubrication regime is largely hydrodynamic.

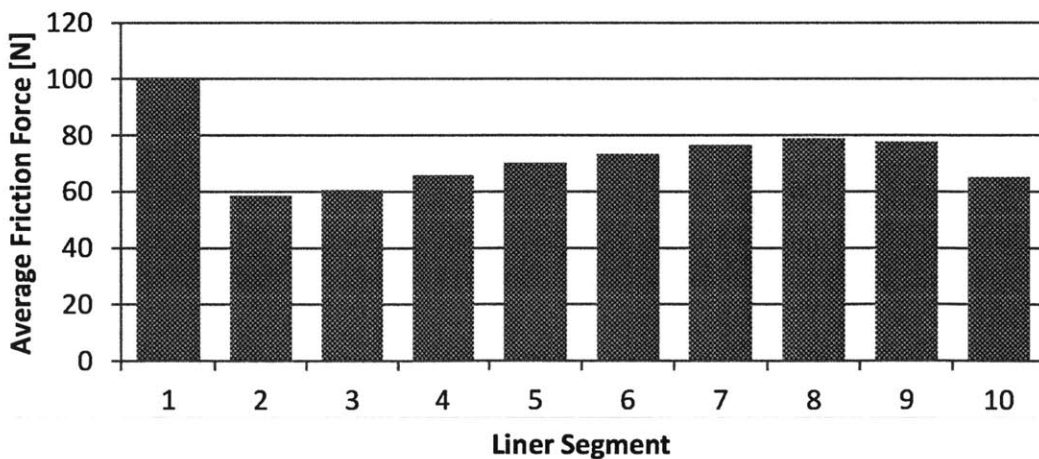


Figure 4.27 Average Friction Force for Each Liner Segment

Figure 4.28 shows the average friction work losses over the engine cycle for each liner segment. It is calculated using the average friction force times the liner segment length. Figure 4.29 shows the average power losses over the engine cycle. As expected the mid-stroke region is responsible for the majority of the power losses in the piston/ring/liner system.

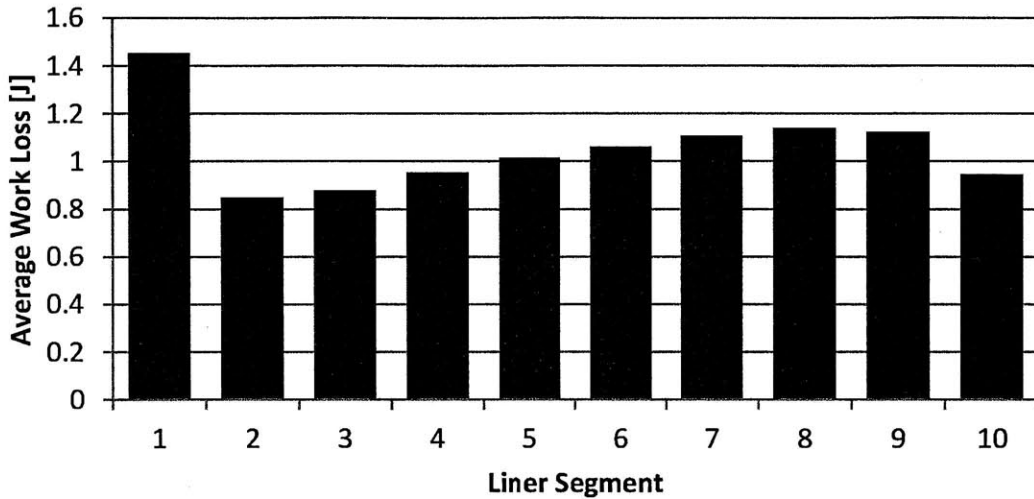


Figure 4.28 Average Friction Work Losses for Each Liner Segment

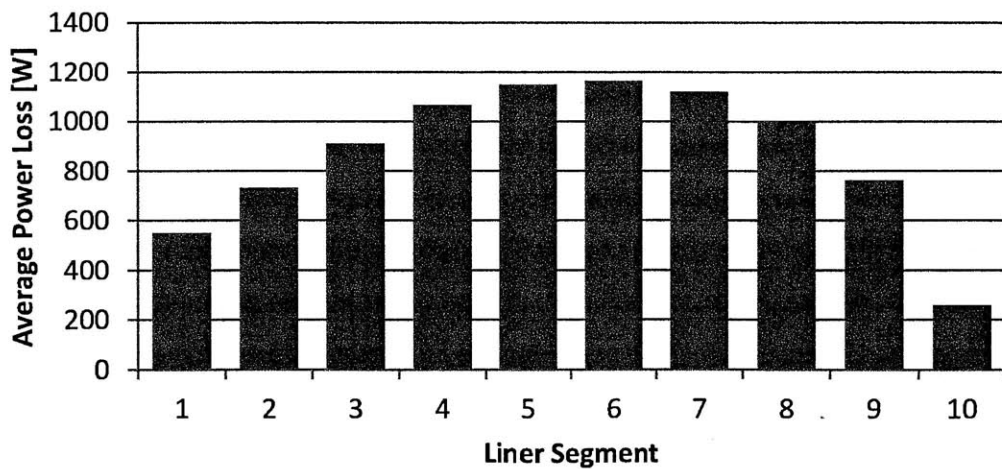


Figure 4.29 Average Friction Power Losses for Each Liner Segment

For piston-ring/liner lubrication, the friction force from hydrodynamic lubrication is expected to be proportional to viscosity and varies inversely with the film thickness, i.e. μ/h . Since film thickness, h , varies with the square root of viscosity, friction varies with the square root of μ . Quantifying the exact distribution of boundary and hydrodynamic friction for each liner segment requires extensive modeling dependent on the specific engine geometry and specifications. Therefore a survey of the literature was conducted to determine a general trend in the distribution of boundary and hydrodynamic friction for each segment of the liner. Figure 4.30 shows the contribution of hydrodynamic and boundary friction for the OCR of a large natural gas engine [42]. As expected the boundary friction is high at TDC and BDC, at -315° and -135° the boundary and hydrodynamic friction forces are approximately equal. This corresponds to segments 1, 2, 9, and 10. Figure 4.31 shows how hydrodynamic and boundary lubrication change in the power cylinder as the mean lubricant viscosity is changed [42]. As expected when mean viscosity decreases boundary friction increases, hydrodynamic friction decreases and vice versa.

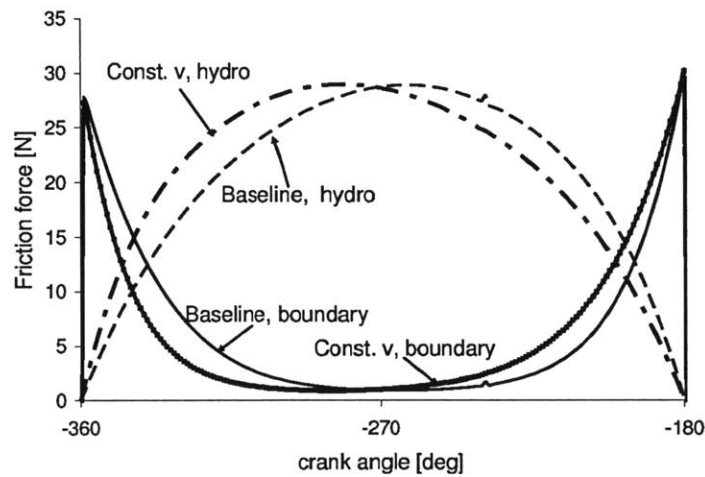


Figure 4.30 Hydrodynamic and Boundary Friction Forces in the Ring Pack [42]

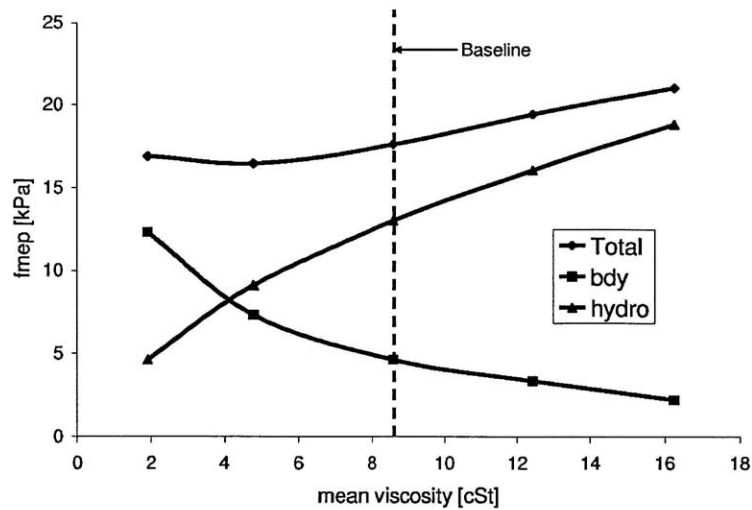


Figure 4.31 Hydrodynamic and Boundary Friction FMEP for Varying Mean Lubricant Viscosities [42]

To calculate the friction reduction from the various TBC applications a set of weighting factors was developed based on the data above. These factors are the ratio of hydrodynamic to boundary friction for each liner segment. These weighting factors based on Figure 4.30 can be seen in Table 4.3 below.

Table 4.3 Hydrodynamic Friction Weighting Factors

Liner Segment	1	2	3	4	5	6	7	8	9	10
Weighting Factor	0.32	0.68	0.77	0.82	0.95	0.97	0.97	0.97	0.94	0.45

Equation (4.22) shows the formula used to calculate the reduced friction force for the TBC coating applications. F_i is the friction force, ω_i is the weighting factor from Table 4.3, ν is the lubricant viscosity with the TBC, and ν_0 is the reference viscosity from the baseline case. The boundary lubrication component does not receive any viscosity scaling due to the TBC and remains constant. The hydrodynamic portion is scaled by the square root of the viscosity with TBC applied over the baseline viscosity for each liner segment and weighted based on the proportion of boundary to hydrodynamic friction. This was then compared with the baseline values to determine the percent decrease in the friction force expected over each liner segment because of the TBC application.

$$F_{i,TBC} = (1 - \omega_i)F_i + \omega_i \sqrt{\frac{v}{v_0}} F_i \quad (4.22)$$

Results from this calculation can be seen in Figure 4.32 for 1 mm TBC applications to the mid-stroke (segments 4,5 and 6), the bottom 60% of the liner (segments 4-10), and TBC on segments 4 through 8 and natural convection of segments 9 and 10. Predicted reductions in the piston/ring/liner interface for a TBC in the mid-stroke region vary from 20% to 30% depending on liner segment and application zone. TDC and BDC friction is largely unaffected except for the case of natural convection on the bottom of the cylinder liner.

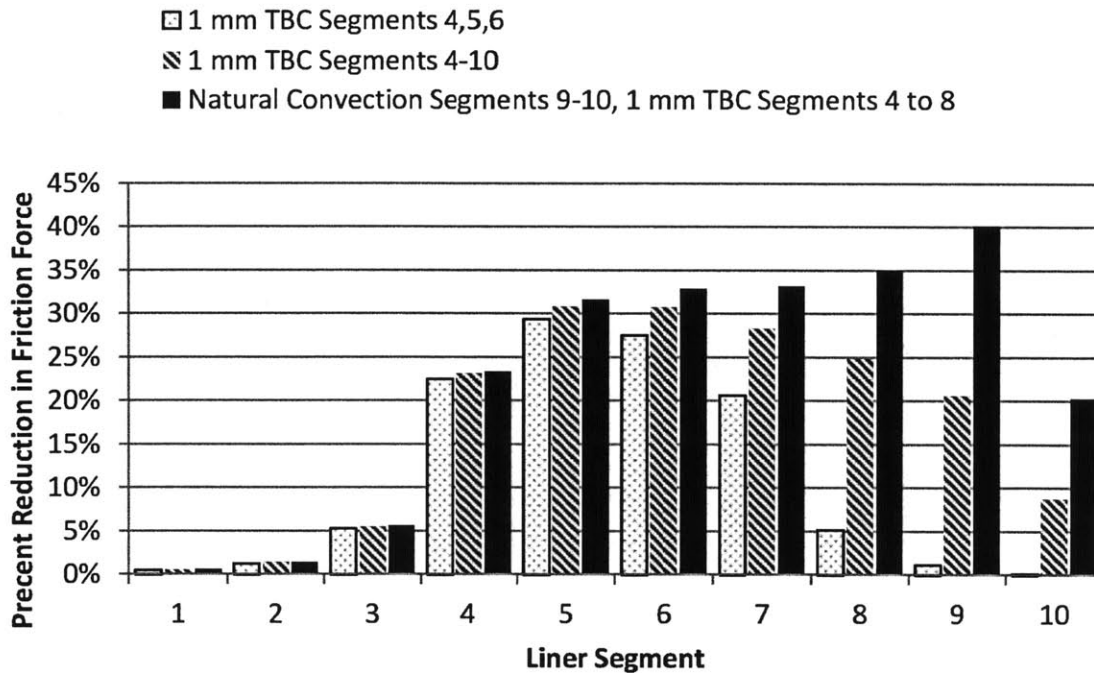


Figure 4.32 Decrease in Liner Segment Friction Force for TBC Applications

The reduction in power losses from the piston/ring/liner assembly was calculated using the average piston speed over each segment length. This result is shown below in Figure 4.33.

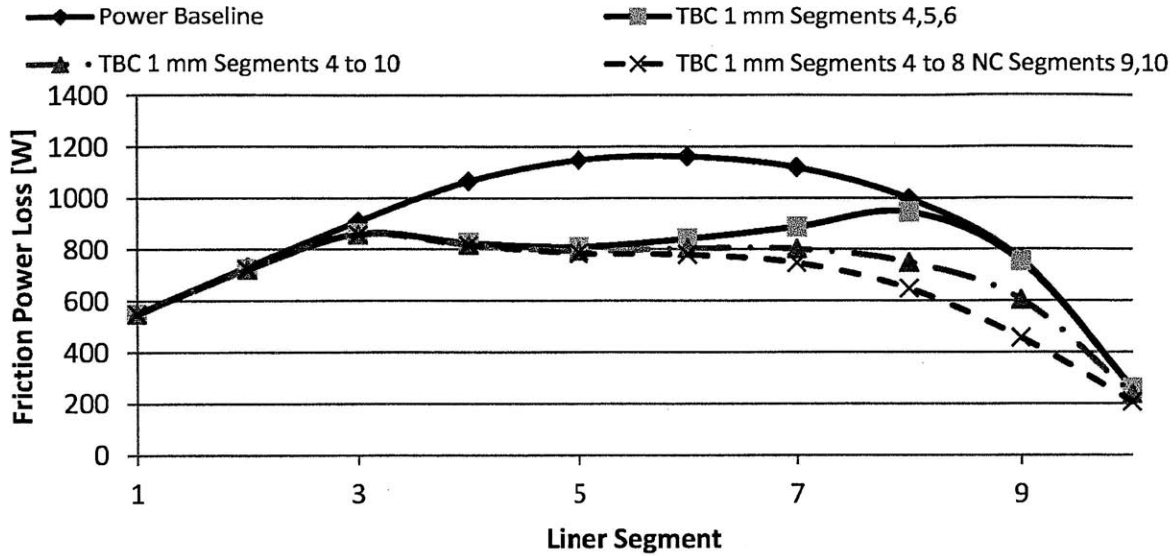


Figure 4.33 Decrease in Liner Segment Friction Power Losses for TBC Applications

The cumulative reduction in work loss for the entire cylinder liner over the engine cycle was calculated for the three TBC application zones in thicknesses varying from 0.5 to 3mm. The work reduction was calculated with Equation (4.23) shown below. The liner segments are equal length and therefore are not required to calculate the ratio of work losses over the engine cycle.

$$\text{Cycle Friction Work Reduction} = \frac{\sum_{i=1}^{10} (1 - \omega_i) F_i + \omega_i \sqrt{\frac{v}{v_0}} F_i}{\sum_{i=1}^{10} F_i} \quad (4.23)$$

The results of this calculation are shown in Figure 4.34. TBC application on the mid-stroke, segments 4 through 6 have a calculated work loss reduction of 7.6% for a 0.5 mm coating and a 16.5% improvement for a 3 mm coating application. Coating the bottom 60% of the liner with a TBC (segments 4-10) led to 11% reduction at 0.5 mm coating thickness to 29% for a 3 mm coating. Combining TBC on the mid-stroke with natural convection on the bottom 20% of the cylinder liner increased the predicted friction reductions to 15.9% and 32.5% reductions at 0.5 mm and 3 mm respectively.

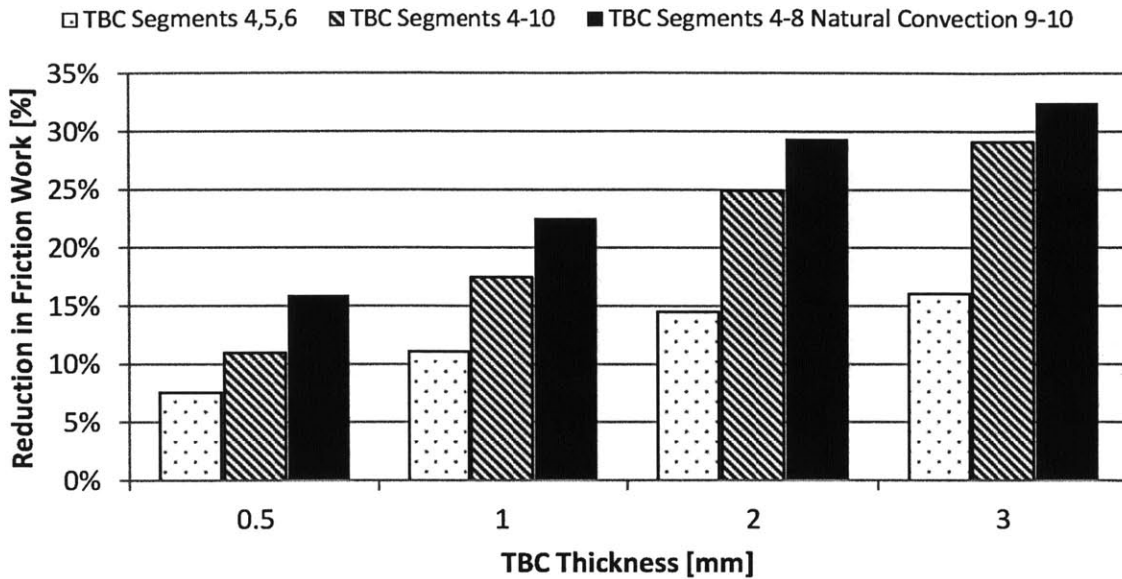


Figure 4.34 Reduction in Engine Friction for Various TBC Application Zones

The previous calculations assume that there is no change in the lubrication regime due to the lower lubricant viscosity. Reduced lubricant viscosity near the BDC region is expected to increase boundary lubrication and wear diminishing the gains in friction reduction. However, for even modest levels of TBC and reduced lubricant viscosity, a large improvement in power cylinder friction is predicted. Figure 4.32 shows the reduction in friction for each liner segment for a 1 mm thermal barrier coating applied to the mid-stroke and the lower 60% of the cylinder liner. As intended, mid-stroke friction reductions are on the order of 30% for both cases while the TDC region remains essentially unchanged.

Based on these results a 1 mm TBC on the bottom 60% of the liner is predicted to reduce power cylinder work losses 17.5%. Based on the assumption that the power cylinder is responsible for 40% of total friction losses in the engine, this translates to approximately 7% decrease in engine FMEP or a 0.7% improvement in fuel consumption for an engine with mechanical efficiency of 90%. This represents a very significant improvement in vehicle fuel economy and engine efficiency.

4.5.5 Study of Thermal Barrier Coating Thickness and Application Zone on Coolant Heat Rejection and Exhaust Gas Enthalpy

Application of TBC to the cylinder liner has additional benefits to engine efficiency besides friction reduction through decreased lubricant viscosity. The TBC reduces heat rejection to the engine coolant, which results in reduced energy required for heat removal. This could allow for reduced radiator sizing, smaller water pumps, and reduced cooling “fan-on” time which would improve vehicle fuel efficiency. Additionally, the exhaust gas temperature and enthalpy will increase with lower coolant heat rejection providing more energy for the turbocharger, turbocompound, and waste heat recovery systems on the vehicle.

Figure 4.35 shows the net exhaust enthalpy, calculated in the simulation, for TBC coating thicknesses of 0.5 mm to 3 mm and application regions of the entire liner, only the mid-stroke, the bottom 60% and the bottom 40% of the liner. It is desirable to increase exhaust gas enthalpy to provide increased available energy for the turbocharger, turbocompound, and/or waste heat recovery systems installed on the engine. Increased exhaust enthalpy may also have a windfall benefit of reducing DPF regeneration cycle durations and/or frequency, as higher exhaust temperatures under normal operating conditions will oxidize more soot accumulated in the DPF. A significant increase in exhaust enthalpy of 17.8% was predicted when the entire cylinder liner is coated with 3 mm of PSZ. A much more modest increase in exhaust enthalpy was expected when the TDC region of the cylinder liner was left uncoated. The largest expected increase was 3.44% when liner segments 4 through 10 were coated with 3 mm of PSZ.

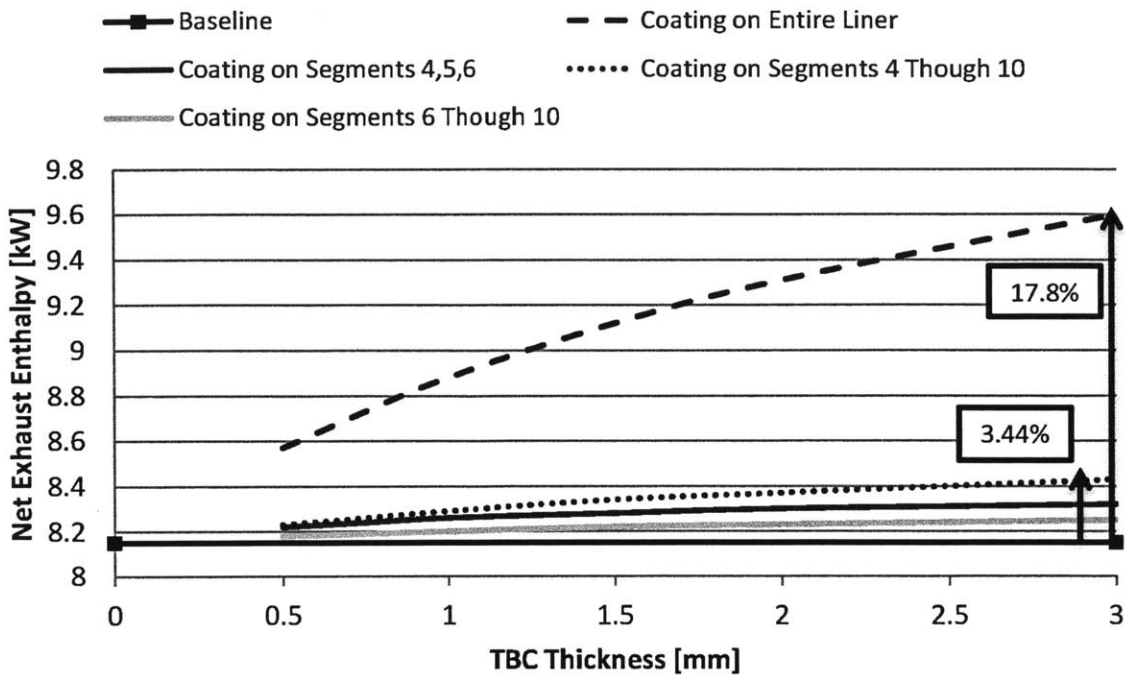


Figure 4.35 Coating Thickness and Type versus Exhaust Enthalpy

Figure 4.36 shows the cylinder liner heat rejection over the engine cycle for various thicknesses of TBC and application zones. Thicknesses of 0.5 mm to 3 mm and application regions of the entire liner, only the mid-stroke, the bottom 60%, and the bottom 40% of the liner were studied. Reducing cylinder liner heat rejection is beneficial to engine efficiency because it reduces the cooling load on the engine, reducing vehicle fan-on time and cooling system size requirements. Coating the entire liner reduces cylinder liner heat rejection 11% for a 0.5 mm thick coating to 36.6% for 3 mm coating.

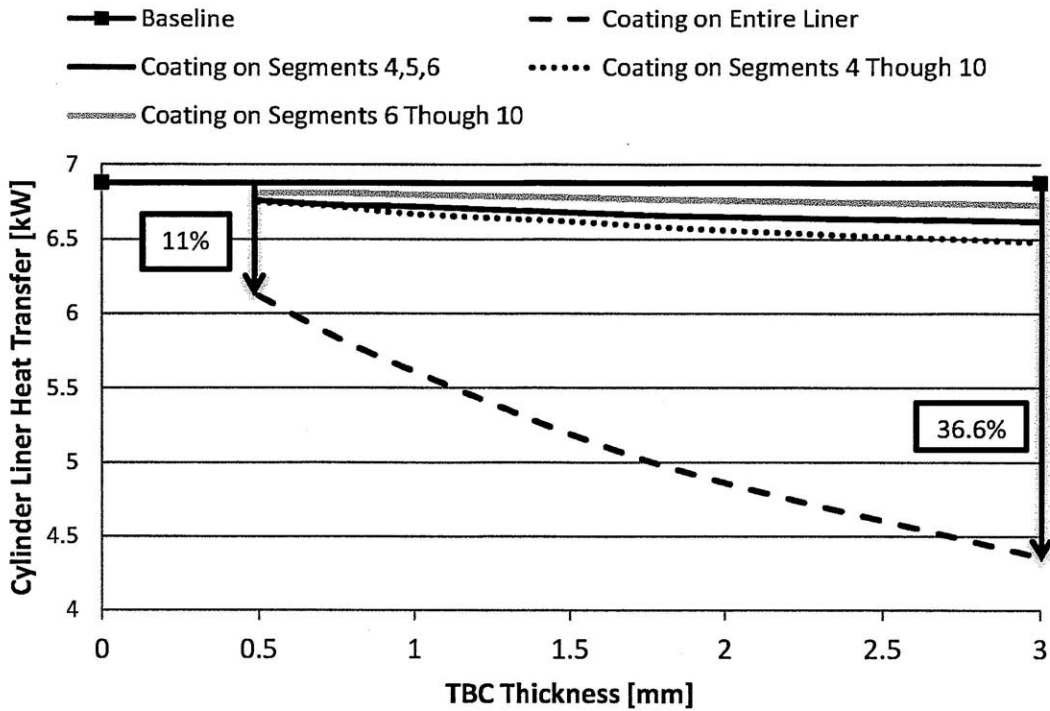


Figure 4.36 Liner Heat Rejection for Different TBC Thickness and Application Zone

When the TDC region of the cylinder liner is uncoated, the reduction in heat rejection is much smaller than for a fully coated liner. Figure 4.37 shows the same data as Figure 4.36 with the fully coated liner data removed to provide greater clarity. Coating the bottom 60% of the liner (segments 4-10) reduces liner heat rejection 3.0% for a 0.5 mm coating and 5.8% for a 3 mm coating.

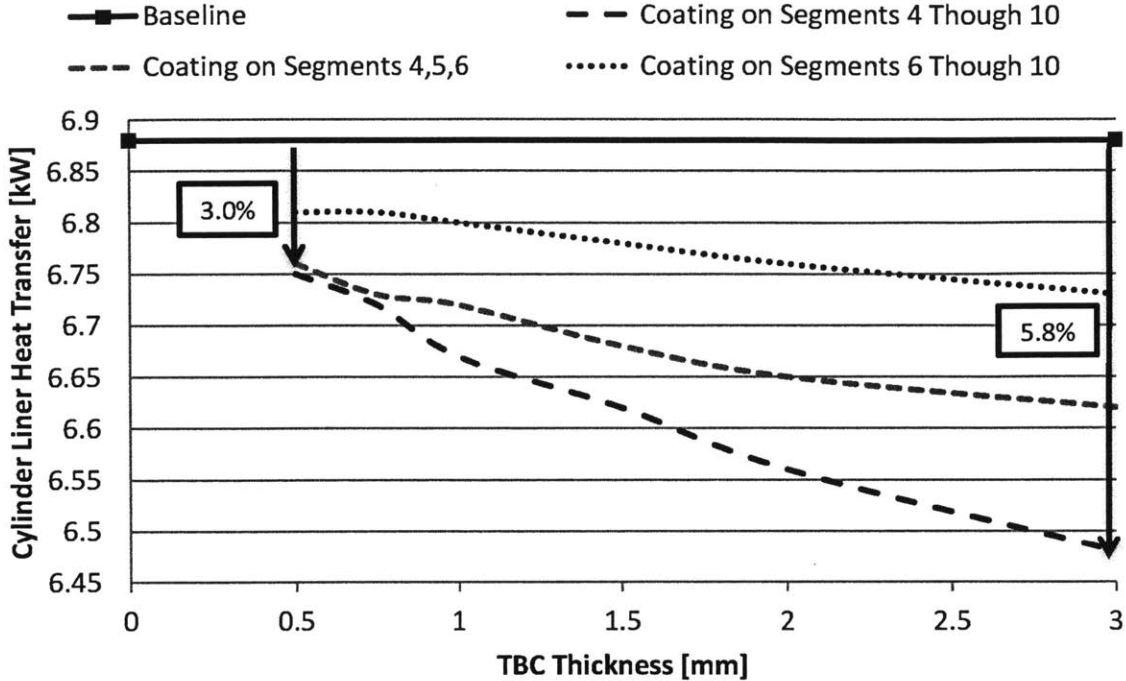


Figure 4.37 Liner Heat Rejection for Different TBC Thickness and Application Zone

From these simulation results, a relatively small, but not insignificant benefit from partially coated cylinder liners exists in regards to exhaust gas enthalpy and reduced cylinder liner heat rejection can be realized. Fundamentally, coatings further down the cylinder liner provide much smaller gains because the high cycle temperatures occur during combustion when the piston is near the TDC of the stroke. Cylinder gas temperature versus crank angle as calculated in the model is shown in Figure 4.38. Here the peak temperatures occur from approximately 360 CA to 450 CA, because during this time the majority of the liner is insulated from the cylinder gasses by the piston and rings. Figure 4.39 displays the full cycle heat transfer for each liner segment. As can be seen, the vast majority of cylinder liner heat rejection, in this case 71.9% and 74.1%, occurs in the segments 1, 2, and 3. Therefore we see diminished benefits from increased exhaust gas enthalpy and reduced coolant heat rejection as the TBC moves down the cylinder liner.

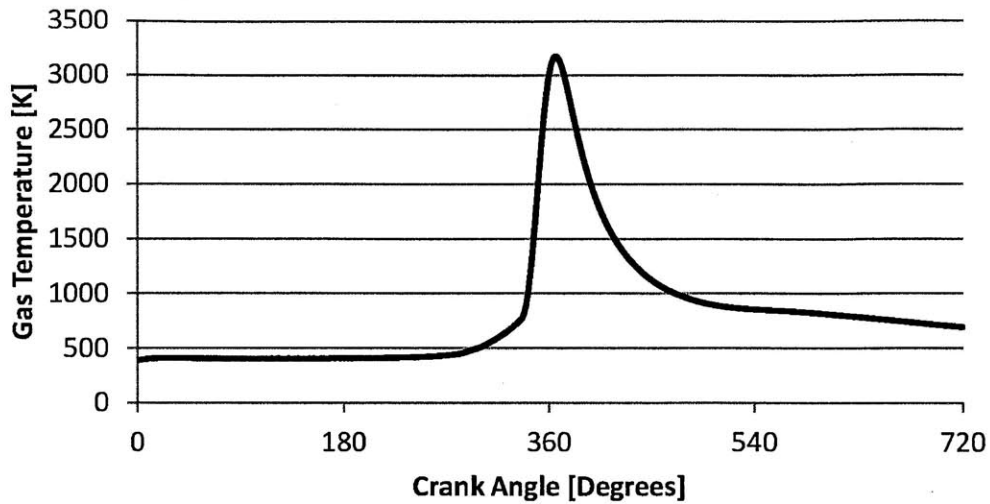


Figure 4.38 Cylinder Gas Temperature versus Crank Angle

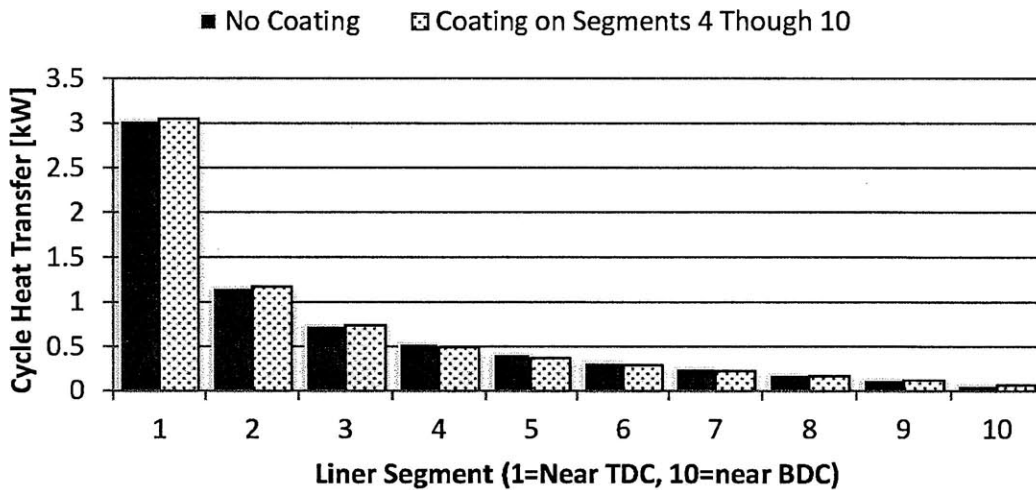


Figure 4.39 Cylinder Liner Full Cycle Heat Transfer by Liner Segment

In summary, exhaust gas enthalpy and the reduction in liner heat rejection can be maximized by using a TBC on the TDC region of the cylinder liner, in addition to coating the top of the piston, cylinder head, and valves. However, this would lead to the numerous drawbacks of TBC coatings previously discussed. These modest gains when coating the mid-stroke and BDC region of the cylinder liner provide increased engine performance without sacrificing engine emissions or durability.

4.5.6 Study of Thermal Barrier Coating Thickness and Application Zone on Engine Thermal Efficiency

Thermal barrier coatings can have additional benefits from increasing the thermal efficiency of the engine. The simulation was used to determine the expected thermal efficiency increase when TBC was applied to the piston, cylinder head, or cylinder liner. Thermal efficiency is expected to increase with the combustion chamber temperature. The greatest increases are realized when the piston or cylinder head is coated with a TBC. The model predicts a 1% and 1.4% increase for the piston and head respectively. Coating the cylinder liner has much less effect on the thermal efficiency, with a modest 0.05% increase expected for a fully insulated cylinder liner. Figure 4.40 below shows the results as a function of TBC thickness.

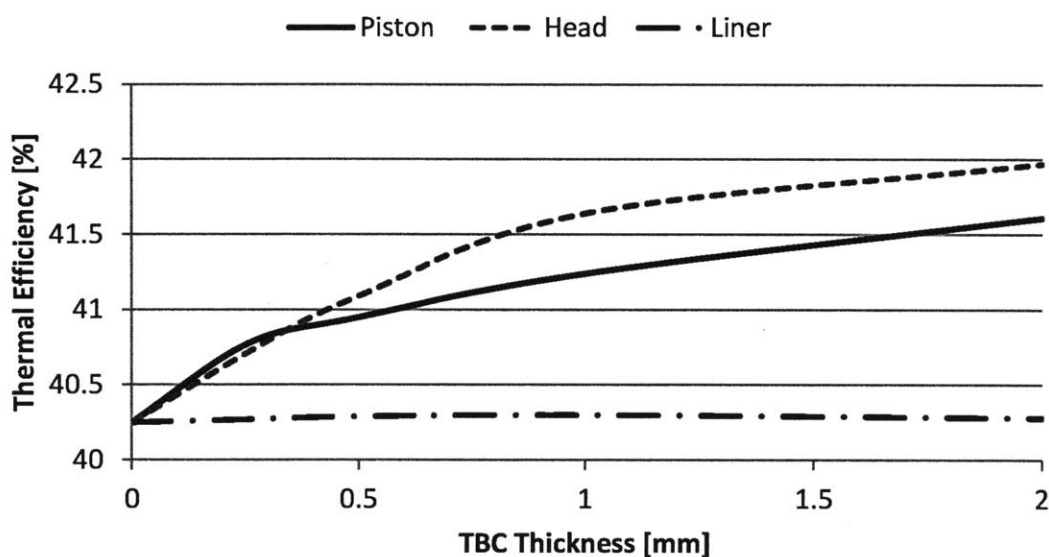


Figure 4.40 Thermal Efficiency as a Function of TBC Thickness

Figure 4.41 shows the thermal efficiency outputs for a partially coated cylinder liner. The results are mixed and actually show an unexpected decrease in thermal efficiency of 0.05% to 0.19%, depending on coating thickness, when the liner is coated in the mid-stroke or the bottom 60%. The reason for this decrease is unclear. These results are likely influenced by the error in the thermodynamic and heat transfer calculation, summation of the indicated work, heat transfer, and exhaust enthalpy typically has an error from 0.5-2% when compared with the fuel energy released in combustion. Therefore, the thermodynamic effects on engine efficiency still require

further verification. This study focuses on the effects of lubricant temperature on friction reduction only, however.

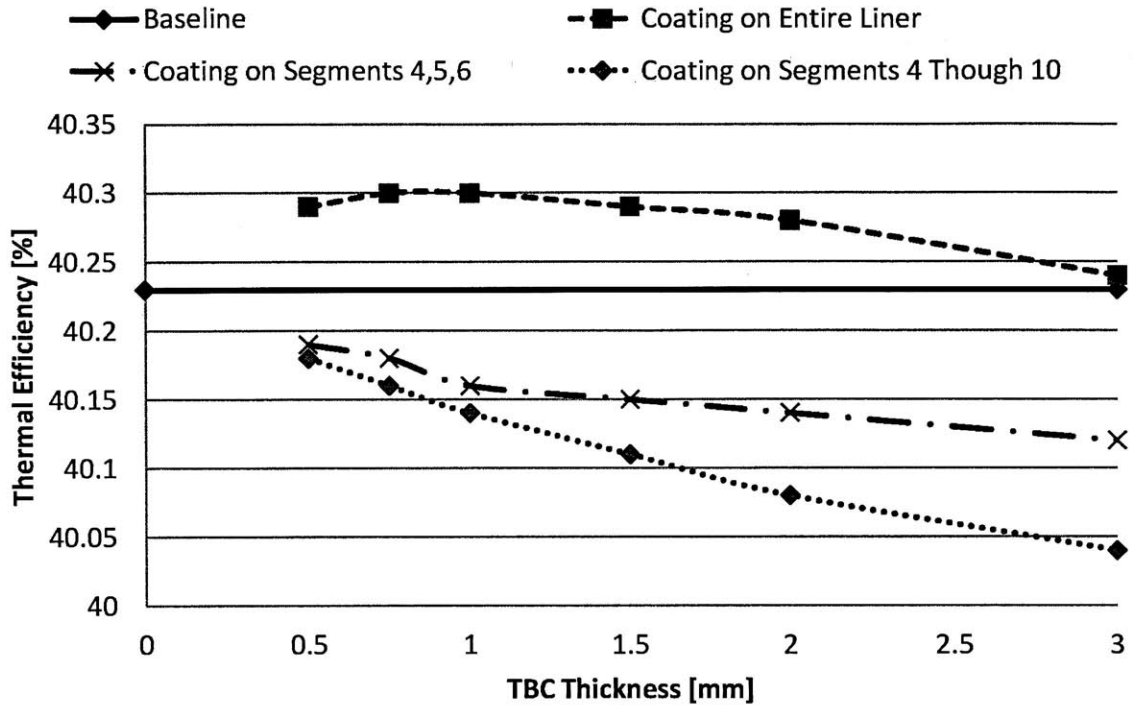


Figure 4.41 Thermal Efficiency for TBC on the Cylinder Liner

4.6 Summary of Thermal Barrier Coating Study

In this research program, the use of thermal barrier coatings was investigated as a novel approach to strategically change cylinder liner temperatures in order to improve the power cylinder frictional losses. A simulation was developed to model the primary physical processes that occur in a complete four stroke engine cycle. Work done by the piston; mass flow rates through the intake and exhaust valves; heat release during combustion; and heat transfer rates at the piston, cylinder head, and liner surfaces were calculated. Overall engine performance characteristics, including thermal efficiency, indicated specific fuel consumption (isfc), indicated power, exhaust gas enthalpy, and turbocharger boost pressure ratio were also determined.

By coating selected parts of the liner where piston speeds are high, the local liner temperature is raised. In this region, the lubrication regime of the piston and liner interface is hydrodynamic and is where the majority of the power cylinder work losses occur due to the high surface speeds. By coating the liner strategically, top dead center temperatures are mostly unaffected. This is important because increasing liner temperature at TDC further decreases the oil film thickness, increasing boundary friction and wear. This approach is expected to maximize friction reduction while minimizing risk to other engine components or directionally increasing component wear rates.

Initial results have shown potential to decrease the piston skirt, piston ring, and cylinder liner interface friction between 15% and 30% depending on coating thickness and application zone. This corresponds to approximately a 0.5% to 1% improvement in vehicle fuel economy, assuming reciprocating power cylinder friction represents 40% of the mechanical losses in the engine with a 90% mechanical efficiency. Additional fuel economy benefits are expected from TBC in the form of increased exhaust gas enthalpy and reduced liner heat rejection. The former will provide more energy to the turbocharger, turbocompound, and waste heat recovery systems, while the later will lower vehicle cooling loads, thereby reducing the power required to pump coolant and operate the vehicle fan. This form of strategic thermal management within the engine has very high potential to increase engine and vehicle efficiency while maintaining the performance and durability demanded in the HD market.

(This page was intentionally left blank)

5 Conclusions

Fuel economy of large, on-road diesel engines is a critical performance metric for engine manufacturers. Demands for increased fuel economy are coupled with corresponding improvements in engine performance, durability, and emissions. One method of improving fuel economy is to reduce the losses due to mechanical friction within the engine. Mechanical friction accounts for between 10% and 15% of the indicated work output of the engine. Reductions in mechanical friction directly improve engine thermal efficiency and fuel economy, and was the focus of the current study.

This project centers on resolving the adverse effects on engine wear, durability, emissions, and oil consumption that often accompany traditional low-friction concepts. A detailed analysis of the sources of friction within a heavy-duty diesel engine was undertaken. Empirical data on engine friction and component wear was collected from industry as well as from studies in literature. Empirical and numerical models were used to determine the sources and distribution of friction losses within the engine. This study provided insight into the most lucrative engine components to target for friction reduction strategies. Analysis was performed to quantify the friction reduction potential through lubricant properties on various engine component groups.

The power cylinder and crankshaft group were calculated to contribute approximately 60% of the total engine mechanical losses. Engine accessories, namely the water pump, oil pump, air compressor, and fuel pump were responsible for an additional 30%. The valve and gear trains accounted for the remaining 10% of mechanical losses. The power cylinder and crankshaft group were selected to study in detail for the potential friction reduction through lubricant formulation. Results of this modeling analysis suggest that a fmep reduction of approximately 10% in the crankshaft assembly is possible through a lubricant viscosity reduction from 15W-40 to 5W-30. Analysis on the power cylinder assembly was performed to determine the friction reduction potential of moving from a 15W-40 lubricant to a 5W-30. Results determined an 11% reduction in power cylinder fmep is possible through this lubricant viscosity reduction. However, the power cylinder is an area of the engine subjected to high wear rates. To optimize the power cylinder, lubricant viscosity must be kept high in the top ring reversal zone to minimize wear while

viscosity can be reduced in the mid-stroke to minimize friction. To achieve this, active thermal management of the power cylinder was investigated.

The use of thermal barrier coatings (TBC) was investigated as a novel approach to strategically increase cylinder liner temperatures in order to reduce power cylinder friction. By coating selected parts of the liner where piston speeds are high, local liner temperature is raised and local lubricant viscosity decreased in that region. In the mid-stroke, the piston is in the hydrodynamic lubrication regime, and high surface speeds generate the majority of the power cylinder work losses which can be reduced through reduced lubricant viscosity. By coating the liner in selected regions only, top dead center temperatures are mostly unaffected thereby minimizing any increase in cylinder liner wear. This approach is expected to maximize friction reduction while minimizing risk to other engine components or increasing component wear rates.

A simulation was developed to model the primary physical processes that occur in a complete four stroke engine cycle. Calculations included work done by the piston, mass flow rates through the intake and exhaust valves, heat release during combustion, and heat transfer rates. The results demonstrate the potential to decrease power cylinder between 15% and 30% depending on coating thickness and application zone. This corresponds to approximately a 0.5% to 1% improvement in vehicle fuel economy. Additional fuel economy benefits from the TBC are expected from increased exhaust gas enthalpy and reduced liner heat rejection. This strategic thermal management approach within the engine has very high potential to increase engine efficiency while maintaining the performance and durability demanded in the HD market.

The use of thermal barrier coatings, as well as changes in the engine lubricant properties has the potential to significantly reduce engine mechanical friction and improve vehicle fuel economy without increasing component wear and failure rates.

5.1 Continuing Work

Initial analysis and modeling has shown the potential for significant improvements in power cylinder friction and vehicle fuel economy. These positive initial results warrant further research and experimentation into this concept.

First, the TBC analysis should be adapted to the specific engine and operating conditions that pertain to the Super Truck project and verify the potential for fmep reduction. Further refinement of the quantification of friction force reduction using experimental data and computer simulation tools should be completed. This will allow for a more accurate prediction of the lubrication regimes present on the cylinder liner with a TBC applied.

Experimental verification of the model accuracy would be informative. This would require a firing engine test to generate and record the cylinder liner temperature profile for each coating application zone and thickness. Testing to validate the friction reduction on a firing engine would also need to be completed. These tests do not have to be commissioned on a large HD diesel but could initially be performed on a smaller engine of similar design e.g diesel, wet liner.

While the focus of this study was TBC, it may also be possible to impose the desired temperature profile on the cylinder liner by other means. Modification of engine coolant flow may change local temperatures and heat transfer coefficients – through reduced flow to the mid-stroke and BDC regions or using natural convection in lieu of coolant along certain parts of the liner.

The main challenge to the successful implementation of this concept will be maximizing the friction reduction while maintaining engine durability, as the higher liner temperatures associated with thermal barrier coatings will likely reduce engine reliability and longevity if not executed correctly.

(This page was intentionally left blank)

Works Cited

- [1] R. Takata, Y. Li and V. Wong, "Effect of Liner Surface Texturing on Ring/Liner Friction in Large-Bore IC Engines," in *Proceedings of ICEF06 ASME Internal Combustion Engine Division 2006 Fall Technical Conference*, Sacramento, CA, 2006.
- [2] W. van Dam, T. Miller and G. Parsons, "Optimizing Low Viscosity Lubricants for Improved Fuel Economy in Heavy Duty Diesel Engines," *SAE Technical Paper 2011-01-1206*, 2011.
- [3] J. Heywood, *Internal Combustion Engine Fundamentals*, New York: McGraw-Hill, 1988.
- [4] S. Kahn Ribeiro, S. Kobayashi, M. Beuthe, J. Gasca, D. Greene, D. S. Lee, Y. Muromachi, P. Newton, S. Plotkin, D. Sperling, R. Wit and P. Zhou, "Transport and its infrastructure. In Climate Change 2007: Mitigation. Contribution of Working Group III to the Fourth Assessment Report of the Intergovernmental Panel on Climate Change [B. Metz, O.R. Davidson, P.R. Bosch, R. Dave, L.A. Meyer (eds)]," Cambridge University Press, Cambridge, United Kingdom and New York, NY, USA, 2007.
- [5] Wärtsilä, "Wärtsilä RTA96C," [Online]. Available: <http://www.wartsila.com/en/engines/low-speed-engines/RT-flex96C>. [Accessed 19 3 2012].
- [6] International Maritime Organization, "International Shipping Facts and Figures - Informatin Resources on Trade, Saftey, Security, Environment," 6 March 2012. [Online]. Available: <http://www.imo.org/KnowledgeCentre/ShipsAndShippingFactsAndFigures/TheRoleandImportanceofInternationalShipping/Documents/International%20Shipping%20-%20Facts%20and%20Figures.pdf>. [Accessed 20 3 2012].
- [7] S. Davis, S. Diegel and R. Boundy, "Transportation Energy Data Book: Edition 30," Oak Ridge National Labratory , 2011.
- [8] J. Ward and S. Davis, "2010 Vehicle Technologies Market Report," U.S. Department of Energy, 2011.
- [9] Charles River Associates, "Diesel Technology and the American Economy," Diesel Technology Forum, Herndon, VA, 2000.
- [10] United States Environmental Protection Agency, "Particulate Matter," 6 July 2011. [Online]. Available: <http://www.epa.gov/pm/>. [Accessed 22 3 2012].

- [11] United States Environmental Protection Agency, "Nitrogen Dioxide," 1 November 2011. [Online]. Available: <http://www.epa.gov/air/nitrogenoxides/>. [Accessed 22 3 2012].
- [12] United States Environmental Protection Agency, "Heavy-Duty Highway Compression-Ignition Engines And Urban Buses -- Exhaust Emission Standards," 7 January 2011. [Online]. Available: <http://epa.gov/oms/standards/heavy-duty/hdci-exhaust.htm>. [Accessed 22 3 2012].
- [13] North American SCR Stakeholders Group, "Meeting EPA 2010," 2008. [Online]. Available: <http://www.factsaboutscr.com/environment/epa2010.aspx>. [Accessed 21 3 2012].
- [14] N. Singh, C. Rutland, D. Foster, K. Narayanaswamy and Y. He, "Investigation into Different DPF Regeneration Strategies Based on Fuel Economy Using Integrated System Simulation," *SAE Paper 2009-01-1275*, 2009.
- [15] United States Environmental Protection Agency, "EPA and NHTSA Propose First-Ever Program to Reduce Greenhouse Gas Emissions and Improve Fuel Efficiency of Medium- and Heavy-Duty Vehicles: Regulatory Announcement," 6 January 2011. [Online]. Available: <http://www.epa.gov/otaq/climate/regulations/420f10901.htm>. [Accessed 22 3 2012].
- [16] G. Fenske, R. Erck, L. Ajayi, A. Erdemir and O. Eryilmaz, "Parasitic Energy Loss Mechanisms Impact on Vehicle System Efficiency," Argonne National Laboratory, 2006.
- [17] K. Fender and D. Pierce, "An Analysis of the Operational Costs of Trucking: A 2011 Update," American Transportation Research Institute, Atlanta, GA, 2001.
- [18] R. Taylor, "Heavy Duty Diesel Engine Fuel Economy: Lubricant Sensitivities," *SAE International Spring Fuels & Lubricants Meeting & Exposition Paris, France*, pp. SAE Paper No 2000-01-2056, 2000.
- [19] U.S. Energy Information Administration, "Gasoline and Diesel Fuel Update," 19 March 2012. [Online]. Available: <http://www.eia.gov/petroleum/gasdiesel/>. [Accessed 23 3 2012].
- [20] D. Richardson, "Review of Power Cylinder Friction for Diesel Engines," *Journal of Engineering for Gas Turbines and Power-Transactions of the ASME*, vol. 122, no. 4, pp. 506-519, 2000.

- [21] P. Shayler, D. Leong, I. Pegg and M. Murphy, "Investigations of Piston Ring Pack and Skirt Contributions to Motored Engine Friction," *SAE Int. J. Engines*, vol. 1, no. 1, pp. 723-734, 2009.
- [22] L. Moughon and V. Wong, "Effects of Lubricant and Piston Design on Reciprocating Engine Friction," in *ASME Paper ICEF2005-1343, Proceedings of ASME Internal Combustion Engine Division Fall Technical Conference*, Ottawa, Canada, 2005 .
- [23] L. Moughon, "Effects of Piston Design and Lubricant Selection on Reciprocating Engine Friction," M.S. Thesis, Department of Mechanical Engineering, Massachusetts Institute of Technology, 2006.
- [24] T. Boschert, "The Lubricant Contribution to Future Low Emission Engine Design," Diesel Particulate and NOx Emissions Course (University of Leeds), Ann Arbor, MI, 2002.
- [25] S. Rizvi, "A Comprehensive Review of Lubricant Chemistry, Technology, Selection, and Design," ASTM International, West Conshohocken, PA, 2009.
- [26] J. Booker, "Dynamically Loaded journal Bearings: Mobility Method of Solution," *ASME Journal of Basic Engineering*, pp. 537-546, 1965.
- [27] K. Hamai, T. Masuda, T. Goto and S. Kai, "Development of a Friction Model for High Performance Engines," *Journal of the Society of Tribologists and Lubrication Engineers*, vol. 47, no. 7, pp. 567-573, 1990.
- [28] G. Livanos and N. Kyrtatos, "A Model of the Friction Losses in Diesel Engines," in *SAE World Congress*, Detroit, Michigan, SAE Paper No. 2006-01-0888, 2006.
- [29] G. Livanos, "Development of a Simplified Instantaneous Friction Model of the Piston-Crank-Slider Mechanism of Internal Combustion Engines," *SAE International Journal of Engines*, vol. 4, no. 1, pp. SAE Paper No. 2011-01-0612, 2011.
- [30] E. Ciulli, "A Review of Internal Combustion Engine Losses Part 1: Specific Studies on the Motion of Pistons, Valves, and Bearings," *Proceedings of the Institution of Mechanical Engineers, Part D: Journal of Automobile Engineering*, vol. 206, no. 4, pp. 223-236, 1992.
- [31] F. Ocvirk, "Short Bearing Approximation for Full Journal Bearings," *NACA TN 2808*, 1952.
- [32] H. Hirani, K. Athre and S. Biswas, "Dynamically Loaded Finite Length Journal Bearings: Analytical Method of Solution," *ASME Journal of Tribology*, vol. 121, no. October, pp. 844-852, 1999.

- [33] A. Raimondi and J. Boyd, "A Solution of Finite Journal Bearing and its Application to Analysis and Design Part, I, II, and III," *ASLE Transactions*, vol. 1, no. 1, pp. 159-202, 1958.
- [34] D. Taraza, N. Henein and W. Bryzik, "Friction Losses in Multi-Cylinder Diesel Engines," in *SAE World Congress, SAE Paper No. 2000-01-0921*, Detroit, MI, 2000.
- [35] V. Wong, T. Tian, H. Lang, J. Ryan, Y. Sekiya, Y. Kobayashi and S. Aoyama, "A Numerical Model of Piston Secondary Motion and Piston Slap in Partially Flooded Elastohydrodynamic Skirt Lubrication," *SAE Paper No 940696*, 1994.
- [36] S. Mansouri and V. Wong, "Effects of Piston Design Parameters on Piston Secondary Motion and Skirt-Liner Friction," *SAE International*, Vols. SAE Paper No. 2004-01-2911, 2004.
- [37] N. Patir and H. Cheng, "Application of Average Flow Model to Lubrication Between Rough Sliding Surfaces," *ASME Journal of Lubrication Technology*, 1979.
- [38] L. Moughon and V. Wong, "Effects of Lubricant and Piston Design on Reciprocating Engine Friction," in *ASME Paper ICEF2005-1343, Proceedings of ASME Internal Combustion Engine Division Fall Technical Conference*, Ottawa, Canada, 2005.
- [39] L. Moughon, "Effects of Piston Design and Lubricant Selection on Reciprocating Engine Friction," *MIT SM Thesis*, 2006.
- [40] T. Tian, V. Wong and J. Heywood, "A Piston Ring Pack Film Thickness and Friction Model for Multigrade Oils and Rough Surfaces," in *SAE International Fall Fuels & Lubricants Meeting & Exposition, SAE Paper No 962032*, San Antonio, Texas, 1996.
- [41] J. Greenwood and J. Tripp, "The Contact of Two Nominally Flat Surfaces," *Proceeding of the Institute of Mechanical Engineers*, vol. 185, pp. 625-633, 1971.
- [42] R. Takata, "Effects of Lubricant Viscosity and Surface Texturing on Ring-pack Performance in Internal Combustion Engines," *MIT SM Thesis*, 2006.
- [43] S. Chen and P. Flynn, "Development of a Single Cylinder Compression Ignition Research Engine," *SAE Paper No. 650733*, 1965.
- [44] E. Ciulli, "A Review of Internal Combustion Engine Losses Part 2: Studies for Global Evaluations," *Proceedings of the Institution of Mechanical Engineers, Part D: Journal of Automobile Engineering*, vol. 207, no. 3, pp. 229-240, 1993.

- [45] B. Millington and E. Hartles, "Friction Losses in Diesel Engines," *SAE Paper No. 680590*, 1968.
- [46] D. Winterbone and D. Tennant, "The Variation of Friction and Combustion Rates During Diesel Engine Transients," *SAE Paper No. 810339*, 1981.
- [47] S. Yagi, Y. Ishibasi and H. Sono, "Experimental Analysis of Total Engine Friction in Four Stroke SI Engines," *SAE Paper No. 900223*, 1990.
- [48] I. Bishop, "Effect of Design Variables on Friction and Economy," *SAE Transactions*, vol. 73, 1965.
- [49] K. J. Patton, R. G. Nitschke and J. B. Heywood, "Development and Evaluation of a Friction Model for Spark-Ignition Engines," *SAE paper 890836*, 1989.
- [50] A. Cameron, *The Principles of Lubrication*, Wiley, 1966.
- [51] D. Sandoval and J. Heywood, "An Improved Friction Model for Spark-Ignition Engines," *SAE World Congress Detroit Michigan*, Vols. SAE Paper No. 2003-01-0725, 2003.
- [52] Car-Repair.com, "Water-Cooled Engines," 5 April 2012. [Online]. Available: <http://www.car-repair.com/engine/water-cooled-engines.html>. [Accessed 5 April 2012].
- [53] S. Jaichandar and P. Tamilporai, "Low Heat Rejection Engines - An Overview," in *SAE World Congress*, *SAE Paper No. 2003-01-0405*, Detroit Michigan, 2003.
- [54] T. Morel, R. Keribar, P. Blumberg and E. Fort, "Examination of Key Issues in Low Heat Rejection Engines," *SAE Paper No. 860316*, 1986.
- [55] K. Hoag, M. Brands and W. Bryzik, "Cummins/TACOM Adiabatic Engluie Program," *SAE Paper No. 850356*, 1985.
- [56] W. Wade, R. Havstad, E. Ounsted, F. Trinkler and I. Garwin, "Fuel Economy Opportunities with an Uncooled DI Diesel Engine," *Imech/SAE*, vol. C432, pp. 11-24, 1984.
- [57] R. Thring, "Low Heat Rejection Engines," *SAE Paper No. 860314*, 1986.
- [58] G. Quian, T. Nakamura and C. Berndt, "The Effect of Thermal Gradient and Residual Stresses on Thermal Barrier Coating Fracture," *Mechanics of Materials*, vol. 27, pp. 91-110, 1998.

- [59] D. Saad, P. Saad, L. Kamo, M. Mekari, W. Bryzik and E. J. Schwarz, "Thermal Barrier Coatings for High Output Turbocharged Diesel Engine," in *SAE 2007 World Congress*, SAE Paper No. 2007-01-1442, Detroit, Michigan, 2007.
- [60] Detroit Diesel Corporation, "Super Truck Program: Engine Project Review Recovery Act - Class 8 Truck Freight Efficiency Improvement Project," 12 May 2011. [Online]. Available: http://www1.eere.energy.gov/vehiclesandfuels/pdfs/merit_review_2011/adv_combustion/ace058_sisken_2011_o.pdf. [Accessed 6 April 2012].
- [61] V. Wong, W. Bauer, R. Kamo, W. Bryzik and e. al., "Assessment of Thin Thermal Barrier Coatings for I.C. Engines," *SAE Paper No 950980*, 1995.
- [62] C. Ferguson and A. Kirkpatrick, *Internal Combustion Engines*, New York: John Wiley & Sons, Inc., 2001.
- [63] F. Shabir, S. Authars, S.Ganesan, R. Karthik and S. Madhan, "Low Heat Rejection Engines - Review," *SAE International Paper No. 2010-01-1510*, 2010.
- [64] K. Ha, J. Kim, M. Cho and D. Oh, "Development of Piston Friction Force Measurement System," in *SAE Powertrain & Fluid Systems Conference & Exhibition*, SAE Paper No. 2002-01-2902, San Diego, CA, 2002.
- [65] K. Kim, P. Shah, M. Takiguchi and S. Aoki, "Part 3: A Study of Friction and Lubrication Behavior for Gasoline Piston Skirt Profile Concepts," *SAE International*, pp. SAE Paper No 09PFL-1163, 2009.
- [66] M. Hoshi, Y. Baba and S. Furuhamo, "A Study of Piston Friction Force in an Internal Combustion Engine (Number 2)," *Tribology Transactions*, vol. 32, no. 4, pp. 453-460, 1989.
- [67] K. Liao, H. Chen and T. Tian, "The Study of Friction between Piston Ring and Different Cylinder Liners using Floating Liner Engine - Part 1," *SAE International*, pp. SAE Paper No. 2012-01-1334, 2012.
- [68] T. Tian, "Modeling the Performance of the Piston Ring-Pack in Internal Combustion Engines," *PhD Thesis, Massachusetts Institute of Technology*, 1997.
- [69] G. Smedley, "Piston Ring Design for Reduced Friction in Modern Internal Combustion Engines," *MIT SM Thesis*, 2002.

- [70] E. Thiele, "Determination of Friction Losses in Internal Combustion Engines,"
Motortechnische Z., vol. 43, no. 6, pp. 253-258, 1982.

(This page was intentionally left blank)

Appendix A

**Table A.0.1 Lubricant Properties and Constants Used in Vogel and Cross Equations
Various**

Viscosity Data for Various Oil Grades							
Oil Grade	k (cSt)	θ_1 (°C)	θ_2 (°C)	ratio of high shear to low shear	c1	c2 (°C) ⁻¹	VI
10W-30	0.1403	869.72	104.4	0.76	2.3	0.0225	157
15W-40	0.03435	1424.3	137.2	0.79	2.5	0.026	142
SAE30	0.0246	1432.29	132.94	1	2.3	0.0225	106
SAE50	0.0384	1349.94	115.16	1	2.3	0.0225	102
5W20	0.04576	1224	134.1	0.94	2.5	0.029	141
5W40	0.15	1018.74	125.91	0.8	2.3	0.0225	203